

Aus der Klinik und Poliklinik für Nuklearmedizin  
der Ludwig-Maximilians-Universität München

Direktor: Prof. Dr. med. Peter Bartenstein

# Diagnostic and therapeutic applications of CA XII targeting 6A10 Fab – radiochemical and biological studies

Kumulative Dissertation  
zum Erwerb des Doktorgrades der Naturwissenschaften (Dr. rer. nat.)  
an der Medizinischen Fakultät  
der Ludwig-Maximilians-Universität München

vorgelegt von  
Luise Fiedler, M.Sc.  
aus Stralsund

2018





Mit Genehmigung der Medizinischen Fakultät  
der Ludwig-Maximilians-Universität München

Betreuer: Priv. Doz. Dr. rer. nat. Guido Böning

Zweitgutachterin: Prof. Dr. Kirsten Lauber

Dekan: Prof. Dr. med. dent. Reinhard Hickel

Tag der mündlichen Prüfung: 14.01.2019



## Eidesstattliche Versicherung

---

Fiedler, Luise

---

Name, Vorname

Ich erkläre hiermit an Eides statt, dass ich die vorliegende Dissertation mit dem Thema

Diagnostic and therapeutic applications of CA XII targeting 6A10 Fab – radiochemical and biological studies

selbständig verfasst, mich außer der angegebenen keiner weiteren Hilfsmittel bedient und alle Erkenntnisse, die aus dem Schrifttum ganz oder annähernd übernommen sind, als solche kenntlich gemacht und nach ihrer Herkunft unter Bezeichnung der Fundstelle einzeln nachgewiesen habe.

Ich erkläre des Weiteren, dass die hier vorgelegte Dissertation nicht in gleicher oder in ähnlicher Form bei einer anderen Stelle zur Erlangung eines akademischen Grades eingereicht wurde.

München, 15.01.2019

Luise Fiedler

---

Ort, Datum

Unterschrift



## Summary

---

The high energy demand of fast and aggressively growing tumor cells is covered by both anaerobic and aerobic glycolysis. This results in an intracellular accumulation of mostly acidic metabolic products. Thus, balancing the intracellular pH is demanding for tumor cells, yet crucial for their optimal proliferation and survival. The carbonic anhydrases (CA) constitute a family of enzymes that catalyse the hydration of carbon dioxide, yielding the bicarbonate ion, which serves as the main buffer system in most organisms. CA XII is a membrane-tethered isozyme on several types of tumors and an excellent target for nuclear medicine diagnosis and therapy. The specific CA XII binding 6A10 Fab (fragment antigen binding) was shown to be of great interest as a new carrier molecule for a radioactive nuclide. A suitable radionuclide for therapeutic applications accompanied with single photon emission computed tomography (SPECT) imaging techniques is lutetium-177. In this study, the  $^{177}\text{Lu}$ -labelled 6A10 Fab was for the first time evaluated *in vitro* and *in vivo* as an agent for local intracavitary radioimmunotherapy (RIT) of glioblastomas. To extend the 6A10 Fab's application beyond the local treatment in the brain, a systemic injection for the detection of CA XII expressing tumors was investigated. For this purpose, this study evaluated the automated production of copper-64 for radiolabelling purposes to provide  $^{64}\text{Cu}$ -labelled 6A10 Fab for positron emission tomography (PET) studies.

For therapeutic applications, the protein was conjugated with *p*-SCN-Bn-CHX-A''-DTPA at a molar chelator-to-protein ratio of 1:0.96 and radiolabelled with lutetium-177 with a specific activity of 1.5 GBq/mg. Radio-TLC revealed a radiochemical purity of greater than 96%. The radioconjugate was analyzed via flow cytometry, confirming the persisting CA XII binding capacity after successful modification. The radiochemical stability of the compound was determined to be greater than 90% after 72 h of incubation in human cerebrospinal fluid (37 °C), human plasma (37 °C) and labelling buffer (room temperature). A mouse xenograft model with CA XII-positive glioma cells was used for biodistribution studies, autoradiographic examinations and first *in vivo* imaging experiments. The tumor revealed a moderate uptake of up to  $3.1 \pm 0.9$  %ID/g 6 h post injection (p.i.) while significantly high and long-lasting kidney retention ( $55.6 \pm 13.0$  %ID/g 48 h p.i.) was found. Tumor slices were analyzed autoradiographically and microscopically to confirm that regions of high activity uptake also show high cell density and vice versa. Tumors were suc-

cessfully visualized using planar scintigraphy or SPECT/CT techniques and a tumor-to-contralateral ratio of 2.4 (5 h p.i.) was measured.

Copper-64 was produced using an automated setup and characterized with respect to its use as a radiolabelling nuclide. Nickel-64, which was used as target material, was electrochemically deposited with yields of up to 96%, automatically sent to a cyclotron, and irradiated with protons (2 - 5 h, 11 – 14.5 MeV, 20 - 30  $\mu$ A), yielding a maximum activity of approx. 5 GBq. In addition to copper-64, irradiation by-products were quantified by gamma spectroscopy as  $0.03 \pm 0.10$  At%  $^{55}\text{Co}$ ,  $0.004 \pm 0.014$  At%  $^{57}\text{Co}$ , and  $1.4 \pm 3.4$  At%  $^{61}\text{Co}$  at the end of irradiation. Ion chromatography of the dissolved target led to a radiochemical purity of >99% in the final product fraction. The copper-64, dissolved in 9 ml HCl, was evaporated to dryness and taken up in 400  $\mu$ l of 0.1 M HCl. Optimization of the module rinsing methods lead to molar activities of up to 133 GBq/ $\mu$ mol. The efficiency of rinsing methods was evaluated by determination of non-radioactive metal contaminations via ICP-OES while the molar activity was calculated by titration of the copper-64 with 1,4,8,11-Tetraazacyclotetradecane-1,4,8,11-tetraacetic acid (TETA). For diagnostic purposes, the 6A10 Fab was conjugated with p-NCS-Bn-NODA-GA, radiolabelled with copper-64 and used for PET imaging and a biodistribution study in mice. First *in vivo* experiments of the  $^{64}\text{Cu}$ -labelled 6A10 Fab showed a high tumor uptake of up to  $6.9 \pm 1.6$  %ID/g. PET analysis revealed a tumor-to-contralateral ratio of  $11.8 \pm 0.3$  (n = 2) 4 h p.i..

The results of this study showed the high potential of the radiolabelled 6A10 Fab fragment for possible therapeutic and diagnostic applications. Radiolabelled with lutetium-177, the protein is suitable for the local therapeutic application in the brain since it showed a moderate tumor uptake, and a good radiochemical stability under physiological conditions. Additionally, it does not cross the blood-brain barrier (BBB). Further investigations on an orthotopic animal model to generate data closer to the final clinical application would be beneficial to estimate the compound's distribution after a local application. By radiolabelling the Fab with copper-64, high tumor uptake enabling high resolution PET images was achieved, which encourages further investigations concerning a future systemic application for diagnostic purposes. The automated production of copper-64 resulted in good radioactive yields, moderate molar activities and high radiochemical purity. Reproducibility of the production process still needs to be improved further for routine supply of copper-64 with high quality for radiolabelling procedures.

## Zusammenfassung

---

Aufgrund ihres schnellen und aggressiven Wachstums benötigen Tumorzellen überdurchschnittlich viel Energie. Dieser Bedarf wird größtenteils über aerobe und anaerobe Glykolyse gedeckt, was intrazellulär zur Entstehung von sauren Stoffwechselprodukten führt. Um einer Übersäuerung entgegenzuwirken sind Puffermoleküle wie Hydrogencarbonate notwendig, die u.a. von der Membran-assoziierten Carboanhydrase XII (CA XII) zur Verfügung gestellt werden. Aus diesem Grund ist dieses Enzym auf vielen Arten von Tumorzellen überexprimiert und stellt somit ein vielversprechendes Zielmolekül für nuklearmedizinische Ansätze in Diagnostik und Therapie dar. Das 6A10 Fab Fragment bindet spezifisch an CA XII, weshalb es als Trägermolekül eines radioaktiven Nuklides prädestiniert ist. In dieser Arbeit wurde das Protein mit Lutetium-177 markiert und durch diverse in-vitro und in-vivo Charakterisierungen auf seine mögliche Eignung für die lokale Therapie von Glioblastomen untersucht. Darüber hinaus ist eine diagnostische Anwendung erstrebenswert, weshalb die automatisierte Produktion des PET-Nuklids Kupfer-64 etabliert und dieses charakterisiert wurde. Schlussendlich wurde das Fab Fragment mit Kupfer-64 markiert und damit erste in-vivo Daten mittels PET-Bildgebung generiert.

Das Protein wurde zunächst mit dem Chelator *p*-SCN-Bn-CHX-A''-DTPA in einem Verhältnis von 1:0,96 gekoppelt und anschließend mit 1,5 GBq <sup>177</sup>Lu/mg Fab radiomarkiert. Die radiochemische Reinheit von mehr als 96% wurde mittels Dünnschichtchromatographie ermittelt. Der Erhalt der Bindungsaffinität des modifizierten Fab Fragments am Zielmolekül CA XII wurde mittels Durchflusszytometrie bestätigt und eine radiochemische Stabilität von über 90% nach 72 h Inkubation in verschiedenen Medien (Liquor, Plasma und Markierungspuffer) gefunden. Autoradiographie-, Biodistributions- und erste Bildgebungsexperimente wurden an Mäusen mit subkutanen Tumortransplantaten durchgeführt. Der Tumor zeigte 6 h p.i. eine moderate Aktivitätsaufnahme von  $3,1 \pm 0,9$  %ID/g, während signifikant hohe Aktivitätswerte in der Niere gefunden wurden, die auch 48 h p.i. noch bei  $55,6 \pm 13,0$  %ID/g lagen. Durch autoradiographische Untersuchungen an Tumorschnitten, gefolgt von HE-Färbungen und entsprechender mikroskopischer Charakterisierung konnte eine Korrelation zwischen Bereichen mit hoher Aktivitätsakkumulation und hoher Zelldichte und vice versa festgestellt werden. Die Verteilung des radioaktiven Konjugats konnte außerdem in ersten Bildgebungsexperimenten (planare Szintigraphie und

SPECT/CT) visualisiert und ein Tumor-zu-kontralateral Verhältnis von 2,4 (5 h p.i.) bestätigt werden.

Im zweiten Teil dieser Arbeit wurde die Konjugation und Radiomarkierung des 6A10 Fabs mit p-NCS-Bn-NODA-GA und Kupfer-64 angestrebt, um erste Information zum in-vivo Verhalten der Verbindung mittels PET-Bildgebung und Biodistribution zu erhalten. Dazu wurde die Herstellung des Nuklids unter Verwendung der automatisierten Alceo-Module etabliert und das Produkt hinsichtlich seiner Eignung zur Radiomarkierung von Proteinen charakterisiert. Elementares Nickel-64 wurde mit Ausbeuten über 96% abgeschieden, automatisch im Strahlengang des Zyklotrons positioniert und bis zu 5 h lang bei 11,0 – 14,5 MeV und 20 - 30  $\mu$ A mit Protonen bestrahlt. Ausbeuten von maximal 5 GBq konnten erzielt werden. Entstandene Nebenprodukte wurden mittels Gammaskopie quantifiziert und auf das Ende der Bestrahlung zerfallskorrigiert ( $0,03 \pm 0,10$  At%  $^{55}\text{Co}$ ,  $0,004 \pm 0,014$  At%  $^{57}\text{Co}$  und  $1,4 \pm 3,4$  At%  $^{61}\text{Co}$ ). Das Nuklidgemisch wurde mittels Ionenchromatographie aufgetrennt, was zu einer radiochemischen Reinheit der  $^{64}\text{Cu}$ -Fraktion von über 99% führte. Nach Volumenreduktion lag das Produkt in 400  $\mu$ l einer 0,1 M HCl vor. Die molare Aktivität des Kupfers, ermittelt durch Titration mit TETA, konnte auf 133 GBq/ $\mu$ mol angehoben werden, nachdem durch Optimierung der Reinigungsmethodik der Anteil an nicht-radioaktiven Metallkontaminationen, quantifiziert mittels ICP-OES Messungen, signifikant reduziert wurde. Erste Biodistributionsergebnisse mit dem  $^{64}\text{Cu}$ -markiertem 6A10 Fab zeigten eine hohe Tumoranreicherung von bis zu  $6,9 \pm 1,6$  %ID/g 5 h p.i.. Die PET-Quantifizierung ergab 4 h p.i. ein Tumor-zu-kontralateral Verhältnis von  $11,8 \pm 0,3$  (n = 2).

Die ersten in-vivo und in-vitro Charakterisierungen des 6A10 Fab in Hinblick auf zukünftige therapeutische und diagnostische Anwendungen zeigten vielversprechende Ergebnisse. Durch die Radiomarkierung mit Lutetium-177 in Hinblick auf die lokale Applikation in das Gehirn, konnte eine moderate Tumoranreicherung und eine ausreichende radiochemische Stabilität unter physiologischen Bedingungen im systemisch applizierten Xenograft-Modell nachgewiesen werden. Zusätzlich dazu zeigte die mangelnde Anreicherung im Gehirn, dass das Radiokonjugat die Blut-Hirn-Schranke nicht passiert. Weitere Informationen über das in-vivo Verhalten des Moleküls nach der lokalen Applikation können zudem durch die Etablierung eines anwendungsnäheren Tiermodells generiert werden.

Die systemische Gabe des  $^{64}\text{Cu}$ -markierten Proteins führte zu einer guten Tumoranreicherung und ermöglichte hochauflösende PET-Bildgebung, was zu weiteren Studien in Hinblick auf die Anwendung des Konjugats im Bereich der Krebsdiagnostik motiviert. Die wissenschaftliche Re-

Levanz dieser ersten Ergebnisse sollte in ausführlichen Biodistributions- und Bildgebungsstudien bestätigt werden um das weitere Vorgehen in Richtung der humanen Anwendung zu rechtfertigen. Die genutzten Alceo-Module ermöglichen die automatische Produktion von Kupfer-64 in guter radioaktiver Ausbeute, moderaten molaren Aktivitäten und hoher radiochemischer Reinheit. Die Reproduzierbarkeit des Herstellungsprozesses sollte durch weitere Modifikationen weiter verbessert werden, um die regelmäßige Bereitstellung von Kupfer-64 in hoher Qualität für Radiomarkierungszwecke gewährleisten zu können.



## List of publications

---

In this thesis the following publications are summarized to a cumulative dissertation according to the examination rules for natural sciences in the medical faculty of the Ludwig-Maximilians-Universität München:

**L. Fiedler**, M. Kellner, A. Gosewisch, R. Oos, G. Böning, S. Lindner, N. Albert, P. Bartenstein, H.-J. Reulen, R. Zeidler and F. J. Gildehaus. „Evaluation of  $^{177}\text{Lu}$ - CHX-A''-DTPA-6A10 Fab as a Radioimmunotherapy Agent Targeting Carbonic Anhydrase XII". In: Nuclear Medicine and Biology 60, 55-62 (2018)

**L. Fiedler**, M. Kellner, R. Oos, G. Böning, S. Ziegler, P. Bartenstein, R. Zeidler, F. J. Gildehaus and S. Lindner. "Fully automated production and characterization of  $^{64}\text{Cu}$  and proof-of-principle small animal PET imaging using  $^{64}\text{Cu}$ -labelled CA XII targeting 6A10 Fab". In: ChemMedChem 13 (2018) DOI: 10.1002/cmdc.201800130

### Conference abstracts

This work was presented in national and international conferences. The corresponding abstracts were published:

**L. Fiedler**, M. Kellner, A. Delker, G. Böning, S. Lindner, P. Bartenstein, R. Zeidler, F.J. Gildehaus. „Carboanhydrase 12 als Target für die Radioimmuntherapie von Glioblastomen“. In: Nuklearmedizin 56, A26, (2017).  
DGN Dresden, Germany 2017

**L. Fiedler**, M. Kellner, A. Delker, G. Böning, S. Lindner, P. Bartenstein, R. Zeidler, F.J. Gildehaus. „Evaluation of Lu-177 labelled 6A10 Fab as an agent targeting carbonic anhydrase 12“. In: Journal of Labelled Compounds and Radiopharmaceuticals 60 (Suppl. 1), S561, (2017).  
ISRS, Dresden, Germany 2017

**L. Fiedler**, M. Kellner, A. Delker, G. Böning, S. Lindner, P. Bartenstein, R. Zeidler, F.J. Gildehaus. „Evaluation of Lu-177 labelled 6A10 Fab as an agent targeting carbonic anhydrase 12“. In: European Journal of Nuclear Medicine and Molecular Imaging 44 (Suppl. 2), S162-S163, (2017). EANM, Vienna, Austria 2017

## Contents

---

Eidesstattliche Versicherung .....	I
Summary .....	III
Zusammenfassung .....	V
List of publications .....	IX
Contents .....	XI
1 Nomenclature.....	1
2 Introduction .....	3
3 Studies .....	11
4 Conclusion and Outlook.....	21
5 Bibliography .....	23
6 Original Publications .....	29
List of Figures .....	47
List of Tables .....	49
Danksagung .....	51



## 1 Nomenclature

---

%ID/g	Percentage injected dose per gram
$A_m$	Molar activity [GBq/ $\mu$ mol]
$A_s$	Specific activity [GBq/mg]
BBB	Blood-brain barrier
CA	Carbonic Anhydrase
CA XII	Carbonic Anhydrase 12
CT	Computed Tomography
EOB	End of beam
EOP	End of preparation
Fab	Fragment antigen binding
GMP	Good Manufacturing Practice
PET	Positron Emission Tomography
$ph_e$	Extracellular pH
$ph_i$	Intracellular pH
p.i.	Post injection
RIT	Radioimmunotherapy
ROI	Region of interest
RT	Room temperature
SPECT	Single Photon Emission Computed Tomography
Tu/Cl	Tumor-to-contralateral



## 2 Introduction

---

With an increasing mortality rate from 7.8 Mio deaths in 2008 up to 8.2 Mio deaths in 2012, cancer is still one of the leading causes of death worldwide [1, 2]. In order to improve survival rates of cancer patients, early detection and effective therapies are mandatory. Nuclear medicine uses radiation emitted from incorporated radioactively labelled biomolecules to localize and treat tumor cells in the living organism. Each radionuclide used for radiolabelling shows its individual decay characteristics, which makes it suitable for different applications. Positron Emission Tomography (PET), for instance, utilizes the 511 keV annihilation photons resulting from the interaction of positrons emitted by the nuclide and electrons in the surrounding tissue. Consequently, a PET - suitable nuclide is characterized by  $\beta^+$  decay [3]. Single Photon Emission Computed Tomography (SPECT) on the other hand detects low energy gamma rays from relaxation processes of an excited nuclear state [3]. Both imaging techniques, PET and SPECT, are often used in combination with an X-ray Computed Tomography (CT) scan to combine metabolic and morphologic information with the aim to improve the diagnostic localization of the radiation source in the body. Radionuclides with short-ranged radiation from  $\alpha$  - or  $\beta^-$  - decay with high linear energy transfer are commonly used for internal radiation treatment for therapeutic purposes [4, 5].

For each application, therapy or diagnosis, accumulation of the radioactivity in the desired target region is achieved by binding the nuclide to an appropriate carrier molecule. The radioactive compound distributes in the organism and accumulates at the desired target. One of the most prominent examples for metabolism-based tumor uptake is the tracer [ $^{18}\text{F}$ ]fluorodeoxyglucose ([ $^{18}\text{F}$ ]FDG) [6, 7]. The high energy demand of fast growing tumor cells leads to an increased glucose uptake. Since FDG is taken up and phosphorylated in the same manners as glucose, glucose metabolism can be quantified by FDG-PET. A more specific tumor uptake can be achieved when the radiomolecule binds to the cells using biochemical reactions between the carrier molecule and cell structures [3]. Using a receptor exclusively expressed on the target tissue in combination with a carrier molecule which binds specifically to this target optimizes image quality or therapeutic output, while sparing healthy tissue from unnecessary radiation.

Such a target is the enzyme carbonic anhydrase (CA XII). It is overexpressed on several tumor tissues, for instance breast carcinoma [8-10], astrocytomas [11], gliomas [12-14], renal carcinoma [15-17] and ovarian tumors [18]. CA XII is located on the membrane and has a major influence on the pH stabilization of the cell. The enzyme catalyzes the hydration of  $\text{CO}_2$  to  $\text{HCO}_3^-$ , which is a buffer in the cytosol. In general, tumor tissue is known for its acidic extracellular pH ( $\text{pH}_e$ ) ( $< 6.9$ ) in comparison to its slightly alkaline intracellular pH ( $\text{pH}_i$ ) ( $> 7.0$ ) [19-22]. A change in  $\text{pH}_i$  would significantly affect cell proliferation and cell function. It might even cause apoptosis [23-27]. Hence, stabilization of the optimal pH range is essential for the cell, which is why CA XII is overexpressed on many tumors.

The fast growth of tumors often leads to a chaotic vascular distribution and insufficient vessel function, resulting in a lack of oxygen supply to the cells [21, 28-30]. Additionally, tumors cover their large energy demand with a high respiration rate [20, 21, 25]. As a result of these effects the tumor cells become hypoxic [21, 28]. Therefore, tumor cells use extensively anaerobic glycolysis to ensure their energy supply. In comparison to healthy cells, they produce a much higher amount of acidic metabolic products in the cytosol which would result in an acidic  $\text{pH}_i$  [21, 31-34], since only  $\text{CO}_2$ , but not  $\text{H}^+$  can easily cross the membrane [21, 35-37].

A cell can rely on several pH regulating mechanisms to extrude protons from the cytosol. An active  $\text{H}^+$  transport is achieved by  $\text{Na}^+/\text{H}^+$  exchangers [21, 32, 38-41], proton channels [42] or V-type ATPase  $\text{H}^+$  ion pumps [32, 43, 44]. An indirect co-transport of protons is attained by monocarboxylate transporters [32, 38, 45]. Additionally, protons can be buffered by intracellular available  $\text{HCO}_3^-$  ions, resulting in  $\text{CO}_2$  which is able to leave the cell [21, 31]. To enable this buffering reaction, bicarbonate ions have to be available in the cytosol. Transporter systems such as  $\text{Cl}^- - \text{HCO}_3^-$  exchanger [46] or  $\text{Na}^+ - \text{HCO}_3^-$  transporter proteins [21] transfer the ions into the cell by diffusion. For these mechanisms, bicarbonate has to be extracellularly available. This is achieved by tumor-associated transmembrane carbonic anhydrases (CA) [38, 47-49]. Figure 2-1 shows a schematic illustration of a tumor cell in context with these pH regulating processes.

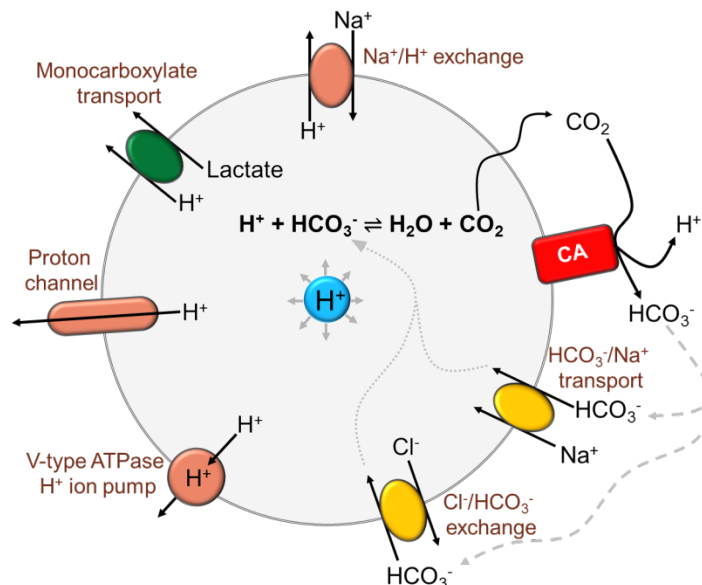


**Figure 2-1:** Schematic drawing of the pH regulation in a tumor cell. Next to extruding  $H^+$  with exchange or transport mechanisms, bicarbonate is used as a buffer system. The escaped  $CO_2$  is extracellularly converted into bicarbonate by carbonic anhydrases and transported back into the cell.

Membrane-tethered CAs with an extracellularly located active site such as CA IX and CA XII have been reported to be of significant importance for tumor cells since they use the escaped  $CO_2$  to provide bicarbonates for transportation back into the cell [21, 31, 50, 51]. CAs are a family of zinc metalloenzymes known to catalyze the hydration of carbon dioxide and water to bicarbonate and proton ( $CO_2 + H_2O \rightarrow H^+ + HCO_3^-$ ) [13, 14, 47, 48, 50, 52, 53], as presented in Figure 2-2.

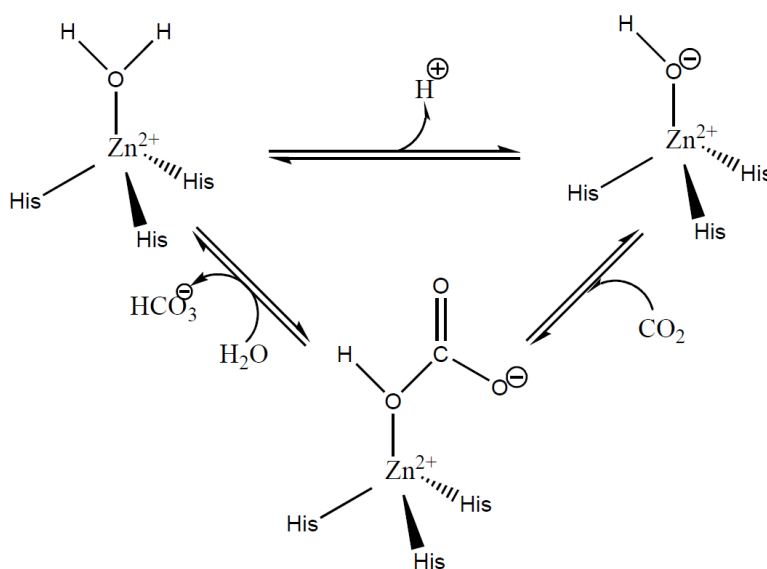


**Figure 2-2:** Reaction mechanism of the formation of bicarbonate catalyzed by carbonic anhydrases.

The reaction is initiated by trapping a water molecule on the zinc ion at the active site, followed by the formation of a hydroxide ion [51, 52]. Carbon dioxide is attacked by the nucleophilic hydroxide ion and the resulting bicarbonate ion is replaced from the  $Zn^{2+}$  with water, which regenerates the initial hydroxide ion and provides the bicarbonate as a buffer to stabilize the cell's pH milieu [51, 52].

The expression of CAs IX and XII has been confirmed on a variety of tumor tissues [50, 54] and is even enhanced under hypoxic conditions [10, 12, 22, 49, 50]. As a target in clinical applications, CA IX has already been intensively investigated [13, 36, 38, 50]. Targeting CA XII might equally be interesting since it is expressed on different malignant cells such as breast carcinoma [8-10], astrocytomas [11], gliomas [12-14], renal carcinoma [15-17] and ovarian tumors [18]. To deliver a radionuclide for diagnostic or therapeutic purposes to CA XII expressing tumor cells, a suitable carrier molecule is needed. The tracer should accumulate homogeneously at the tumor and not on healthy tissue with - especially for therapy - a long retention time on the target [55].

Radiolabelled biomolecules, such as antibodies, have already been investigated to be promising agents for therapeutic and diagnostic approaches in nuclear medicine [56-62]. Antibodies are characterized by a molecular mass of approx. 150 kDa and consist of two heavy and two light chains (see Figure 2-3). The light and the heavy chains together are forming the antigen binding site at the N-terminated area of the antibody.

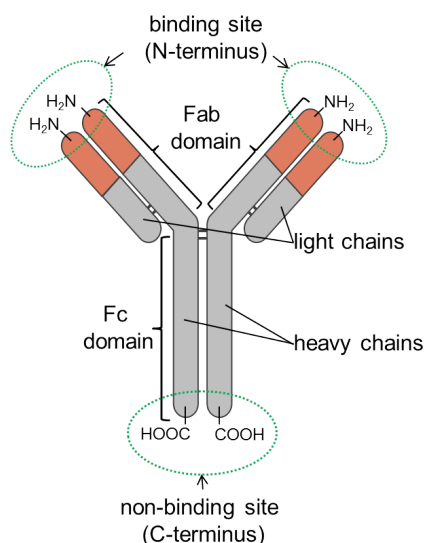


**Figure 2-3:** Schematic illustration of an antibody structure containing the N-terminated binding sites on the Fab-domains, the C-terminated Fc-domain and the allocation in heavy and light chains.

Since a Fab (fragment antigen binding) with approx. 55 kDa consists of one of the two binding sites of an antibody, identical target specificity to the full-length antibody can be expected. Nevertheless, the size difference between these two molecules has significant impact on the pharmacokinetics. *In vivo* distribution and digestion of antibodies is known to be slow, which result in prolonged availability in the blood [63-65]. As a result, the antibody is available for a continued distribution in both, target and non-target tissue. In case of radiolabelled antibodies, this may entail unintended exposure of healthy tissue and an impaired contrast in nuclear images [55, 66]. Due to their high molecular weight, full-length antibodies have worse diffusion properties than Fab fragments so an inhomogeneous distribution in solid tumors due to a limited vascular permeability has been reported [66]. Fab fragments accumulate faster in the tumor and are cleared rapidly from the blood through the kidney. This leads to lower tumor uptakes in comparison to antibodies [55, 62, 67]. Due to this shortened availability in the blood, radiolabelled Fab fragments allow high resolution nuclear imaging since the tumor to background signal is improved in comparison to antibody applications [55, 68]. Fab fragments have just 1/3 of the antibody's molecular weight, resulting in an improved diffusion ability [69, 70]. This contributes to an enhanced clearance of normal tissue, better uptake homogeneity in tumors and improved targeting of disseminated metastases [62, 66, 67].

In this study, the Fab fragment of the 6A10 antibody was used to target CA XII expressing tumor cells. The 6A10 antibody has been shown to be a promising agent for this purpose [13, 14]. Besides its highly specific *in vitro* CA XII binding capacity this antibody inhibits the catalytic function of the target enzyme, which results in antitumor activity both *in vivo* and *in vitro* [13, 14]. Further modification and radiolabelling of the 6A10 Fab in connection with the confirmation of its preserved biological function, as well as *in vivo* and *in vitro* experiments are presented in this study.

The first part of this study focused on investigating the possible therapeutic application of radiolabelled 6A10 Fab against gliomas, which are known to overexpress CA XII in comparison to healthy brain tissue [12-14]. Gliomas are the most common brain tumors in adults accompanied with poor prognosis for patients [71, 72]. Standard treatment includes maximum surgery of the tumor and all visible affected tissue, but due to the gliomas highly infiltrative growth behavior full resection of all disseminated tumor cells is nearly impossible [73]. Also, standard radiation and chemotherapy cannot prevent long-term recurrences [74]. Local intracavitary radioimmunotherapy (RIT) offers an alternative therapeutic approach, where a radiolabelled conjugate is locally applied into the resection cavity, from where it diffuses into the surrounding brain tissue and targets disseminated glioma cells through direct irradiation [59, 74, 75]. A fast distribution in the

brain tissue in combination with a highly specific binding to malignant cells is mandatory for a successful therapy. Previous studies investigated the diffusion properties of anti-tenascin full-length antibodies against their Fab fragments in rat brains and confirmed the superior diffusion velocity and distance of the fragments [76]. Using even smaller molecules to further increase the diffusion gradient and therefore the diffusion distance [69, 70] is not expected to be of advantage, since most tumor recurrences occur in a 2 cm margin around to the resection cavity [77]. A wider diffusion extent would increase the exposure of healthy tissue, which should be avoided. Since an antibody fragment with moderate diffusion properties shows the most promising characteristics for RIT purposes, this study investigates the possibility to use the 6A10 Fab for RIT applications against glioblastomas.

To generate a significant therapy effect on the spread tumor cells and simultaneously spare as much healthy tissue as possible, the 6A10 Fab has to be radiolabelled with a suitable radionuclide. Nuclides like iodine-131 and yttrium-90 have previously been used for RIT studies [74, 78, 79]. Yttrium-90 is not considered in this study, since it has a soft tissue range of 11 mm [80], which is too large to precisely irradiate small targets in otherwise healthy tissue. Iodine-131 and lutetium-177 on the other hand offer similar soft tissue ranges (approx. 2 mm), half-lives (8 days and 6.7 days, respectively) and beta decay characteristics [80]. In addition to the emission of therapy-relevant particles, it is clinically advantageous to use a nuclide with photon emission for imaging. However, lutetium-177 is used in this study since it offers, due to its 208 keV gamma energy, a better SPECT imaging quality than iodine-131. This improved imaging data can be used for individual patient dose calculations in future therapy trials. Lutetium-177 is furthermore available in high radiopharmaceutical quality, in accordance to the Good Manufacturing Practice (GMP) guidelines, which is essential for the clinical application of the produced radioconjugate.

A first evaluation of the  $^{177}\text{Lu}$ -labelled 6A10 Fab with regard to a potential application for RIT was performed in this study. These characterization experiments included *in vitro* stability studies in labelling buffer, cerebrospinal fluid and plasma, *in vitro* blocking studies on tumor slices, autoradiography and HE-staining of tumor slices, biodistribution studies and proof-of-principle planar imaging and SPECT/CT experiments on mice bearing a glioma tumor xenograft.

Besides gliomas, CA XII expression has been reported on different tumors cells such as breast, ovarian or lung cancer. Extending the range of application of the 6A10 Fab beyond the local glioblastoma therapy might therefore be a promising development in anti-cancer research. By using a suitable  $\beta^+$  emitting nuclide for radiolabelling, this Fab fragment could be used for PET-

based diagnostics of CA XII expressing tumors. Since this includes a systemic administration of the compound, the used radionuclide should have appropriate characteristics in correlation with the Fab's pharmacokinetic and metabolic profile. Full-length antibodies have previously been radiolabelled with nuclides such as zirconium-89 ( $T_{1/2} = 3.27$ ) [81, 82] or iodine-124 ( $T_{1/2} = 4.18$ ) [82], which enable PET-imaging of even very slow biological distribution processes due to their long half-lives. To track the fate of a Fab fragment *in vivo*, which has a faster pharmacokinetic profile in comparison to antibodies, a radionuclide with a more suitable, intermediate half-life such as copper-64 ( $T_{1/2} = 12.7$  h) is promising. Copper-64 is superior to zirconium-89 and iodine-124, since its decay scheme has an additional  $\beta^-$  component (probability 39.0 (3)%) [83-85]. This may even enable therapeutic applications [86-88]. Labelling of biological carrier molecules such as antibodies and their fragments with copper-64 is commonly achieved by using chelators, such as Diamsar, NOTA, NODA-GA, PCTA and their derivatives [89, 90]. Several promising studies of chelator-conjugated,  $^{64}\text{Cu}$ -radiolabelled antibodies and their fragments have recently been published against pancreatic cancer [91], malignant lymphoma [92], breast cancer [93-95], ovarian cancer [94], head and neck cancers [96] and CA IX expressing malignant tissue [97]. Other types of molecules, such as RGD-peptides or RGD<sub>2</sub>-BBN heterotrimers have also been radiolabelled with copper-64 via chelators and investigated for PET-imaging of gliomas and prostate cancer, respectively [98, 99]. Due to this well-established coordination chemistry, radiolabelling of the 6A10 Fab with copper-64 is feasible and very promising for further investigations.

The production of copper-64 according to the  $^{64}\text{Ni}(p,n)^{64}\text{Cu}$  reaction in a biomedical cyclotron has already been established by several groups [100-105]. However, all production related steps including electrochemical deposition of the nickel-64 solid target, irradiation, dissolution and purification of the irradiated target, and final preparation of the copper-64 for labelling purposes were performed using individual methods and mostly custom-made, semi-automated setups. An automated commercially available setup for this purpose (the so-called "Alceo" modules), is provided by Comecer S.p.A. (Castel Bolognese, Italy). In this study, the production of copper-64 using the first generation Alceo modules was evaluated and established. The amount of co-produced radionuclides, the radiochemical purity and identity after separation, as well as the non-radioactive metal impurities and the molar activity were determined to characterize the product with regard to further radiolabelling applications. Finally, the 6A10 Fab was radiolabelled with copper-64 for the first time. The conjugate was systemically injected into mice bearing a CA XII-expressing tumor xenograft and proof-of-principle PET-imaging experiments were performed.



### <sup>177</sup>Lu-labelled 6A10 Fab for therapeutic RIT applications

The 6A10 Fab fragment was firstly radiolabelled and evaluated for the use as a therapeutic agent against glioma recurrences in this study. The Fab was conjugated with the chelator *p*-SCN-Bn-CHX-A''-DTPA at alkaline pH. This induces the formation of a thiourea bond between the chelators' isothiocyanate residue and the amino groups of lysines, located in the amino acid sequence of the 6A10 Fab. Using nap-5 columns, unbound chelator was removed and the amount of bound chelator per molecule Fab was determined to be 1:0.96 via Maldi-TOF analysis. A concentration calculation of the conjugation product was performed based on photometric absorption. The lutetium-177 was complexed to the chelator in a slightly acidic sodium acetate buffer, yielding a specific activity ( $A_s$ ) of up to 1.5 GBq/mg with radiochemical purities >96%. Figure 3-1 shows the structural drawing of the final radioimmunoconjugate.

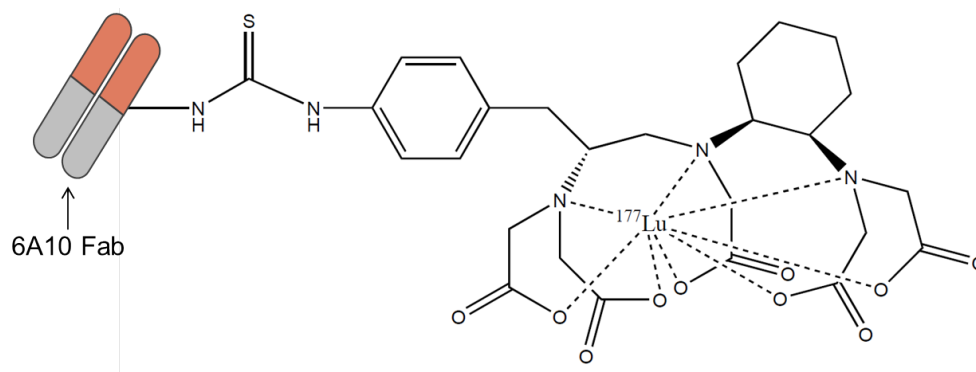


**Figure 3-1:** Structural drawing of the [<sup>177</sup>Lu]LuDTPA-Fab.

The absence of any free lutetium-177 or [<sup>177</sup>Lu]LuDTPA was confirmed using radio-TLC techniques. Flow cytometry investigations with the conjugated and radiolabelled Fab on CA XII expressing cell lines were performed, which verified the sustained biological function of the Fab *in vitro*. The immunoconjugate was incubated in cerebrospinal fluid (37 °C), plasma (37 °C), and labelling buffer (RT) over 96 h, which resulted in a remaining radiochemical purity of 86%, 90% and 90%, respectively. Autoradiographic and microscopic examinations of glioma tumor slices revealed that areas with high activity accumulation also have a high cell density and vice versa. Furthermore, an *in vitro* blocking experiment on tumor slices resulted in a 50% reduced uptake after blocking the CA XII with native 6A10 antibody.

A suitable animal model would require tumor inoculation and resection followed by chemo- and radiotherapy and finally local application of the Fab. Since such a model is currently not available, a xenograft animal model was used in this study to determine the *in vivo* behavior of the conjugate. SCID-mice with glioma xenografts on the right flank were used for biodistribution studies. The mice were systemically injected with  $4.3 \pm 0.4$  MBq of the  $^{177}\text{Lu}$ -labelled conjugate and sacrificed after different time points (1 h, 3 h, 6 h, 24 h, 48 h). The relevant tissue was collected, the distribution of the radioactive compound was determined via gamma counter measurement, decay corrected to the time of sacrifice, and expressed as percentage injected dose per gram (%ID/g). After 3 h, the tumor retained a maximum of activity with  $3.1 \pm 0.9\%$ ID/g, successively decreasing to  $1.8 \pm 0.5\%$ ID/g after 48 h. Compared with other studies investigating radiolabelled Fab fragments, such as Mandler et al. 2015 [68, 106], this means a moderate uptake. High kidney retention was observed over all time points, with  $55.6 \pm 13.0\%$ ID/g even after 48 h, which may be critical for therapeutic applications. Nevertheless, the aim of this study was a local RIT application, so the compound would not leave the brain in the first place, assuming on an intact blood-brain barrier (BBB) after tumor resection. According to the biodistribution results, the brain does not accumulate activity which is an indicator for the inability of the Fab to cross the BBB.

Finally, first planar imaging experiments on a clinical T2 Siemens Symbia were performed 4 h p.i. on tumor bearing mice ( $n = 5$ ), after the injection of  $16.6 \pm 2.1$  MBq, resulting in a good visualization of the tumor. The tumor-to-contralateral ratio (Tu/Cl) determined by region of interest (ROI) analysis was approx. 2/3 smaller than the one determined by biodistribution, which is mainly a consequence of using a human scanner with a limited spatial resolution for small-animal imaging.

As a consequence, the  $^{177}\text{Lu}$ -labelled 6A10 Fab was found to be a promising compound for further investigations with regard to RIT application. Detailed descriptions of all relevant material, methods and corresponding results in conjunction with a detailed discussion is provided in Fiedler et al. 2018 [107].

A successful RIT approach against gliomas can only be guaranteed by using an optimized amount of radioactivity applied in the resection cavity. SPECT/CT imaging is a valuable tool to generate the data necessary for those dose calculations. Thus, for one animal (5 h p.i.) an additional 60-minute SPECT/CT on a dual-headed T2 Siemens Symbia was acquired directly after the first planar scintigraphy. The SPECT data acquisition was based on a  $180^\circ$ -rotation of both detectors in 60 projections, a detector radius of 10 cm and a measurement time of 60 s per view. Projections were measured in  $256 \times 256$  pixels with zoom 2 (isotropic voxels of 1.2 mm). The

SPECT image was reconstructed using CT-based attenuation correction, triple-energy-window scatter correction (lower peak:  $170 \text{ keV} \pm 20\%$ , upper peak  $240 \pm 20\% \text{ keV} \pm 15\%$ ) and compensation for geometrical detector response as described in Delker et al. [108]. Figure 3-2 shows the coronal and transversal SPECT/CT image slice of this mouse. In analogy to the planar scintigraphy and biodistribution experiments, kidneys and bladder were strongly visible. ROI analysis revealed a tumor-to-contralateral ratio of 2.4. This value differs from the corresponding mean ratio of  $3.3 \pm 0.3$  generated from planar scintigraphy, since SPECT/CT values are corrected for attenuation and scattering effects and the exclusion of signal superposition is possible.

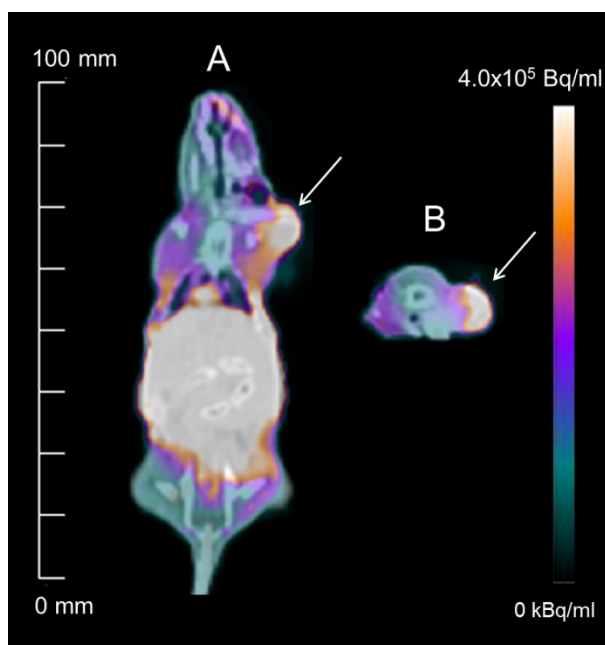


**Figure 3-2:** Coronal (A) and transversal (B) SPECT/CT image of a mouse 5 h after the injection of 16.1 MBq  $^{177}\text{Lu}$ -6A10 Fab. The tumor on the right shoulder is indicated by white arrows.

### **$^{64}\text{Cu}$ -labelled 6A10 Fab for diagnostic PET applications**

Copper-64 is considered as a suitable nuclide to label the 6A10 Fab for the possible use as a diagnostic agent in PET studies. The cyclotron-based production of this radiometal using the automated Alceo setup was evaluated in this study in order to establish a routine production of copper-64 suitable for radiolabelling.

The Alceo setup consists of three modules to cover all necessary steps of the copper-64 production: the “EDS”, where the electrochemical nickel-64 deposition on the so-called “shuttle” and the dissolution of the irradiated nickel-64 target takes place, the “PTS” which is responsible for target positioning and cooling during the irradiation and the “PRF” for separation of the irradiated product from possible co-products and target material. The Alceo modules use a dynamic electrochemical deposition method, in which the nickel-64 solution is pumped through the electrochemical cell at a constant flow between 1.2 – 1.4 ml/min. Up to 85 mg nickel-64 were deposited in

20-24 h at 2.6 V and a varying current. The shuttle equipped with the nickel deposit was automatically sent through tubes to the PETtrace 800 series cyclotron for irradiation. The beam position was successfully confirmed to be in the beamline by performing a paper burn test. Beam parameters between 11 – 14.5 MeV, up to 5 h irradiation duration and up to 30  $\mu\text{A}$  were tested in this study. High irradiation currents and long durations with a 14.5 MeV proton beam have so far resulted in yields greater than 5 GBq copper-64 at the end of beam (EOB). Irradiation by-products were separated from the copper-64 fraction and quantified using gamma spectroscopy. The purified copper-64, available in 9 ml hydrochloric acid (HCl), was evaporated to dryness and re-dissolved in 400  $\mu\text{l}$  0.1 M HCl in order to set appropriate conditions for further radiolabeling experiments. Gamma spectroscopy analysis and half-life determination confirmed the nuclide identity of copper-64 and its purity (>99%). The molar activity ( $A_m$ ) was calculated using a TETA titration method introduced by McCarthy et al. 1997 [100] and decayed samples of the product were analyzed via ICP-OES. The amount of metal impurities was used to evaluate the module cleaning method and a correlation with the measured molar activity was made. Improving the cleaning procedure has led to an  $A_m$  of up to 133 GBq/ $\mu\text{mol}$ . The insufficient reproducibility during target preparation was discovered to be one of the most limiting factors when using the Alceo modules for the automated production of copper-64. Nevertheless, it was possible to provide copper-64 in good yields, high purity and moderate molar activity for medical purposes. Finally, the 6A10 Fab fragment was conjugated with p-NCS-Bn-NODA-GA, radiolabelled with the produced copper-64 (see Figure 3-3) with an  $A_s$  of  $208.6 \pm 49.7$  MBq/mg and a radiolabelling purity of higher than 93%. A first PET image was generated on a tumor xenograft mouse model. A full description of the performed experiments concerning the copper-64 production, characterization, radiolabelling and final PET application with the 6A10 Fab, including all relevant material, is provided in Fiedler et al. 2018 [109].

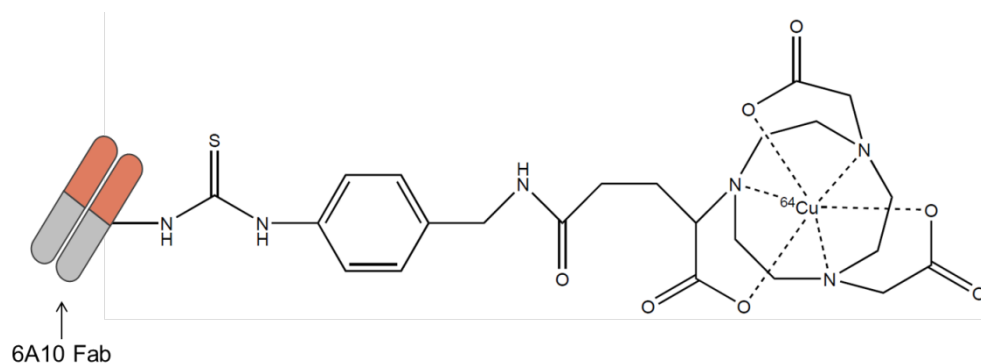


**Figure 3-3:** Structural drawing of the [ $^{64}\text{Cu}$ ]CuNODA-GA-Fab.

---

PET imaging and biodistribution of four tumor bearing mice (M1, M2, M4 and M5), injected with the  $^{64}\text{Cu}$ -labelled 6A10 Fab, were performed. Data gained from the biodistribution experiments with  $^{64}\text{Cu}$ -6A10 Fab were subsequently compared to the data previously obtained from biodistribution with the  $^{177}\text{Lu}$ -6A10 Fab.

Tumors were subcutaneously inoculated with  $5 \times 10^6$  U87 cells into the right shoulder of female SCID-mice (6 - 8 weeks, 20 - 25 g). A growth time of 12 days resulted in tumor sizes of  $140 \pm 89 \text{ mm}^3$ . The mice were intravenously injected with  $13.1 \pm 2.4 \text{ MBq}$  of the  $^{64}\text{Cu}$ -labelled 6A10 Fab (approx. 250  $\mu\text{l}$ ). M1 and M2 were scanned 4 h p.i. (see Figure 3-4) and M3 and M4 23 h p.i. (see Figure 3-5) for 1 h on an Inveon P120  $\mu\text{PET}$  device under constant anaesthesia. The images were analyzed with the Inveon Research Workplace software and tumor-to-contralateral ratios were determined by ROI analysis, using a tumor ROI based on 40% threshold. Immediately after the scans the mice were sacrificed, all relevant tissue was harvested, collected, weighed and measured by gamma counter. These data were decay corrected to the time of biodistribution (5 h p.i. for M1 and M2; 24 h p.i. for M4 and M5) and expressed as %ID/g (see Table 3-1). This table additionally includes the comparison between the  $^{64}\text{Cu}$ - and the  $^{177}\text{Lu}$ -generated biodistribution data at similar time points ( $^{64}\text{Cu}$ -compound 5 h p.i. with the  $^{177}\text{Lu}$ -compound 6 h p.i., and the results of both studies 24 h p.i.).

Both, biodistribution and imaging data showed good tumor uptake and high accumulations in organs such as kidney, liver, bladder, spleen and the intestines. Especially in comparison to the values obtained from the  $^{177}\text{Lu}$ -labelled compound it is notable, that the tumor as well as every other harvested tissue shows higher amounts of the  $^{64}\text{Cu}$ -labelled compound. Next to the biodistribution data listed in Table 3-1, a graphical comparison of the results gained 5 h, 6 h and 24 h p.i. is shown in Figure 3-6 and Figure 3-7, respectively.

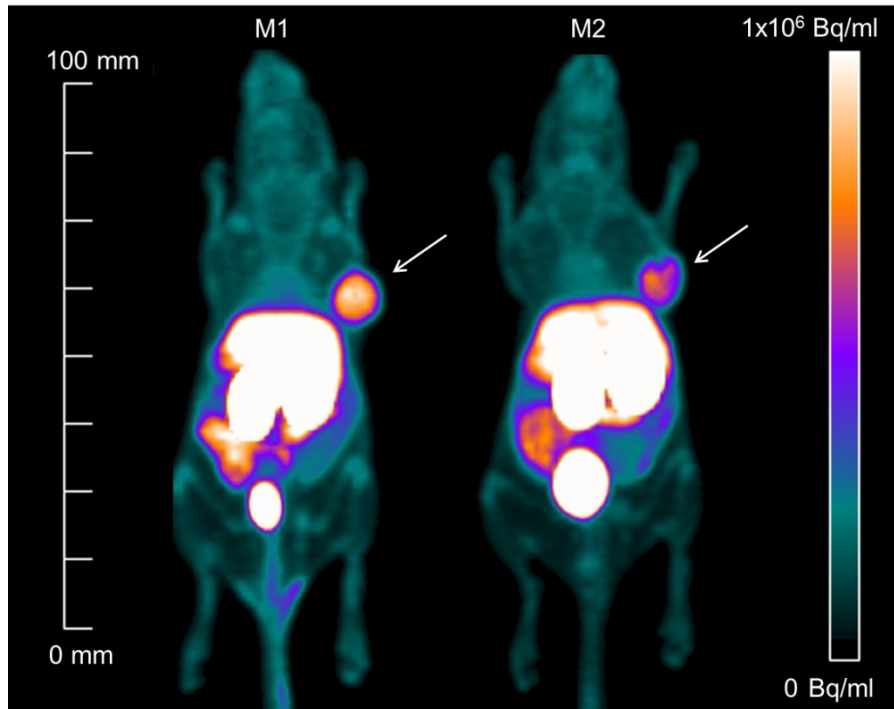


**Figure 3-4:** PET images of M1 and M2 4 h after the injection of 14.7 MBq and 13.9 MBq of the  $^{64}\text{Cu}$ -6A10 Fab, respectively. Tumors on the right shoulder are indicated with white arrows.

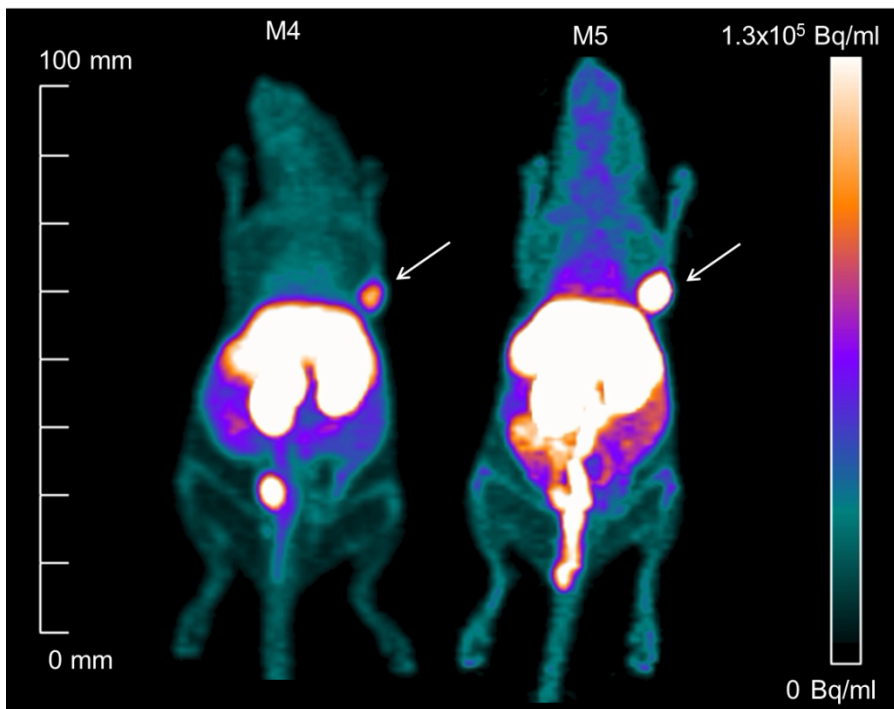


**Figure 3-5:** PET images of M4 and M5 23 h after the injection of 9.6 MBq and 14.2 MBq of the  $^{64}\text{Cu}$ -6A10 Fab, respectively. Tumors on the right shoulder are indicated with white arrows.

**Table 3-1:** Comparison of the biodistribution results (in %ID/g) gained using n = 2 and n = 4 mice injected with  $^{64}\text{Cu}$ - and  $^{177}\text{Lu}$ -labelled 6A10 Fab, respectively.

	$^{64}\text{Cu}$ -Fab (5 h p.i.)	$^{177}\text{Lu}$ -Fab (6 h p.i.) [107]	$^{64}\text{Cu}$ -Fab (24 h p.i.)	$^{177}\text{Lu}$ -Fab (24 h p.i.) [107]
Blood	1.9 ± 0.2	1.2 ± 0.3	0.9 ± 0.1	0.2 ± 0.1
Heart	1.7 ± 0.2	0.9 ± 0.2	1.4 ± 0.2	0.6 ± 0.2
Lung	3.3 ± 0.2	1.5 ± 0.7	3.9 ± 1.0	0.5 ± 0.3
Liver	13.5 ± 1.6	5.4 ± 0.7	8.2 ± 1.3	2.6 ± 1.0
Spleen	6.0 ± 0.7	1.8 ± 0.7	4.2 ± 0.9	2.1 ± 1.1
Stomach	2.5 ± 0.4	0.6 ± 0.1	1.9 ± 0.2	0.5 ± 0.1
Small int.	3.3 ± 0.4	0.6 ± 0.1	2.5 ± 0.3	0.4 ± 0.1
Large int.	4.4 ± 0.4	1.5 ± 0.4	3.3 ± 0.5	0.7 ± 0.2
Kidney	84.2 ± 19.7	83.5 ± 18.5	21.4 ± 4.9	93.1 ± 5.0
Brain	0.2 ± 0.0	0.1 ± 0.0	0.1 ± 0.0	0.0 ± 0.0
Muscle	0.5 ± 0.1	0.3 ± 0.1	0.3 ± 0.1	0.3 ± 0.1
Tumor	6.9 ± 1.6	3.0 ± 0.8	5.7 ± 2.0	2.5 ± 0.6
Thyroid	1.3 ± 0.4	0.4 ± 0.1	1.0 ± 0.2	0.4 ± 0.3

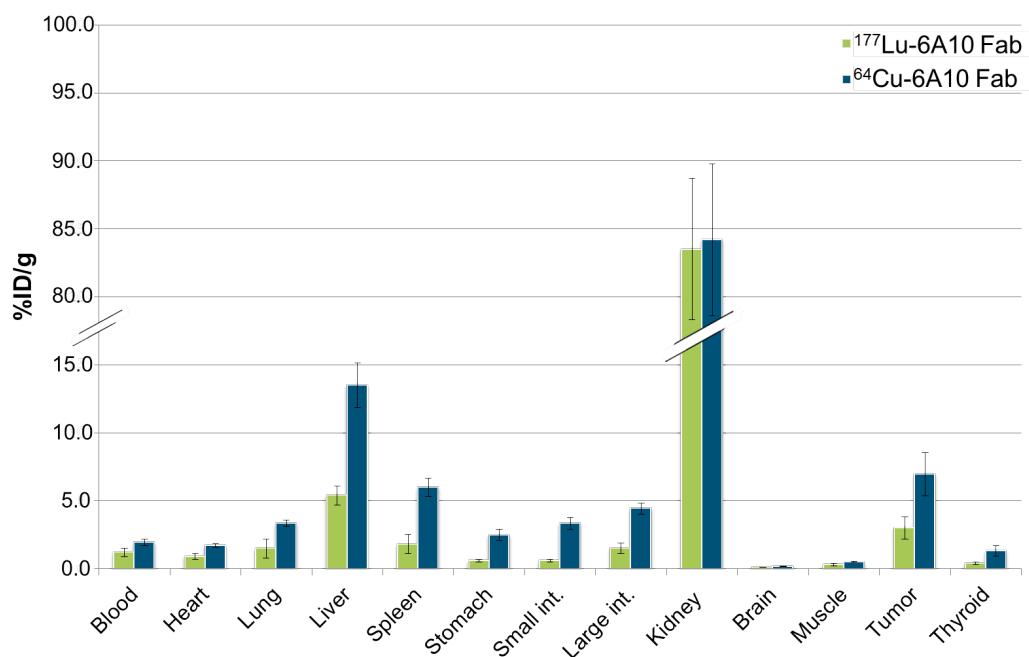


**Figure 3-6:** Biodistribution results 6 h and 5 h after injecting tumor xenograft bearing mice with  $4.3 \pm 0.4$  MBq  $^{177}\text{Lu}$ -6A10 Fab (n = 4) [107] and  $13.1 \pm 2.4$  MBq  $^{64}\text{Cu}$ -6A10 Fab (n = 2).

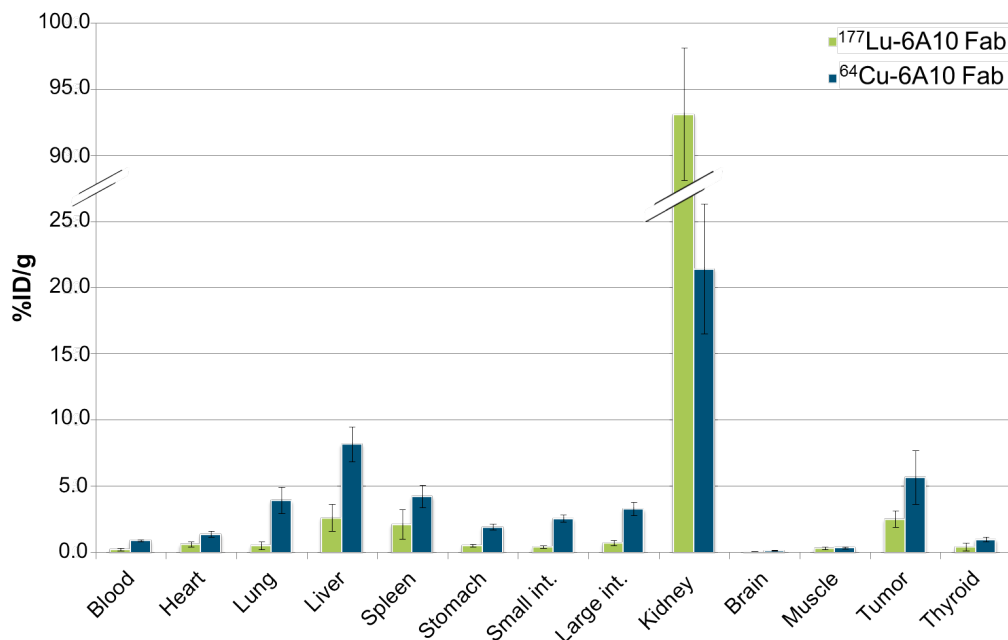


**Figure 3-7:** Biodistribution results 24 h after injecting tumor xenograft bearing mice with  $4.3 \pm 0.4$  MBq  $^{177}\text{Lu}$ -6A10 Fab (n = 4) [107] and  $13.1 \pm 2.4$  MBq  $^{64}\text{Cu}$ -6A10 Fab (n = 2).

Molecules with the size of a Fab undergo mainly renal metabolic processes. As a result, an activity of approx. 84%ID/g was found in the kidney 5 and 6 h p.i. in both studies. 24 h p.i. the  $^{64}\text{Cu}$ -compound shows a more rapid clearance (20%ID/g) in comparison to the  $^{177}\text{Lu}$ -compound (over 90%ID/g). Protein-chelate-metal-conjugates are metabolized in the kidney's lysosomes. Lysosomes catabolize these complexes into metal-chelate fragments, which cannot cross the cell membrane easily and therefore show a long retention in the kidney [110, 111]. The first results of this study indicate, that the  $^{64}\text{Cu}$  complex may overcome the lysosomes membrane much faster than the  $^{177}\text{Lu}$  complex. The liver accumulated approx. 3 times more of the  $^{64}\text{Cu}$ -compound than the  $^{177}\text{Lu}$ -compound with a slow reduction from  $13.5 \pm 1.6$  to  $8.2 \pm 1.3$  %ID/g after 24 h, similar to the spleen which shows three times more activity 5 h p.i. and two times more activity after 24 h. The blood and other tissues also retained increased amounts of activity of the  $^{64}\text{Cu}$ -labelled in comparison to the  $^{177}\text{Lu}$ -labelled compound. Most importantly, the tumor uptake was improved using the  $^{64}\text{Cu}$ -Fab, with  $6.9 \pm 1.6$  %ID/g and  $5.7 \pm 2.0$  %ID/g at 5 h and 24 h p.i., respectively, which was twice as high compared to the  $^{177}\text{Lu}$ -Fab uptake with  $3.0 \pm 0.8$  ID/g and  $2.5 \pm 0.6$  %ID/g. Conjugation and radiolabelling of a molecule with different chelating agents and radionuclides are known to alter the pharmacokinetics of the compound significantly. This effect may also be visible in this study, as NODA-GA conjugation and  $^{64}\text{Cu}$ -labelling seems to result in enhanced diffusion properties and improved vascular permeability of the 6A10 Fab, evidenced by a more persisting activity retention of the  $^{64}\text{Cu}$ -compound in all tissues com-

pared to the  $^{177}\text{Lu}$ -compound 24 h p.i.. *In vivo* stability data for the compound is not yet available, therefore radiometal loss from the conjugate, for example through trans-chelating processes, cannot be excluded. Several proteins are known to bind copper in the human body and might therefore have a major influence on the activity distribution observed in this study. Superoxide dismutase for instance, which is strongly present in liver, kidney, adrenal and red blood cells, binds copper and leads to an enhanced retention of the metal in the corresponding tissue [112-114] in case of copper-64. The measured activity in the liver might also be caused by Ceruloplasmin, a copper-storage protein synthesized in the liver, which is able to bind up to 6 atoms of the metal in its structure [112, 113].

A comparison of all measured tumor-to-contralateral ratios calculated from biodistribution and PET data, the amount of injected activity and the individual tumor volumes in  $\text{mm}^3$  are provided in Table 3-2. The table also revealed that tumor-to-contralateral ratios from biodistribution and PET differ slightly. Limitations of the PET resolution might lead to too small activity quantifications in the tumor with the result of decreased tumor-to-contralateral ratios. Especially small structures with little activity uptake are affected by those limitations, best visible at M4 with the smallest tumor and the lowest injected activity.

**Table 3-2:** Tumor volume, applied activity and the correlating Tu/Cl values generated from biodistribution and PET data of each mouse investigated with the  $^{64}\text{Cu}$ -compound.

Mouse	Tumor volume [ $\text{mm}^3$ ]	Inj. Activity [MBq]	Tu/Cl – Biodis.	Tu/Cl - PET
M1	240	14.7	15.2 (5 h p.i.)	12.0 (4 h p.i.)
M2	190	13.9	12.6 (5 h p.i.)	11.5 (4 h p.i.)
M4	60	9.6	14.6 (24 h p.i.)	9.9 (23 h p.i.)
M5	70	14.2	17.8 (24 h p.i.)	16.6 (23 h p.i.)



## 4 Conclusion and Outlook

---

In this study, the CA XII targeting 6A10 Fab, radiolabelled with lutetium-177 or copper-64, was studied as a potential new therapeutic and diagnostic anti-cancer agent in medical applications.

### **<sup>177</sup>Lu-labelled 6A10 Fab for therapeutic RIT applications**

To produce a compound for local intracavitary RIT against the recurrences of resected gliomas, the 6A10 Fab was conjugated with DTPA and radiolabelled with lutetium-177 for the first time. A comprehensive *in vitro* and *in vivo* characterization confirmed the conjugate to be suitable for this application.

In this study, a tumor-xenograft model was used to investigate the compound's pharmacokinetics although this model does not entirely reflect the clinical situation. But an animal model for investigating a therapeutic approach similar to the final application would require an inoculated tumor to be removed, followed by radio- and chemotherapy. The local application of the drug has to occur after a sufficient recovery time to guarantee an intact BBB. However, such a complex animal model is not available so far.

The approach of local intracavitary RIT using radiolabelled antibodies, such as <sup>131</sup>I-antitennascin, has already been established in several clinical studies, resulting in an improved survival time of patients suffering from gliomas [74, 78]. Since this work demonstrated the highly promising characteristics of the <sup>177</sup>Lu-labelled 6A10 Fab for RIT purposes, a clinical trial is currently in preparation to treat glioma patients with the compound. The high radiopharmaceutical quality of the compound for first in-human applications will be ensured by the establishment of a GMP compliant production.

To spare sensitive organs from unintended exposure during therapy, any activity leakage through the BBB has to be reduced or even avoided. Biodistribution studies on mice showed no brain accumulation after a systemic application, which might indicate the compounds incapability to cross the BBB. In order to further guarantee the brain's integrity a so-called leakage test is part of pre-therapeutic examinations of RIT patients [74].

### **Production of the PET nuclide copper-64**

In order to use the 6A10 Fab fragment for PET applications, a fully automated production of copper-64 utilizing the Alceo modules was successfully established and resulted in copper-64 with good radiolabelling quality, high radioactive yields and excellent radiochemical purity. Further improvement of the process reproducibility may be achieved by setup changes, such as line-shortening, or by using a system based on disposable kits. Such a system would also reduce non-radioactive metallic impurities, thus increasing the molar activity of the produced copper-64.

### **<sup>64</sup>Cu-labelled 6A10 Fab for diagnostic PET applications**

The 6A10 Fab was conjugated with NODA-GA and successfully radiolabelled with the produced copper-64, resulting in a compound well suitable for the proof-of-principle PET imaging experiments performed in this work. Biodistribution results further revealed a good tumor uptake, even superior to the tumor uptake previously determined with the <sup>177</sup>Lu-compound. All tissue samples, except kidney, showed a longer retention time for the <sup>64</sup>Cu-compound compared to the <sup>177</sup>Lu-compound. This encourages further investigations of the compound for applications in PET diagnostics of CA XII expressing diseases, e. g. breast cancer. Such investigations will comprise biodistribution and PET imaging experiments at different time points, including *in vivo* blocking strategies to confirm the specific tumor uptake of the conjugate.

The radiolabelled 6A10 Fab investigated in this work showed highly promising characteristics for its application in nuclear medicine. Radiolabelled with <sup>177</sup>Lu, a phase I clinical trial for the treatment of glioma patients with the 6A10 Fab will be initiated shortly. Furthermore, the implementation of the above suggested improvements regarding the <sup>64</sup>Cu-labelled 6A10 Fab will be an important step towards its application in clinical PET studies.

## 5 Bibliography

---

- [1]. J. Ferlay *et al.*, Cancer incidence and mortality worldwide: Sources, methods and major patterns in GLOBOCAN 2012. *Int. J. Cancer* **136**, E359-E386 (2015).
- [2]. A. Jemal *et al.*, Global Cancer Statistics. *CA Cancer* **61**, 69-90 (2011).
- [3]. N. Long, W.-T. Wong, *The Chemistry of Molecular Imaging*. (Wiley, Hoboken, New Jersey, 2015).
- [4]. C.-H. Yeong, M. Cheng, K.-H. Ng, Therapeutic radionuclides in nuclear medicine: current and future prospects. *Biomed. Biotechnol.* **15**, 845-863 (2014).
- [5]. S. Guhlke, A. M. Verbruggen, S. Vallabhajosula, in *Clinical Nuclear Medicine*. (Springer, Berlin, Heidelberg, 2007).
- [6]. I. Kayani *et al.*, Functional Imaging of Neuroendocrine Tumors With Combined PET/CT Using <sup>68</sup>Ga-DOTATATE (Dota-D<sup>1</sup>Phe<sup>1</sup>, Tyr<sup>3</sup>-octreotate) and <sup>18</sup>F-FDG. *Cancer* **112**, 2447 - 2455 (2008).
- [7]. H. Zhuang *et al.*, Dual Time Point <sup>18</sup>F-FDG PET Imaging for Differentiating Malignant from Inflammatory Processes. *J. Nucl. Med.* **42**, 1412 - 1417 (2001).
- [8]. D. H. Barnett *et al.*, Estrogen Receptor Regulation of Carbonic Anhydrase XII through a Distal Enhancer in Breast Cancer. *Cancer Res.* **68**, 3505-3515 (2008).
- [9]. P. H. Watson *et al.*, Carbonic anhydrase XII is a marker of good prognosis in invasive breast carcinoma. *Br. J. Cancer* **88**, 1065-1070 (2003).
- [10]. C. C. Wykoff *et al.*, Expression of the Hypoxia-Inducible and Tumor-Associated Carbonic Anhydrases in Ductal Carcinoma *in Situ* of the Breast. *Am. J. Pathol.* **158**, 1011-1019 (2001).
- [11]. J. Haapasalo *et al.*, Identification of an alternatively spliced isoform of carbonic anhydrase XII in diffusely infiltrating astrocytic gliomas. *Neuro-Oncology* **10**, 131-138 (2008).
- [12]. M. A. Proescholdt *et al.*, Expression of hypoxia-inducible carbonic anhydrases in brain tumors. *Neuro-Oncol.* **7**, 465-475 (2005).
- [13]. C. Battke *et al.*, Generation and characterization of the first inhibitory antibody targeting tumour-associated carbonic anhydrase XII. *Cancer Immunol. Immunother.* **60**, 649-658 (2011).
- [14]. G. Gondi *et al.*, Antitumor Efficacy of a Monoclonal Antibody That Inhibits the Activity of Cancer-Associated Carbonic Anhydrase XII. *Cancer Res.* **73**, 6494-6503 (2013).
- [15]. A. J. Kivelä *et al.*, Expression of a Novel Transmembrane Carbonic Anhydrase Isozyme XII in Normal Human Gut and Colorectal Tumors. *American Journal of Pathology* **156**, 578-584 (2000).
- [16]. S. Parkkila *et al.*, Expression of the Membrane-associated Carbonic Anhydrase Isozyme XII in the Human Kidney and Renal Tumors. *J. Histochem. Cytochem.* **48**, 1601-1608 (2000).
- [17]. Ö. Türeci *et al.*, Human carbonic anhydrase XII: cDNA cloning, expression, and chromosomal localization of a carbonic anhydrase gene that is overexpressed in some renal cell cancers. *Proc. Natl. Acad. Sci. USA* **95**, 7608-7613 (1998).
- [18]. P. Hynninen *et al.*, Expression of transmembrane carbonic anhydrases IX and XII in ovarian tumours. *Histopathol.* **49**, 594-602 (2006).
- [19]. M. Stubbs, P. M. J. McSheehy, J. R. Griffiths, C. L. Bashford, Causes and consequences of tumour acidity and implications for treatment. *Mol. Med. Today* **6**, 15-19 (2000).

- [20]. P. Vaupel, F. Kallinowski, P. Okunieff, Blood Flow, Oxygen and Nutrient Supply, and Metabolic Microenvironment of Human Tumors: A Review. *Cancer Res.* **49**, 6449-6465 (1989).
- [21]. P. Swietach, R. D. Vaughan-Jones, A. L. Harris, Regulation of tumor pH and the role of carbonic anhydrase 9. *Cancer Metastasis Rev.* **26**, 299-310 (2007).
- [22]. A. Waheed, W. S. Sly, Carbonic anhydrase XII functions in health and disease. *Gene* **623**, 33-40 (2017).
- [23]. A. Roos, W. F. Boron, Intracellular pH. *Physiol. Rev.* **61**, 296–434 (1981).
- [24]. M. De Brabander, G. Geuens, R. Nuydens, R. Willebrords, J. De Mey, Microtubule stability and assembly in living cells: The influence of metabolic inhibitors, taxol and pH. *Cold Spring Harbor Symp. Quant. Biol.* **1**, 227-240 (1982).
- [25]. R. J. Isfort *et al.*, Induction of protein phosphorylation, protein synthesis, immediate-early-gene ex- pression and cellular proliferation by intracellular pH modula- tion. Implications for the role of hydrogen ions in signal transduction. *Eur. J. Biochem.*, 349-357 (1993).
- [26]. D. J. McConkey, S. Orrenius, Signal transduction pathways in apoptosis. *Stem Cells* **14**, 619-631 (1996).
- [27]. H. J. Park, J. C. Lyons, T. Ohtsubo, C. W. Song, Acidic environment causes apoptosis by increasing caspase activity. *Br. J. Cancer*, 1892–1897 (1999).
- [28]. D. G. Hirst, Oxygen Delivery to Tumors. *Int. J. Radiat. Oncol., Biol., Phys.* **12**, 1271-1277 (1986).
- [29]. M. Höckel *et al.*, Association between tumor hypoxia and malignant progression in advanced cancer of the uterine cervix. *Cancer Res.* **56**, 4509–4515 (1996).
- [30]. D. M. Brizel *et al.*, Tumor oxygenation predicts for the likelihood of distant metastases in human soft tissue sarcoma. *Cancer Res.* **56**, 941-943 (1996).
- [31]. D. Neri, C. T. Supuran, Interfering with pH regulation in tumours as a therapeutic strategy. *Nat. Rev. Drug Discovery* **10**, 767-777 (2011).
- [32]. Y. Kato *et al.*, Acidic extracellular microenvironment and cancer. *Cancer Cell Int.* **13**, 89-98 (2013).
- [33]. O. Warburg, *The metabolism of tumours*. (London: Arnold Constable, 1930).
- [34]. F. Horn *et al.* (Thieme, 2002).
- [35]. P. Swietach, S. Patiar, C. T. Supuran, A. L. Harris, R. D. Vaughan-Jones, The Role of Carbonic Anhydrase 9 in Regulating Extracellular and Intracellular pH in Three-dimensional Tumor Cell Growths. *J. Biol. Chem.* **284**, 20299-20310 (2009).
- [36]. P. Swietach *et al.*, Tumor-associated Carbonic Anhydrase 9 Spatially Coordinates Intracellular pH in Three-dimensional Multicellular Growths. *J. Biol. Chem.* **283**, 20473-20483 (2008).
- [37]. A. Hulikova, R. D. Vaughan-Jones, P. Swietach, Dual Role of CO<sub>2</sub>/HCO<sub>3</sub> Buffer in the Regulation of Intracellular pH of Three-dimensional Tumor Growths. *J. Biol. Chem.* **286**, 13815-13826 (2011).
- [38]. J. Chiche *et al.*, Hypoxia-Inducible Carbonic Anhydrase IX and XII Promote Tumor Cell Growth by Counteracting Acidosis through the Regulation of the Intracellular pH. *Cancer Res.* **69**, 358-368 (2009).
- [39]. J. Orlowski, S. Grinstein, Diversity of the mammalian sodium/proton exchanger SLC9 gene family. *Pfluegers Arch.* **447**, 549 –565 (2004).
- [40]. H. Murer, U. Hopfer, R. Kinne, Sodium/Proton Antiport in Brush-Border-Membrane Vesicles Isolated from Rat Small Intestine and Kidney. *Biochem. J.* **154**, 597–604 (1976).
- [41]. C. Sardet, A. Franchi, J. Pouysségur, Molecular Cloning, Primary Structure, and Expression of the Human Growth Factor-Activatable Na<sup>+</sup>/H<sup>+</sup> Antiporter. *Cell* **56**, 271–280 (1989).
- [42]. T. E. DeCoursey, V. V. Cherny, An electrophysiological comparison of voltage-gated proton channels, other ion channels, and other proton channels. *Isr. J. Chem.* **39**, 409–418 (1999).

- [43]. P. L. Pedersen, E. Carafoli, Ion motive ATPases. I. Ubiquity, properties, and significance to cell function. *Trends Biochem. Sci.* **12**, 146-150 (1987).
- [44]. R. Martinez-Zaguilan, R. M. Lynch, G. M. Martinez, R. J. Gillies, Vacuolar-type H(+)-ATPases are functionally expressed in plasma membranes of human tumor cells. *Am. J. Physiol.* **265**, C1015–C1029 (1993).
- [45]. A. P. Halestrap, D. Meredith, The SLC16 gene family-from monocarboxylate transporters (MCTs) to aromatic amino acid transporters and beyond. *Pfluegers Arch.* **447**, 619–628 (2004).
- [46]. A. H. Lee, I. F. Tannock, Heterogeneity of Intracellular pH and of Mechanisms That Regulate Intracellular pH in Populations of Cultured Cells. *Exp. Ther.* **58**, 1901-1908 (1998).
- [47]. R. E. Tashian, The Carbonic Anhydrases: Widening Perspectives on Their Evolution, Expression and Function. *BioEssays* **10**, 186-189 (1989).
- [48]. W. S. Sly, P. Y. Hu, Human Carbonic Anhydrases and Carbonic Anhydrase Deficiencies. *Annu. Rev. Biochem.* **64**, 375-401 (1995).
- [49]. C. C. Wykoff *et al.*, Hypoxia-inducible Expression of Tumor-associated Carbonic Anhydrases<sup>1</sup>. *Cancer Res* **60**, 7075-7083 (2000).
- [50]. S. Ivanov *et al.*, Expression of Hypoxia-Inducible Cell-Surface Transmembrane Carbonic Anhydrases in Human Cancer. *Am. J. Pathol.* **158**, 905-919 (2001).
- [51]. C. T. Supuran, Carbonic anhydrases: novel therapeutic applications for inhibitors and activators. *Nat. Rev. Drug Discovery* **7**, 168-181 (2008).
- [52]. D. A. Whittington *et al.*, Crystal structure of the dimeric extracellular domain of human carbonic anhydrase XII, a bitopic membrane protein overexpressed in certain cancer tumor cells. *PNAS* **98**, 9545-9550 (2001).
- [53]. S. Lindskog, Structure and Mechanism of Carbonic Anhydrase. *Pharmacol. Ther.* **74**, 1-20 (1997).
- [54]. R. M. Torczynski, A. P. Bollon. (1996), vol. U.S. Patent 5,589,579.
- [55]. M. S. Dennis *et al.*, Imaging Tumors with an Albumin-Binding Fab, a Novel Tumor-Targeting Agent. *Cancer Res* **67**, 254-261 (2007).
- [56]. D. D. Bigner *et al.*, Iodine-131-Labeled Antitenascin Monoclonal Antibody 81C6 Treatment of Patients With Recurrent Malignant Gliomas: Phase I Trial Results. *J. Clin. Oncol.* **16**, 2202-2212 (1998).
- [57]. R. Chakravarty *et al.*, <sup>90</sup>Y/<sup>177</sup>Lu-labelled Cetuximab immunoconjugates: radiochemistry optimization to clinical dose formulation. *J. Labelled Compd. Radiopharm.* **59**, 354-363 (2016).
- [58]. J. Dahle *et al.*, Evaluating Antigen Targeting and Anti-tumor Activity of a New Anti-CD37 Radioimmunoconjugate Against Non-Hodgkin's Lymphoma. *Anticancer Res.* **33**, 85-96 (2013).
- [59]. P. De Bonis *et al.*, Radioimmunotherapy for High-Grade Glioma. *Immunotherapy* **5**, 647-659 (2013).
- [60]. S. M. Larson, J. A. Carrasquillo, N.-K. V. Cheung, O. W. Press, Radioimmunotherapy of human tumours. *Nat. Rev. Cancer* **15**, 347–360 (2015).
- [61]. R. M. Sharkey, D. M. Goldenberg, Cancer radioimmunotherapy. *Immunotherapy* **3**, 349–370 (2011).
- [62]. V. Kenanova, A. M. Wu, Tailoring antibodies for radionuclide delivery. *Expert Opin. Drug Delivery* **3**, 53-70 (2006).
- [63]. D. G. Covell *et al.*, Pharmacokinetics of Monoclonal Immunoglobulin G<sub>1</sub>, F(ab')<sub>2</sub>, and Fab' in Mice. *Cancer Res* **46**, 3969-3978 (1986).
- [64]. R. W. Kinne *et al.*, Rat Adjuvant Arthritis: Imaging with Technetium-99m-Anti-CD4 Fab' Fragments. *J. Nucl. Med.* **36**, 2268-2275 (1995).
- [65]. T. Behr, W. Becker, E. Hannappel, D. M. Goldenberg, F. Wolf, Targeting of Liver Metastases of Colorectal Cancer with IgG, F(ab')<sub>2</sub>, and Fab' Anti-Carcinoembryonic

- Antigen Antibodies Labeled with  $^{99m}\text{Tc}$ : The Role of Metabolism and Kinetics'. *Cancer Res. (Suppl.)* **55**, 5777s-5785s (1995).
- [66]. G. M. Thurber, S. C. Zajic, K. D. Wittrup, Theoretic Criteria for Antibody Penetration into Solid Tumors and Micrometastases. *J. Nucl. Med.* **48**, 995-999 (2007).
- [67]. P. Holliger, P. J. Hudson, Engineered antibody fragments and the rise of single domains. *Nat. Biotechnol.* **23**, 1126-1136 (2005).
- [68]. C. T. Mendler, T. Gehring, H.-J. Wester, M. Schwaiger, A. Skerra,  $^{89}\text{Zr}$ -Labeled Versus  $^{124}\text{I}$ -Labeled aHER2 Fab with Optimized Plasma Half-Life for High-Contrast Tumor Imaging In Vivo. *J. Nucl. Med.* **56**, 1112-1118 (2015).
- [69]. M. E. Young, P. A. Carroad, R. L. Bell, Estimation of Diffusion Coefficients of Proteins. *Biotechnol. Bioeng.* **22**, 947-955 (1980).
- [70]. D. P. Valencia, F. J. González, Understanding the linear correlation between diffusion coefficient and molecular weight. A model to estimate diffusion coefficients in acetonitrile solutions. *Electrochem. Commun.* **13**, 129-132 (2011).
- [71]. W. Stummer *et al.*, Fluorescence-guided surgery with 5-aminolevulinic acid for resection of malignant glioma: a randomised controlled multicentre phase III trial. *Lancet Oncol.* **7**, 392-401 (2006).
- [72]. R. Stupp *et al.*, Effects of radiotherapy with concomitant and adjuvant temozolomide versus radiotherapy alone on survival in glioblastoma in a randomised phase III study: 5-year analysis of the EORTC-NCIC trial. *Lancet Oncol.* **10**, 459-466 (2009).
- [73]. A. Claes, A. J. Idema, P. Wesseling, Diffuse glioma growth: a guerilla war. *Acta Neuropathol* **114**, 443-458 (2007).
- [74]. H.-J. Reulen *et al.*, Long-term outcome of patients with WHO Grade III and IV gliomas treated by fractionated intracavitary radioimmunotherapy. *J. Neurosurg.* **123**, 760-770 (2015).
- [75]. M. R. Zalutsky, Targeted radiotherapy of brain tumors. *Br. J. Cancer* **90**, 1469-1473 (2004).
- [76]. C. M. Goetz *et al.*, Distribution of labelled anti-tenascin antibodies and fragments after injection into intact or partly resected C6-gliomas in rats. *Cancer Immunol. Immunother.* **54**, 337-344 (2005).
- [77]. D. A. Reardon *et al.*, A pilot study:  $^{131}\text{I}$ -Antitenascin monoclonal antibody 81c6 to deliver a 44-Gy resection cavity boost. *J. Neuro-Oncol.* **10**, 182-189 (2008).
- [78]. C. Goetz *et al.*, Locoregional radioimmunotherapy in selected patients with malignant glioma: experiences, side effects and survival times. *J. Neuro-Oncol.* **62**, 321-328 (2003).
- [79]. K. Hopkins, Direct Injection of  $^{90}\text{Y}$  Moabs into Glioma Tumor Resection Cavities leads to Limited Diffusion of the Radioimmunoconjugates into Normal Brain Parenchyma: A Model to Estimate Absorbed Radiation Dose. *Int. J. Radiat. Oncol., Biol., Phys.* **40**, 835-844 (1998).
- [80]. in *NIST Database for Physical Reference Data*. vol. 2017.
- [81]. G. W. Severin, J. W. Engle, R. J. Nickles, T. E. Barnhart,  $^{89}\text{Zr}$  Radiochemistry for PET. *J. Med. Chem.* **7**, 389-394 (2011).
- [82]. S. M. Cheal *et al.*, ImmunoPET Imaging of Endogenous and Transfected Prolactin Receptor Tumor Xenografts. *Mol. Pharmaceutics*, Doi: 10.1021/acs.molpharmaceut.1027b01133 (2018).
- [83]. C. Wanke, K. Kossert, O. J. Nähle, O. Ott, Activity standardization and decay data of  $^{64}\text{Cu}$ . *Appl. Radiat. Isot.* **68**, 1297-1302 (2010).
- [84]. G. Wermann *et al.*, Determination of the b- branching ratio of  $^{64}\text{Cu}$  by mass spectrometric investigations of the decay products in neutron transmuted copper. *Appl. Radiat. Isot.* **56**, 145-151 (2001).
- [85]. S. M. Qaim, T. Bisinger, K. Hilgers, D. Nayak, H. H. Coenen, Positron emission intensities in the decay of  $^{64}\text{Cu}$ ,  $^{76}\text{Br}$  and  $^{124}\text{I}$ . *Radiochim. Acta* **95**, 67-73 (2007).

- [86]. A. H. Al Rayyes, Y. Ailouti, Production and Quality Control of  $^{64}\text{Cu}$  from High Current Ni Target. *World J. Nucl. Sci. Technol.* **3**, 72-77 (2013).
- [87]. M. Shokeen, C. J. Anderson, Molecular Imaging of Cancer with Copper-64 Radiopharmaceuticals and Positron Emission Tomography (PET). *Acc. Chem. Res.* **42**, 832-841 (2009).
- [88]. A. N. Asabella *et al.*, The Copper Radioisotopes: A Systematic Review with Special Interest to  $^{64}\text{Cu}$ . *BioMed Res. Int.* **2014**, 1-9 (2014).
- [89]. M. S. Cooper *et al.*, Comparison of  $^{64}\text{Cu}$ -complexing bifunctional chelators for radioimmunoconjugation: labeling efficiency, specific activity and *in vitro/in vivo* stability. *Bioconjugate Chem.* **23(5)**, 1029-1039 (2012).
- [90]. C. J. Anderson, R. Ferdani, Copper-64 Radiopharmaceuticals for PET Imaging of Cancer: Advances in Preclinical and Clinical Research. *Cancer Biother. Radiopharm.* **24**, 379-393 (2009).
- [91]. H. Wang *et al.*, Small-Animal PET Imaging of Pancreatic Cancer Xenografts Using a  $^{64}\text{Cu}$ -Labeled Monoclonal Antibody, MAb159. *J. Nucl. Med.* **56**, 908-913 (2015).
- [92]. Q. Xie *et al.*, Establishing Reliable Cu-64 Production Process: From Target Plating to Molecular Specific Tumor Micro-PET Imaging. *Molecules* **22**, 641-650 (2017).
- [93]. J. E. Mortimer *et al.*, Tumor Uptake of  $^{64}\text{Cu}$ -DOTA-Trastuzumab in Patients with Metastatic Breast Cancer. *J. Nucl. Med.* **59**, 38-43 (2018).
- [94]. K. Lam, C. Chan, R. M. Reilly, Development and preclinical studies of  $^{64}\text{Cu}$ -NOTA-pertuzumab F(ab')<sub>2</sub> for imaging changes in tumor HER2 expression associated with response to trastuzumab by PET/CT. *mAbs* **9**, 154-164 (2017).
- [95]. L. Y. Kwon, D. A. Scollard, R. M. Reilly,  $^{64}\text{Cu}$ -Labeled Trastuzumab Fab-PEG24-EGF Radioimmunoconjugates Bispecific for HER2 and EGFR: Pharmacokinetics, Biodistribution, and Tumor Imaging by PET in Comparison to Monospecific Agents. *Mol. Pharmaceutics* **14**, 492-501 (2017).
- [96]. L. K. van Dijk *et al.*, PET of EGFR with  $^{64}\text{Cu}$ -cetuximab-F(ab')<sub>2</sub> in mice with head and neck squamous cell carcinoma xenografts. *Contrast Media Mol. Imaging* **11**, 65-70 (2016).
- [97]. A. Čepa *et al.*, In vitro evaluation of the monoclonal antibody  $^{64}\text{Cu}$ -IgG M75 against human carbonic anhydrase IX and its in vivo imaging. *Appl. Radiat. Isot.* **133**, 9-13 (2018).
- [98]. S. Sarkar *et al.*, High in Vivo Stability of  $^{64}\text{Cu}$ -Labeled Cross-Bridged Chelators Is a Crucial Factor in Improved Tumor Imaging of RGD Peptide Conjugates. *J. Med. Chem.* **61**, 385-395 (2018).
- [99]. E. Lucente *et al.*, Novel  $^{64}\text{Cu}$  labeled RGD2-BBN heterotrimers for PET imaging of prostate cancer. *Bioconjugate Chem.*, (2018).
- [100]. D. W. McCarthy *et al.*, Efficient production of high specific activity  $^{64}\text{Cu}$  using a biomedical cyclotron. *Nucl. Med. Biol.* **24**, 35-43 (1997).
- [101]. S. Thieme *et al.*, Module-assisted preparation of  $^{64}\text{Cu}$  with high specific activity. *Appl. Radiat. Isot.* **70**, 602-608 (2012).
- [102]. T. Ohya *et al.*, Efficient preparation of high-quality  $^{64}\text{Cu}$  for routine use. *Nucl. Med. Biol.* **43**, 685-691 (2016).
- [103]. A. Obata *et al.*, Production of therapeutic quantities of  $^{64}\text{Cu}$  using a 12 MeV cyclotron. *Nucl. Med. Biol.* **30**, 535-539 (2003).
- [104]. M. Matarrese *et al.*, Automated production of copper radioisotopes and preparation of high specific activity [ $^{64}\text{Cu}$ ]Cu-ATSM for PET studies. *Appl. Radiat. Isot.* **68**, 5-13 (2010).
- [105]. M. A. Avila-Rodriguez, J. A. Nye, R. J. Nickles, Simultaneous production of high specific activity  $^{64}\text{Cu}$  and  $^{61}\text{Co}$  with 11.4 MeV protons on enriched  $^{64}\text{Ni}$  nuclei. *Appl. Radiat. Isot.* **65**, 1115-1120 (2007).

- [106]. C. T. Mendler *et al.*, High contrast tumor imaging with radio-labeled antibody Fab fragments tailored for optimized pharmacokinetics via PASylation. *mAbs - Taylor & Francis* **7**, 96-109 (2015).
- [107]. L. Fiedler *et al.*, Evaluation of  $^{177}\text{Lu}$ -CHX-A''-DTPA-6A10 Fab as a Radioimmunotherapy Agent Targeting Carbonic Anhydrase XII *Nucl. Med. Biol.* **60**, 55-62 (2018).
- [108]. A. Delker *et al.*, Dosimetry for  $^{177}\text{Lu}$ -DKFZ-PSMA-617: a new radiopharmaceutical for the treatment of metastatic prostate cancer. *Eur. J. Nucl. Med. Mol. Imaging* **43**, 42-51 (2016).
- [109]. L. Fiedler *et al.*, Fully automated production and characterization of  $^{64}\text{Cu}$  and proof-of-principle small animal PET imaging using  $^{64}\text{Cu}$ -labelled CA XII targeting 6A10 Fab. *ChemMedChem* **13**, DOI: 10.1002/cmdc.201800130 (2018).
- [110]. T. M. Behr *et al.*, Overcoming the Nephrotoxicity of Radiometal-Labeled Immunoconjugates. *Cancer Supplement* **80**, 2591-2610 (1997).
- [111]. J. R. Duncan, T. M. Behr, S. J. DeNardo, Intracellular Fate of Radiometals [letter to the editor]. *J. Nucl. Med.* **38**, 829-829 (1997).
- [112]. B. E. Rogers *et al.*, Comparison of Four Bifunctional Chelates for Radiolabeling Monoclonal Antibodies with Copper Radioisotopes: Biodistribution and Metabolism. *Bioconjugate Chem.* **7**, 12 (1996).
- [113]. E. W. Price, C. Orvig, Matching chelators to radiometals for radiopharmaceuticals. *Chemical Society Reviews* **43**, 260-290 (2014).
- [114]. L. A. Bass, M. Wang, M. J. Welch, C. J. Anderson, In Vivo Transchelation of Copper-64 from TETA-Octreotide to Superoxide Dismutase in Rat Liver. *Bioconjugate Chem.* **11**, 527-532 (2000).

## 6 Original Publications

---

**L. Fiedler**, M. Kellner, A. Gosewisch, R. Oos, G. Böning, S. Lindner, N. Albert, P. Bartenstein, H.-J. Reulen, R. Zeidler and F. J. Gildehaus. „Evaluation of  $^{177}\text{Lu}$ - CHX-A''-DTPA-6A10 Fab as a Radioimmunotherapy Agent Targeting Carbonic Anhydrase XII". In: Nuclear Medicine and Biology 60, 55-62 (2018)

**L. Fiedler**, M. Kellner, R. Oos, G. Böning, S. Ziegler, P. Bartenstein, R. Zeidler, F. J. Gildehaus and S. Lindner. "Fully automated production and characterization of  $^{64}\text{Cu}$  and proof-of-principle small animal PET imaging using  $^{64}\text{Cu}$ -labelled CA XII targeting 6A10 Fab". In: ChemMedChem 13 (2018) DOI: 10.1002/cmdc.201800130



Contents lists available at ScienceDirect

## Nuclear Medicine and Biology

journal homepage: [www.elsevier.com/locate/nucmedbio](http://www.elsevier.com/locate/nucmedbio)

## Evaluation of $^{177}\text{Lu}$ -CHX-A''-DTPA-6A10 Fab as a radioimmunotherapy agent targeting carbonic anhydrase XII

L. Fiedler <sup>a,\*</sup>, M. Kellner <sup>b</sup>, A. Gosewisch <sup>a</sup>, R. Oos <sup>a</sup>, G. Böning <sup>a</sup>, S. Lindner <sup>a</sup>, N. Albert <sup>a</sup>, P. Bartenstein <sup>a</sup>, H.-J. Reulen <sup>d</sup>, R. Zeidler <sup>b,c</sup>, F.J. Gildehaus <sup>a,\*</sup>

<sup>a</sup> Department of Nuclear Medicine, University Hospital, LMU Munich, Munich, Germany

<sup>b</sup> German Research Center for Environmental Health, Research Group Gene Vectors, Helmholtz-Center Munich, Germany

<sup>c</sup> Department of Otorhinolaryngology, University Hospital, LMU Munich, Munich, Germany

<sup>d</sup> Department for Neurosurgery, University Hospital, LMU Munich, Munich, Germany

## ARTICLE INFO

## Article history:

Received 4 October 2017

Received in revised form 5 February 2018

Accepted 18 February 2018

Available online xxxx

## Keywords:

Glioblastoma

Fab

Carbonic anhydrase XII

Radioimmunotherapy

 $^{177}\text{Lu}$ 

## ABSTRACT

**Introduction:** Due to their infiltrative growth behavior, gliomas have, even after surgical resection, a high recurrence tendency. The approach of intracavitary radioimmunotherapy (RIT) is aimed at inhibiting tumor re-growth by directly administering drugs into the resection cavity (RC). Direct application of the radioconjugate into the RC has the advantage of bypassing the blood-brain barrier, which allows the administration of higher radiation doses than systemic application. Carbonic anhydrase XII (CA XII) is highly expressed on glioma cells while being absent from normal brain and thus an attractive target molecule for RIT. We evaluated a CA XII-specific 6A10 Fab (fragment antigen binding) labelled with  $^{177}\text{Lu}$  as an agent for RIT.

**Methods:** 6A10 Fab fragment was modified and radiolabelled with  $^{177}\text{Lu}$  and characterized by MALDI-TOF, flow cytometry and radio-TLC. *In vitro* stability was determined under physiological conditions. Biodistribution studies, autoradiography tumor examinations and planar scintigraphy imaging were performed on SCID-mice bearing human glioma xenografts.

**Results:** The *in vitro* CA XII binding capacity of the modified Fab was confirmed. Radiochemical purity was determined to be >90% after 72 h of incubation under physiological conditions. Autoradiography experiments proved the specific binding of the Fab to CA XII on tumor cells. Biodistribution studies revealed a tumor uptake of 3.0%ID/g after 6 h and no detectable brain uptake. The tumor-to-contralateral ratio of 10/1 was confirmed by quantitative planar scintigraphy.

**Conclusion:** The radiochemical stability in combination with a successful *in vivo* tumor uptake shows the potential suitability for future RIT applications with the 6A10 Fab.

© 2018 Elsevier Inc. All rights reserved.

### 1. Introduction

WHO grade IV Glioblastoma multiforme (GBM) represent the most aggressive and common subtype of brain tumors [1,2]. Despite improvements in surgery and radio- and chemotherapy approaches, the clinical prognosis for GBM patients is still desperate [3,4]. Due to their invasive growth, GBM cannot be resected completely even by radical surgery. Consequently, almost all GBM patients succumb to local recurrence close to the resection margin within 1–2 years after diagnosis [1,2,5–7]. For improved therapy of these infiltrating cells, intracavitary radioimmunotherapy (RIT) has been suggested as interesting option in the past [2,8,9]. Radioimmunoconjugates were

directly injected into the resection cavity via an implanted Ommaya-reservoir and disseminated tumor cells were targeted through diffusion processes of the compound. Local treatment in the brain also enables the application of higher doses, in comparison to systemic application, because sensitive organs such as kidneys and liver are spared. Among other studies [5,10–12], Reulen et al. [9] recently reported on the long-term results of fractionated RIT with  $^{131}\text{I}$  and  $^{90}\text{Y}$ -labelled monoclonal antibody directed against tenascin C, an extracellular matrix glycoprotein which is ubiquitously expressed by malignant glioma cells, but only minimally expressed in normal brain tissue. They observed an increased median survival time of 25.3 and 77.2 months for GBM patients and patients with anaplastic astrocytoma, respectively, which was significantly longer than that described for historic control patients (15 and 36 months, respectively) [13–16], indicating the high clinical potential of RIT.

Carbonic anhydrase XII (CA XII) is a new, promising target molecule for RIT of gliomas. CA XII is a membrane-tethered enzyme that is

\* Corresponding authors at: Department of Nuclear Medicine, University Hospital LMU Munich, Marchioninistrasse 15, 81377 Munich, Germany.

E-mail addresses: [luisse.fiedler@med.uni-muenchen.de](mailto:luisse.fiedler@med.uni-muenchen.de) (L. Fiedler), [franz.gildehaus@med.uni-muenchen.de](mailto:franz.gildehaus@med.uni-muenchen.de) (F.J. Gildehaus).

overexpressed by glioma cells while being absent from healthy brain tissue [17]. To cover their energy demand, aggressively proliferating tumor cells are characterized by extensive anaerobic glycolysis, which causes intracellular acidification. Due to its catalytic properties during the conversion of CO<sub>2</sub> and H<sub>2</sub>O to HCO<sub>3</sub><sup>-</sup> and H<sup>+</sup>, CA XII is essential for the pH stabilization and is overexpressed on the glioma cells [17,18], which makes it a suitable target for glioma therapy. The 6A10 antibody binds very specifically to CA XII [17,18], and is therefore considered as a possible tracer for the intracavitary RIT after tumor resection. Better diffusion properties are expected from the smaller Fab fragment, so the aim of this study was to evaluate the radiolabelled 6A10 Fab fragment with regard to a possible future clinical application. The Fab was therefore modified with *p*-SCN-CHX-A''-DTPA (in the following abbreviated as DTPA), radiolabelled with <sup>177</sup>Lu and extensively characterized *in vitro* and *in vivo*.

## 2. Materials and methods

Unless otherwise stated, all analytic grade chemicals and expendable items were purchased from Sigma Aldrich (Taufkirchen, Germany), Merck (Darmstadt, Germany), Carl Roth (Karlsruhe, Germany) or Eppendorf (Hamburg, Germany).

### 2.1. Conjugation of DTPA with 6A10 Fab

The 6A10 Fab was produced in CHO cells, purified on a CaptureSelect column (Thermo Fisher, Munich, Germany) and delivered in concentrations of up to 5 mg/ml in phosphate buffered saline (PBS). Using Amicon Ultra 2 ml ultracentrifugal (10 kDa cutoff) devices, the buffer was exchanged to 0.1 M phosphate buffer pH 8.5 (Braun, Melsungen, Germany) with concomitant volume reduction to a concentration up to 7.2 mg/ml [19]. As alternative procedure, buffer exchange was also achieved using size exclusion chromatography. Therefore, nap-5 columns (GE-Healthcare, Munich, Germany) were pretreated with 10 ml of the phosphate buffer, a sample volume < 0.5 ml was applied to the resin and eluted with 1 ml buffer. The re-buffered product was collected in fractions. The concentration of the processed Fab was determined by measurement of the photometric absorption at 280 nm (Ultrospec 1100 photometer by Amersham Biosciences now GE Healthcare, Munich, Germany), Quartz UPRASIL® precision cell by Hellma Analytics (Mühlheim, Germany), using an unprocessed Fab calibration standard. A 10-fold molar excess of *p*-SCN-CHX-A''-DTPA (Macrocylics, Dallas, Texas) was added to the Fab and incubated in an Eppendorf Thermomixer at 37 °C for 1 h. Buffer exchange to 0.01 M sodium acetate pH 5.3 and removal of unbound DTPA was achieved by ultracentrifugation or size exclusion chromatography, as previously explained. Absorption measurement was again used for concentration calculation. Final product volumes ranged between 500 and 1000 µl. The number of bound chelator molecules per Fab was analyzed by the Protein Analysis Unit (Ludwig-Maximilians-University Munich) using MALDI-TOF analysis.

### 2.2. <sup>177</sup>Lu-labelling with DTPA-6A10 Fab-conjugate

The required amount of Fab-DTPA conjugate (0.1–1 mg) was diluted with 50–100 µl 0.1 M sodium acetate pH 5.3. 150–1500 MBq of [<sup>177</sup>Lu]LuCl<sub>3</sub> in 0.04 M hydrochloric solution (EndolucinBeta® from ITG, Garching, Germany) was added to the reaction vessel and incubated at 37 °C for 1 h. Radio thin layer chromatography (radio-TLC) on iTLC-SA (Agilent, Waldbronn, Germany) strips with 0.5 M citrate buffer pH 4–5 was performed for quality control purpose. For DC analysis, a miniGITA (Raytest, Straubenhardt, Germany) and the GINA Star TLC software was used.

### 2.3. Flow cytometry

Flow cytometry analysis was performed with a FACSCanto™ Flow Cytometer (BD Biosciences, Heidelberg, Germany) to determine the specific binding ability of the conjugated and labelled Fab in comparison to the unmodified variant on CA XII positive A549 cell line. The cells were incubated with 6A10 Fab, followed by incubation with a fluorochrome-coupled secondary antibody. Incubation of the secondary antibody only, without 6A10, served as control. Furthermore, the CA XII expression of the cell line used in this study was characterized with native 6A10 antibody.

### 2.4. Radiochemical stability

To determine the radiochemical stability of the labelled conjugate, it was incubated in labelling buffer at room temperature and in a 10-fold volume excess of human cerebrospinal fluid (CSF) and human plasma at 37 °C. CSF and plasma was extracted from healthy volunteers. At different time points (2 h; 4 h; 8 h; 16 h; 24 h; 48 h; 72 h; 96 h) an aliquot of the conjugate was analyzed with radio-TLC as previously described.

### 2.5. Cell line

Human glioblastoma cell line U87MG was received by the American Type Culture Collection and cultivated in Gibco MEM medium (Thermo Fischer Scientific, Munich, Germany), supplemented with 10% Fetal Bovine Serum and L-Glutamine (both from Biochrom, Berlin, Germany), and kept under constant conditions of 5% CO<sub>2</sub> and 37 °C in a CB150 incubator (Binder, Tuttlingen, Germany). Cell passages at the time of tumor inoculation ranged from 12 to 16. As a part of our cell culture handling routine, all cell lines are regularly checked for mycoplasma.

### 2.6. Biodistribution

Female SCID-mice (6–8 weeks, 20–25 g, from Charles River, Sulzbad, Germany) were subcutaneously injected with  $5 \times 10^6$  U87MG cells into the right flank. Tumor sizes of approx. 0.5 cm<sup>3</sup> within 2–3 weeks of tumor growth were aspired. <sup>177</sup>Lu-labelled 6A10 Fab was synthesized as described above and  $4.3 \pm 0.4$  MBq ( $2.9 \pm 0.3$  µg Fab) were injected intravenously into the tail vein. At each time point (1 h; 3 h; 6 h; 24 h; 48 h) 4 mice were sacrificed for biodistribution studies. Blood and relevant tissue was harvested, collected in tubes, and weighed. The retained tissue radioactivity was measured by gamma counter (Cobra Quantum 5003 by Canberra Packard, Schwadorf, Austria), decay corrected to the time of biodistribution and expressed as percentage injected dose per gram of tissue (%ID/g).

### 2.7. Autoradiography and HE-staining

U87MG-xenotransplanted female SCID-mice (n = 6) were injected with  $20.7 \pm 1.3$  MBq of the labelled conjugate. After 3–50 h tumors were extracted post mortem, immediately embedded in Tissue-Tek O.C.T. (Sakura Finetek, Staufen, Germany) and stored at –80 °C. Tumors were cut into 20 µm slices with a Leica CM1510 S cryostat (Leica Biosystems, Nussloch, Germany), transferred to microscope slides and dried. A phosphoric photo screen was exposed overnight to the radiating tumor slices, and scanned with a Cr 35 Bio scanner (Dürr Medical, Bietigheim-Bissingen, Germany). Image analysis was performed with an Aida Image Analyzer v.450. Different intensity areas were compared.

Furthermore, *in vitro* blocking experiments on tumor slices, harvested from mice which were not injected with the conjugate, were carried out. The slices were incubated for 1 h with a 100-fold molar excess of native 6A10 to block CA XII, and afterwards rinsed with TRIS-HCl. The dried slices were incubated for 1 h with <sup>177</sup>Lu-labelled 6A10 Fab. Analysis and interpretation of autoradiographs was done as described above.

Additionally, staining with hematoxylin and eosin (HE-staining) was performed. The dry slices were rinsed with distilled water, dried, dyed with hematoxylin and again rinsed with water and a series of hydrochloric-alcoholic solutions. Subsequent staining with eosin was followed by rinsing with water, 70%, 96%, 96%, 100%, 100% ethanol and xylene. The dried slices were covered and microscopically examined at the Pathology Department of the Ludwig-Maximilians-University Munich.

### 2.8. Planar scintigraphy

Mice ( $n = 5$ ; 6–8 weeks; 20–25 g) were subcutaneously injected with U87MG cells into the right shoulder to avoid disturbance from kidney and bladder activity in the final image. An average tumor size of  $0.5 \text{ cm}^3$  was reached after 1.5 weeks of growth time.  $16.6 \pm 2.1 \text{ MBq}$  radioconjugate was injected via a tail vein catheter. A 60-minute planar scintigraphy on the isoflurane anesthetized animals was performed on a T2 Siemens Symbia for all animals 4 h p.i. using a 20% energy window around the  $^{177}\text{Lu}$  photopeak of 208 keV in combination with a medium-energy-low-penetration collimator. A  $1024 \times 1024$  imaging matrix with zoom 2 was chosen. The planar images (pixel size:  $0.2997 \times 0.2997 \text{ mm}^2$ ) were post-processed via a Gaussian filter with a FWHM of 3 mm for noise suppression. Afterwards tumor-to-muscle ratios were evaluated via PMOD (Version 3.609) by drawing circular ROIs of 2 mm radius at the tumor and at the contralateral thigh muscle.

## 3. Results

### 3.1. Conjugation of DTPA with 6A10 Fab

Depending on the chelator quantity, up to 8 centrifugal runs were necessary to successfully remove unbound DTPA. Unbound DTPA could also be removed using nap-5 columns. The resulting conjugate concentration was up to 6 mg/ml in 0.01 M sodium acetate.

MALDI-TOF analysis revealed a molar ratio of chelator to protein of 1:0.96, with a mass shift from 48,329 kDa to 48,904 kDa, native 6A10 Fab to conjugated Fab respectively.

### 3.2. $^{177}\text{Lu}$ -labelling of DTPA-6A10 Fab-conjugate

Specific activities of 1.5 GBq/mg Fab, with radiochemical purities >96% without further purification were achieved. Radio-TLC analysis of the product revealed the sufficient separation of the radiolabelled Fab from radiolabelled DTPA and free  $^{177}\text{Lu}$ . A representative chromatogram is plotted in Fig. 1. Free [ $^{177}\text{Lu}$ ]Lu-DTPA or  $^{177}\text{Lu}$  was detectable at  $R_f$ -values of  $0.2 \pm 0.05$  and  $1.0 \pm 0.1$ , respectively, while the Fab remains at the origin.

### 3.3. Flow cytometry

Flow cytometry confirmed that modification and labelling with  $^{177}\text{Lu}$  does not inhibit the characteristic CA XII binding ability of the 6A10 Fab in comparison to its native form. This is shown in part a of Fig. 2, where conjugated and native Fab-samples are compared using equivalent serial dilution steps on a CA XII expressing cell line. For both, similar fluorescent signals were detectable. Part b of Fig. 2 shows the binding capability of the radiolabelled Fab sample. Using a native 6A10 antibody, the positive CA XII expression of the U87 cells used for this study was confirmed.

### 3.4. Radiochemical stability

Data obtained from different production charges were compared after normalization to 100% radiochemical purity at 0 h and plotted in Fig. 3. Over a period of 72 h the radiochemical stability of the labelled conjugate was determined to be >90% in all the tested media. After 96 h, the conjugate maintained a radiochemical purity of 86% in cerebrospinal fluid and 90% in labelling buffer and plasma.

### 3.5. Biodistribution

In Table 1 and Fig. 4 the results of the biodistribution study on U87MG xenotransplanted SCID-mice are summarized. The tumor showed a quick activity uptake up to  $3.1 \pm 0.9\% \text{ID/g}$ , decreasing to  $1.8 \pm 0.5\% \text{ID/g}$  at 48 h. Blood activity was  $6.4 \pm 2.2\% \text{ID/g}$  after 1 h, followed by a clearance within the next 24 h. The muscle was characterized by

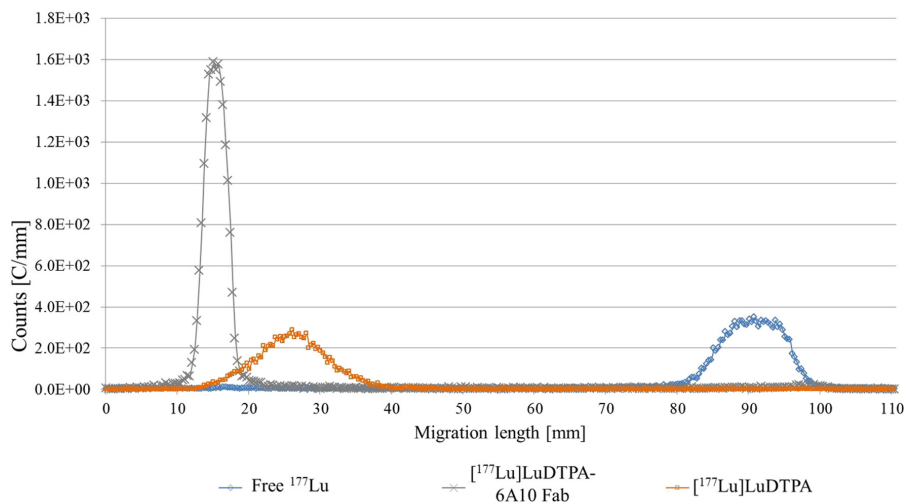
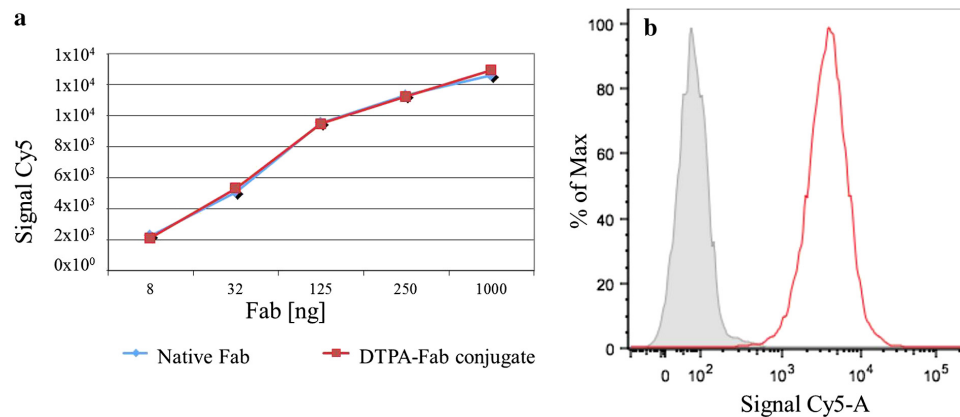


Fig. 1. Comparison of radio-TLC chromatograms of free  $^{177}\text{Lu}$ ,  $^{177}\text{Lu}$ -labelled DTPA and the final  $^{177}\text{Lu}$ -labelled DTPA-6A10 Fab.



**Fig. 2.** Graphic summary of flow cytometry results: a: Evaluation of flow cytometry analysis comparing uncoupled and DTPA-coupled Fab. No significant differences in binding behavior were observed after conjugating the Fab with DTPA. b: Result of flow cytometry analysis of  $^{177}\text{Lu}$  labelled 6A10 Fab (red) in comparison to an isotype control antibody (grey). Successful binding is indicated by shifts on the x-axis. (For interpretation of the references to color in this figure legend, the reader is referred to the web version of this article.)

very small uptake, which never exceeded 1%ID/g. High amounts of activity were detected in the liver and especially in the kidney. Even after 48 h 3%ID/g retained in the liver. Most activity over all time points was found in the kidney, which still held an amount of  $55.6 \pm 13.0\%$ ID/g after 48 h. The other organs, such as lung, spleen, intestines and stomach are characterized by steady decrease of activity over time. The brain showed low values below 0.2%ID/g over all time points.

### 3.6. Autoradiography and HE-staining

Autoradiographic analysis of the tumor slices revealed an inhomogeneous activity distribution. Microscopic analysis of HE-stained slices confirmed furthermore a correlation between cell density and activity accumulation. Examinations of  $n = 6$  tumors, harvested at different time points (1 h, 3 h, 5 h, 30 h and 50 h p.i.) confirmed, that areas of high cell density retain higher activity, and vice versa. A representative example is given in Fig. 5 on a tumor slice, which is harvested 5 h p.i. Blocking experiments on tumor slices with 100-fold molar excess of 6A10 antibody (Fig. 6) revealed a 49% decreased uptake of  $^{177}\text{Lu}$ -labelled Fab ( $n = 8$ ) in comparison to un-blocked slices.

### 3.7. Planar scintigraphy

Tumors were successfully visualized in the planar scintigraphies at 4 h p.i. (Fig. 7). Besides the tumor on the right shoulder (as indicated

with white arrows), kidneys and bladder were strongly visible. Based on this preliminary image data, the mean tumor-to-contralateral ratio ( $n = 5$  mice) was calculated to be  $3.3 \pm 0.3$ .

## 4. Discussion

Improving the overall survival and quality-of-life of glioma patients by inhibiting tumor recurrence is the aim of intracavitary radioimmunotherapy. Studies using anti-tenascin C antibody-conjugates [5,9–12,20] have already indicated the high clinical potential of RIT in this context. Carbonic anhydrase XII is another attractive target molecule, because it is not present on healthy brain while being overexpressed by glioma cells. In order to target CA XII, a specific binding radioimmunoconjugate is required, which has sufficiently high radiochemical stability. When used for local intracavitary application, the conjugate should not cross the blood-brain-barrier and is intended to distribute through diffusion processes into the tissue.

Because the therapeutic effect of intracavitary RIT is based on diffusion out of the cavity into the adjacent brain, Goetz et al. [21] compared the diffusion properties of full-length anti-tenascin antibodies with those of their Fab fragments in rat brains. Their study revealed that both, migration velocity and distance were higher for Fabs as compared to whole antibodies.

As the diffusion velocity depends on the molecular size, a variety of small molecules has been in consideration for RIT, for instance

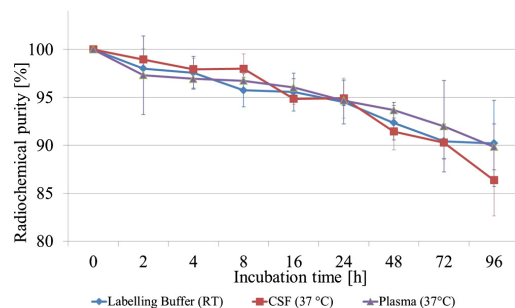


**Fig. 3.** Plots of the radiochemical purities [%] vs incubation time [h] of  $^{177}\text{Lu}$ -Fab samples in labelling buffer, cerebrospinal fluid and plasma ( $n = 6$ ).

**Table 1**

Measured biodistribution values in %ID/g in glioma tumor (U87MG) bearing SCID-mice at 1 h, 3 h, 6 h, 24 h and 48 h after the intravenous application of  $4.3 \pm 0.4$  MBq radioconjugate.

	%ID/g				
	1 h	3 h	6 h	24 h	48 h
Blood	$6.4 \pm 2.2$	$2.7 \pm 0.3$	$1.2 \pm 0.3$	$0.2 \pm 0.1$	$0.1 \pm 0.01$
Heart	$1.8 \pm 1.1$	$1.2 \pm 0.6$	$0.9 \pm 0.2$	$0.6 \pm 0.2$	$0.8 \pm 0.4$
Lung	$1.9 \pm 1.1$	$1.7 \pm 0.3$	$1.5 \pm 0.7$	$0.5 \pm 0.3$	$0.3 \pm 0.1$
Liver	$3.5 \pm 2.4$	$5.0 \pm 2.9$	$5.4 \pm 0.7$	$2.6 \pm 1.0$	$3.1 \pm 1.1$
Spleen	$1.7 \pm 1.3$	$2.5 \pm 1.2$	$1.8 \pm 0.7$	$2.1 \pm 1.1$	$1.6 \pm 0.7$
Stomach	$0.9 \pm 0.8$	$0.8 \pm 0.3$	$0.6 \pm 0.1$	$0.5 \pm 0.1$	$0.2 \pm 0.1$
Small int.	$2.6 \pm 0.6$	$1.0 \pm 0.2$	$0.6 \pm 0.1$	$0.4 \pm 0.1$	$0.3 \pm 0.1$
Large int.	$1.7 \pm 1.0$	$2.2 \pm 0.6$	$1.5 \pm 0.4$	$0.7 \pm 0.2$	$0.4 \pm 0.1$
Kidney	$42.9 \pm 22.6$	$84.3 \pm 28.1$	$83.5 \pm 18.7$	$93.1 \pm 14.1$	$55.6 \pm 13.0$
Brain	$0.2 \pm 0.1$	$0.1 \pm 0.02$	$0.1 \pm 0.01$	$0.04 \pm 0.01$	$0.03 \pm 0.01$
Muscle	$0.4 \pm 0.1$	$0.9 \pm 1.0$	$0.3 \pm 0.1$	$0.3 \pm 0.1$	$0.1 \pm 0.02$
Tumor	$2.4 \pm 1.0$	$3.1 \pm 0.9$	$3.0 \pm 0.8$	$2.5 \pm 0.6$	$1.8 \pm 0.5$
Thyroid	$0.6 \pm 0.2$	$0.3 \pm 0.5$	$0.4 \pm 0.1$	$0.4 \pm 0.3$	$0.4 \pm 0.3$

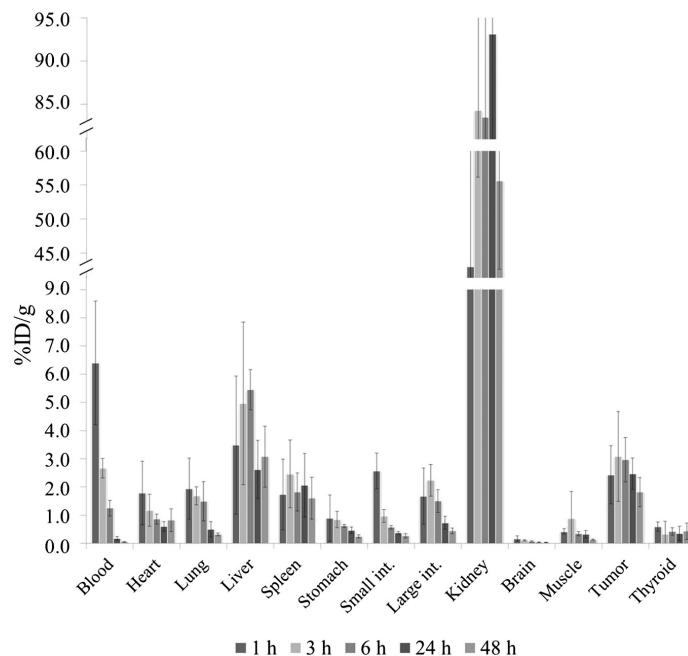


Fig. 4. Biodistribution profile in %ID/g at 1 h, 3 h, 6 h, 24 h and 48 h after the intravenous application of  $4.3 \pm 0.4$  MBq radioconjugate.

pre-targeted  $^{90}\text{Y}$ -biotin [22], Peptidic Vector 1,4,7,10-tetraazacyclododecane-1-glutaric acid-4,7,10-triacetic acid-substance P [23],  $^{131}\text{I}$ -TM-601 [24],  $^{213}\text{Bi}$ -DOTA-[Thi8, Met(02)11]-substance P [25] etc. Migration of the antibody or other molecules into the surrounding parenchyma occurs predominantly by diffusion and depends on the diffusion gradient, the diffusion coefficient and the width and tortuosity of the extracellular space [21,26,27].

The distance, the molecule travels in the tissue, may be extended by increasing the diffusion gradient (activity concentration in the resection cavity), for example by decreasing the molecular size [28,29]. Smaller molecules, with better diffusion properties and higher diffusion velocities may spread too far, which results in unintentional high doses on

healthy brain tissue. Very large molecules on the other hand, such as antibodies (MW approx. 150 kDa) show slower diffusion properties. In this study, a fab fragment (MW approx. 55 kDa) with a moderate diffusion and transit time is used, to treat the tumor cells, which have migrated into the brain tissue adjacent to the resection cavity. Therefore, the radioactive labelled Fab fragment of the 6A10 antibody which binds highly specific to human CA XII [17,18] was further investigated.

Several radionuclides have been considered for radiolabelling the 6A10 Fab. Isotopes such as  $^{131}\text{I}$  and  $^{90}\text{Y}$  were already used for RIT studies [5,9,30]. The 6A10 Fab is intended to bind at the tumor cells infiltrating the healthy brain tissue, which represent a very small target in comparison to a solid tumor. To spare surrounding tissue, a short range  $\beta$ -emitting nuclide is favorable. According to the data provided by NIST (National Institute of Standards and Technology [31]),  $^{90}\text{Y}$  and  $^{131}\text{I}$  have soft tissue ranges of about 11 mm and 2.2 mm, respectively, which excludes  $^{90}\text{Y}$  for our purpose.  $^{131}\text{I}$  and  $^{177}\text{Lu}$  have comparable beta-characteristics, half-lives and soft tissue ranges, but  $^{177}\text{Lu}$  offers with its 208 keV gamma energy a better image quality. Imaging characteristics of the used radionuclide are mandatory for dose calculations based on SPECT/CT data, which will be necessary to calculate the optimal dose for effective tumor treatment. A better image quality results in more precise dose estimations out of the imaging data, which is why  $^{177}\text{Lu}$  is favorable over  $^{131}\text{I}$  in this study. Furthermore,  $^{177}\text{Lu}$  for labelling purposes is easily available in GMP-quality and offers convenient radiolabelling strategies [19,32–35].

Previous studies with  $^{177}\text{Lu}$ -labelled proteins, such as cetuximab [34,36–39] have already investigated the suitability of *p*-SCN-CHX-A'-DTPA for this purpose. It was also reported, that DTPA offers the ability of high labelling yields at ambient temperature in combination with suitable *in vivo* stability.

Modifying the protein with this DTPA derivate and further radiolabelling with  $^{177}\text{Lu}$  was done based on methods reported previously [19,39]. High radiochemical purities of up to 99% were

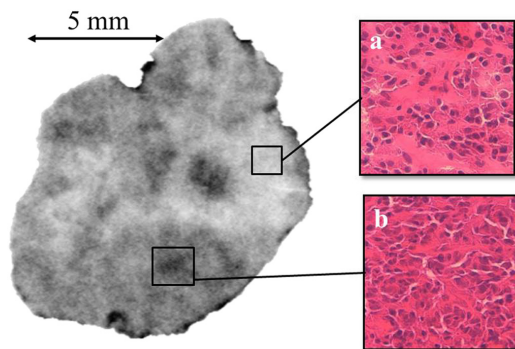


Fig. 5. Autoradiography image of a U87MG tumor slice, harvested from a tumor bearing SCID-mouse 5 h p.i. The typical inhomogeneous activity distribution is analyzed by microscopic examinations after HE-staining. One low (a) and one high (b) activity region correspond to high and low cell densities in a 40-fold magnification.

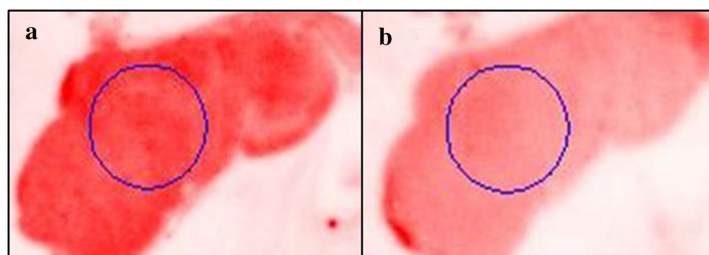


Fig. 6. Autoradiographs of unblocked (a) and blocked (b) tumor slices. CA XII blockade revealed an uptake reduction of 49% in comparison to the unblocked tumor slice.

gained. In addition, flow cytometry confirmed that the radioimmunoconjugate retained the Fab's biological properties.

The radiochemical purity of [ $^{177}\text{Lu}$ ]Lu-DTPA conjugated 6A10 Fab in human plasma was >90% after 72 h. Working with similar antibodies or Fabs, chelated with DTPA or DOTA, and radiolabeled with  $^{177}\text{Lu}$ , different groups reported comparable results to ours [32,33,39,40]. Therefore, the stability of our tested [ $^{177}\text{Lu}$ ]Lu-DTPA-6A10 Fab was found to be sufficient.

Autoradiography and HE-staining experiments on glioma xenograft slices presented a correlation between uptake and cell density. Areas with a high cell density showed a higher uptake while low cell density resulted in lower uptake. This appears reasonable, since a higher number of cells correlates with more CA XII to bind the radiolabelled Fab.

Systemic distribution and uptake tendency of the radiolabelled Fab was investigated by biodistribution studies. The verified activity accumulation in the tumor is comparable to the results other groups presented in previous studies, for example with HER2 and CD20 Fabs [41,42]. In contrast to a whole antibody, the systemic tumor uptake of a Fab fragment is known to be lower and not as long-lasting [43], mainly because of its monovalent binding site and faster digestion [44–47]. Comparing the uptake in tumor, blood and muscle at 48 h ( $1.8 \pm 0.5\%$  ID/g,  $0.1 \pm 0.01\%$  ID/g and  $0.1 \pm 0.02\%$  ID/g respectively), the tumor showed a significant activity level in comparison to the blood. Simultaneously, no retention in muscle tissue occurred. These results, in combination with the reduced uptake detected in first autoradiographic blockage experiments on tumor slices, indicates the specific binding ability of the conjugate on the tumor. The rapid clearance in blood and muscle together with the tumor uptake value implies a good tumor to background ratio, which is favorable for tumor imaging [42]. Furthermore, the significant low brain uptake indicates, that the conjugate does not cross the blood brain barrier. Similar to the blood, organs such as heart, lung, stomach and intestines showed rapid activity reduction. As expected, liver and kidney show high accumulation values around  $3.1 \pm 1.1\%$  ID/g and  $55.6 \pm 13.0\%$  ID/g, respectively.

Renal biomolecule metabolism is highly dependent on molecular size and properties [45,48]. Large proteins, such as antibodies, do not enter the glomerulus ultrafiltration system, which results in longer blood retention times [45,46]. Molecules below ~65 kDa are cleared through the kidney, and undergo ultrafiltration, lysosome metabolism and tubulus reabsorption processes [45,46,48]. According to Duncan et al. and Behr et al. [49,50], lysosomes catabolize the protein-chelate-conjugates into metal chelate fragments. Those fragments can hardly cross the lysosome membrane and remain in the lysosomes for a long time. Those findings are confirmed by the results Mendler et al. [41] reported, as they found a correlation between the radiolabeling chemistry and the kidney uptake. Their comparison of  $^{124}\text{I}$ -iodinated Fab-PAS and  $^{89}\text{Zr}$ -labelled Fab-PAS via chelator conjugation revealed a significant high kidney accumulation up to  $88\%$  ID/g (24 h) of the metal chelate, whereas the iodinated protein only reached a value of  $0.4\%$  ID/g.

To summarize these facts, the long kidney retention time of Fabs labelled with radiometals can be attributed to their specific renal metabolism, consisting of glomerulus ultrafiltration, tubular absorption, degradation and retention through lysosomes and further reabsorption processes. However, the future therapy aim is the local application of the radioconjugate into the brain. In order to protect sensitive organs, such as the kidney, leakage of the conjugate into the blood system should be avoided. To test the leak-tightness of the resection cavity and the Ommaya reservoir system, a small amount of the radioconjugate can be injected prior to the therapy and a whole body scintigram can confirm that the activity remains in the brain [9]. Additionally, the apparent inability of the conjugate to cross the BBB can be regarded as beneficial, since this may avoid systemic distribution of the drug resulting in minimization of radioactive exposure to non-target organs. Further reduction of organ exposure during patient treatment can be achieved by fractionated RIT, where the activity is applied in several fractions to maximise the exposure time on the glioma cells [9,51]. Furthermore, in case of conjugate leakage into the

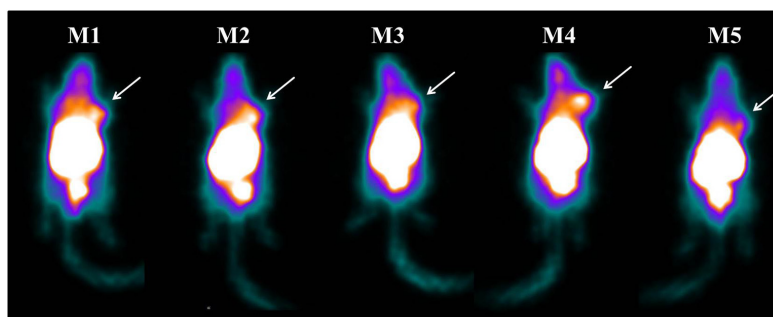


Fig. 7. Planar scintigraphy of 5 mice (M1–M5) 4 h p.i. Tumor localizations at the right shoulders are illustrated by the white arrows.

blood system, several techniques to reduce tubular reabsorption, for example inhibiting the tubular reabsorption by injecting a lysine solution, have been reported [45,48]. The kidneys are reported to express CA XII as well [52]. An intrinsic effect of the biomolecule can be neglected, as the amount of Fab entering the blood system is considered to be rather small, even in case of 10% leakage. Nevertheless, performing a leakage test is even more important.

Biodistribution results were confirmed by preliminary planar scintigraphy images. As discussed, kidneys showed a strong activity accumulation in the planar images. The evaluation of the tumor-to-contralateral ratios based on this images 4 h p.i. revealed a mean ratio of  $3.3 \pm 0.3$ . Biodistribution data, on the other hand, revealed an average tumor-to-contralateral ratio of 3.4 and 10 at 3 h p.i. and 6 h p.i., respectively. The ratios evaluated with biodistribution and planar images are comparable, especially in consideration of the decreasing muscle-blood-activity over time and the limited spatial resolution, as we used a human, which is not optimized for small animal imaging. Further discrepancy between the calculations may be caused because different mice were used for biodistribution and imaging experiments, respectively.

In this study, tumor xenografts on mice were used as a first proof for binding of the radiolabelled 6A10 Fab to the glioma cells *in vivo*. A more accurate and application-oriented research method would be provided by examinations on an orthotopic animal model, since the planned application will be local into the resection cavity in the brain. Nevertheless, realization of such a model is difficult, since this would include tumor inoculation, tumor resection and radiochemotherapy prior to the local application of the Fab. A corresponding suitable and preclinical model does not yet exist for technical and regulatory reasons.

Further investigations in this topic will be focused on establishing a GMP compliant production routine as the next step towards future clinical applications.

## 5. Conclusions

The 6A10 Fab can be successfully conjugated with p-SCN-Bn-CHX-A''-DTPA and radiolabelled with  $^{177}\text{Lu}$ . This conjugate is sufficiently stable under physiological conditions, binds successfully to CA XII, shows significant tumor accumulation in a xenografted model after systemic application and does not cross the blood-brain barrier. As a next step, the establishment of an orthotopic glioma model is planned, to corroborate our first results with special emphasis on tumor accumulation and biodistribution.

## Competing interests

The authors declare that they have no competing interests.

## Compliance with ethical standards

The authors declare that they have no conflict of interest.

All animal experiments were performed according to the current German animal protection laws and protocols of the local authorities. This article does not contain any studies with human participants performed by any of the authors, so no informed consent was required.

## Acknowledgement

This work was supported by grants from the Bundesministerium für Bildung und Forschung: VIP+00560; (BMBF) and the Helmholtz-Validierungsfonds: HVF-046 (HVF) and intramural grants of the Helmholtz-Center Munich to RZ.

## References

- [1] Herold-Mende C, Mueller MM, Bonsanto MM, Schmitt HP, Kunze S, Steiner H-H. Clinical impact and functional aspects of tenascin-C expression during glioma progression. *Int J Cancer* 2002;98:362–9.
- [2] De Bonis P, Lofrese G, Anile C, Pompucci A, Vigo V, Mangiola A. Radioimmunotherapy for high-grade glioma. *Immunotherapy* 2013;5(6):647–59.
- [3] Stummer W, Pichlmeier U, Meinel T, Wiestler OD, Zanella F, Reulen H-J. Fluorescence-guided surgery with 5-aminolevulinic acid for resection of malignant glioma: a randomised controlled multicentre phase III trial. *Lancet Oncol* 2006;7:392–401.
- [4] Stupp R, Hegi ME, Mason WP, van den Bent MJ, Taphoorn MJB, Janzer RC, et al. Effects of radiotherapy with concomitant and adjuvant temozolomide versus radiotherapy alone on survival in glioblastoma in a randomised phase III study: 5-year analysis of the EORTC-NCIC trial. *Lancet Oncol* 2009;10:459–66.
- [5] Goetz C, Riva R, Poepperl G, Gildehaus FJ, Hischa A, Tatsch K, et al. Locoregional radioimmunotherapy in selected patients with malignant glioma: experiences, side effects and survival times. *J Neurooncol* 2003;62:321–8.
- [6] Nestler U, Lutz K, Pichlmeier U, Stummer W, Franz K, Reulen H-J, et al. Anatomic features of glioblastoma and their potential impact on survival. *Acta Neurochir* 2015;157:179–86.
- [7] Claes A, Idema AJ, Wesseling P. Diffuse glioma growth: a guerilla war. *Acta Neuropathol* 2007;114:443–58.
- [8] Zalutsky MR. Targeted radiotherapy of brain tumors. *Br J Cancer* 2004;90(8):1469–73.
- [9] Reulen H-J, Poepperl G, Goetz C, Gildehaus FJ, Schmidt M, Tatsch K, et al. Long-term outcome of patients with WHO Grade III and IV gliomas treated by fractionated intracavitary radioimmunotherapy. *J Neurosurg* 2015;123:760–70.
- [10] Reardon DA, Zalutsky MR, Akabani G, Coleman RE, Friedman AH, Herndon II JE, et al. A pilot study:  $^{131}\text{I}$ -antitenascin monoclonal antibody 81c6 to deliver a 44-Gy resection cavity boost. *J Neurooncol* 2008;10:182–9.
- [11] Reardon DA, Akabani G, Coleman RE, Friedman AH, Friedman HS, Herndon II JE, et al. Salvage radioimmunotherapy with murine iodine-131-labeled antitenascin monoclonal antibody 81C6 for patients with recurrent primary and metastatic malignant brain tumors: phase II study results. *J Clin Oncol* 2006;24(1):115–22.
- [12] Bigner DD, Brown MT, Friedman AH, Coleman RE, Akabani G, Friedman HS, et al. Iodine-131-labeled antitenascin monoclonal antibody 81C6 treatment of patients with recurrent malignant gliomas: phase I trial results. *J Clin Oncol* 1998;16(6):2202–12.
- [13] Chang EL, Loeffler JS, Riese NE, Wen PY, Alexander III E, Black PM, et al. Survival results from a phase I study of etanidazole (SR2508) and radiotherapy in patients with malignant glioma. *Int J Radiat Oncol Biol Phys* 1998;40(1):65–70.
- [14] Madajewicz S, Chowhan N, Tlayil A, Roque C, Meek A, Davis R, et al. Therapy for patients with high grade astrocytoma using intraarterial chemotherapy and radiation therapy. *Cancer* 2000;88(10):2350–6.
- [15] Davis FG, Freels S, Grutsch J, Barlas S, Brem S. Survival rates in patients with primary malignant brain tumors stratified by patient age and tumor histological type: an analysis based on Surveillance, Epidemiology, and End Results (SEER) data, 1973–1991. *J Neurosurg* 1998;88.
- [16] Stupp R, Mason WP, van den Bent M, Weller M, Fisher B, Taphoorn MJB, et al. Radiotherapy plus concomitant and adjuvant temozolomide for glioblastoma. *N Engl J Med* 2005;352:987–96.
- [17] Gondi G, Mysliwicz J, Hulikova A, Jen JP, Swietach P, Kremmer E, et al. Antitumor efficacy of a monoclonal antibody that inhibits the activity of cancer-associated carbonic anhydrase XII. *American Association for Cancer Research*. 2013;73(21):6494–503.
- [18] Battke C, Kremmer E, Mysliwicz J, Gondi G, Dumitru C, Brandau S, et al. Generation and characterization of the first inhibitory antibody targeting tumour-associated carbonic anhydrase XII. *Cancer Immunol Immunother* 2011;60:649–58.
- [19] Kameswaran M, Pandey U, Gamre N, Vimalnath KV, Sarma HD, Dash A. Evaluation of  $^{177}\text{Lu}$ -CHX-A''-DTPA-bevacizumab as a radioimmunotherapy agent targeting VEGF expressing cancers. *Appl Radiat Isot* 2016;114:196–201.
- [20] Akabani G, Reardon DA, Coleman ER, Wong TZ, Metzler SD, Bowsher JE, et al. Dosimetry and radiographic analysis of  $^{131}\text{I}$ -labeled antiTenascin 81C6 murine monoclonal antibody in newly diagnosed patients with malignant gliomas: a phase II study. *J Nucl Med* 2005;46(6):1042–51.
- [21] Goetz CM, Rachinger W, Decker M, Gildehaus FJ, Stocker S, Jung G, et al. Distribution of labelled anti-tenascin antibodies and fragments after injection into intact or partly resected C6-gliomas in rats. *Cancer Immunol Immunother* 2005;54:337–44.
- [22] Paganelli G, Bartolomei M, Ferrari M, Cremonesi M, Broggi G, Maira G, et al. Pre-targeted locoregional radioimmunotherapy with  $^{90}\text{Y}$ -biotin in glioma patients: phase I study and preliminary therapeutic results. *Cancer Biother Radiopharm* 2001;16(3):227–35.
- [23] Kneifel S, Cordier D, Good S, MCS Ionescu, Ghaffari A, Hofer S, et al. Local targeting of malignant gliomas by the diffusible peptidic vector 1,4,7,10-tetraazacyclododecane-1-glutaric acid-4,7,10-triacetic acid-substance P. *Clin Cancer Res* 2006;12(12):3843–50.
- [24] Hockaday DC, Shen S, Fiveash J, Raubitschek A, Colcher D, Liu A, et al. Imaging glioma extent with  $^{131}\text{I}$ -TM-601. *J Nucl Med* 2005;46(4):580–6.
- [25] Cordier D, Forrer F, Bruchertseifer F, Morgenstern A, Apostolidis C, Good S, et al. Targeted alpha-radiation therapy of functionally critically located gliomas with  $^{213}\text{Bi}$ -DOTA-[Th18,Me1(O2)11]-substance P: a pilot trial. *Eur J Nucl Med Mol Imaging* 2010;37(7):1335–44.
- [26] Patlak CS, Blasberg RG, Fenstermacher JD. Graphical evaluation of blood-to-brain transfer constants from multiple-time uptake data. *J Cereb Blood Flow Metab* 1983;3(1):1–7.
- [27] Reulen H, Graham R, Spatz M, Klitzo I. Role of pressure gradients and bulk flow in dynamics of vasogenic brain edema. *J Neurosurg* 1977;46(1):24–35.
- [28] Young ME, Carrood PA, Bell RL. Estimation of diffusion coefficients of proteins. *Biotechnol Bioeng* 1980;22:947–55.

- [29] Valencia DP, González FJ. Understanding the linear correlation between diffusion coefficient and molecular weight. A model to estimate diffusion coefficients in acetonitrile solutions. *Electrochem Commun* 2011;13:129–32.
- [30] Hopkins K. Direct injection of  $^{90}\text{Y}$  Moabs into glioma tumor resection cavities leads to limited diffusion of the radioimmunconjugates into normal brain parenchyma: a model to estimate absorbed radiation dose. *Int J Radiat Oncol Biol Phys* 1998;40(4):835–44.
- [31] NIST database for physical reference data. <https://www.nist.gov/pml/productservices/physical-reference-data>; 2017.
- [32] Thakral P, Singla S, Yadav MP, Vasisht A, Shady M, Gupta SK, et al. An approach for conjugation of  $^{177}\text{Lu}$ -DOTA-SCN-Rituximab (BioSim) & its evaluation for radioimmunotherapy of relapsed & refractory B-cell non Hodgkins lymphoma patients. *Indian J Med Res* 2014;139:544–54.
- [33] Salouti M, Babaei MH, Rajabi H, Rasaei MJ. Preparation and biological evaluation of  $^{177}\text{Lu}$  conjugated PR81 for radioimmunotherapy of breast cancer. *Nucl Med Biol* 2011;38:849–55.
- [34] Milenic DE, Garmestani K, Chapel L, Dadachova E, Yordanov A, Ma D, et al. In vivo comparison of macrocyclic and acyclic ligands for radiolabeling of monoclonal antibodies with  $^{177}\text{Lu}$  for radioimmunotherapeutic applications. *Nucl Med Biol* 2002;29:431–42.
- [35] Maddalena ME, Fox J, Chen J, Feng W, Cagnolini A, Lindner KE, et al.  $^{177}\text{Lu}$ -AMBA biodistribution, radiotherapeutic efficacy, imaging, and autoradiography in prostate cancer models with low GRP-R expression. *J Nucl Med* 2009;50(12):2017–24.
- [36] Price EW, Orvig C. Matching chelators to radiometals for radiopharmaceuticals. *Chem Soc Rev* 2014;43:260–90.
- [37] Perk LR, Visser GWM, Vosjan MJWD, Stigter-van Walsum M, Tjink BM, Leemans CR, et al.  $^{89}\text{Zr}$  as a PET surrogate radioisotope for scouting biodistribution of the therapeutic radiometals  $^{90}\text{Y}$  and  $^{177}\text{Lu}$  in tumor-bearing nude mice after coupling to the internalizing antibody cetuximab. *J Nucl Med* 2005;46(11):1898–906.
- [38] Chakravarty R, Chakraborty S, Dash A. A systematic comparative evaluation of  $^{90}\text{Y}$ -labeled bifunctional chelators for their use in targeted therapy. *J Label Compd Radiopharm* 2013;57:65–74.
- [39] Chakravarty R, Chakraborty S, Sarma HD, Nair KVV, Rajeswari A, Dash A.  $^{90}\text{Y}/^{177}\text{Lu}$ -labelled cetuximab immunoconjugates: radiochemistry optimization to clinical dose formulation. *J Label Compd Radiopharm* 2016;59:354–63.
- [40] Hermanto S, Haryuni RD, Ramli M, Mutalib A, Hudiyono S. Synthesis and stability test of radioimmunconjugate  $^{177}\text{Lu}$ -DOTA-F(ab')<sub>2</sub>-trastuzumab for theranostic agent of HER2 positive breast cancer. *J Radiat Res Appl Sci* 2016;9:441–8.
- [41] Mendler CT, Gehring T, Wester H-J, Schwaiger M, Skerra A.  $^{89}\text{Zr}$ -labeled versus  $^{124}\text{I}$ -labeled aHER2 Fab with optimized plasma half-life for high-contrast tumor imaging in vivo. *J Nucl Med* 2015;56:1112–8.
- [42] Mendler CT, Friedrich L, Laitinen I, Schlapschy M, Schwaiger M, Wester H-J, et al. High contrast tumor imaging with radio-labeled antibody Fab fragments tailored for optimized pharmacokinetics via PAsylation. *mAbs* - Taylor & Francis; 2015; 96–109.
- [43] Dennis MS, Jin H, Dugger D, Yang R, McFarland L, Ogasawara A, et al. Imaging tumors with an albumin-binding Fab, a novel tumor-targeting agent. *Cancer Res* 2007;67(1):254–61.
- [44] Covell DG, Barbet J, Holton OD, Black CDV, Parker RJ, Weinstein JN. Pharmacokinetics of monoclonal immunoglobulin G<sub>1</sub>, F(ab')<sub>2</sub>, and Fab' in mice. *Cancer Res* 1986;46(8):3969–78.
- [45] Vejt E. Renal toxicity of radiolabeled peptides and antibody fragments: mechanisms, impact on radionuclide therapy, and strategies for prevention. *J Nucl Med* 2010;54: 1049–58.
- [46] Freise AC, Wu AM. In vivo imaging with antibodies and engineered fragments. *Mol Immunol* 2015;67:142–52.
- [47] Holliger P, Hudson PJ. Engineered antibody fragments and the rise of single domains. *Nat Biotechnol* 2005;23(9):1126–36.
- [48] Akizawa H, Uehara T, Arano Y. Renal uptake and metabolism of radiopharmaceuticals derived from peptides and proteins. *Adv Drug Deliv Rev* 2008;60:1319–28.
- [49] Duncan JR, Behr TM, DeNardo SJ. Intracellular fate of radiometals [letter to the editor]. *J Nucl Med* 1997;38:829.
- [50] Behr TM, Sharkey RM, Sgouros G, Blumenthal RD, Dunn RM, Kolbert K, et al. Overcoming the nephrotoxicity of radiometal-labeled immunoconjugates. *Cancer Suppl* 1997;80(12):2591–610.
- [51] Ocean AJ, Pennington KL, Guarino MJ, Sheikh A, Bekaii-Saab T, Serafini AN, et al. Fractionated radioimmunotherapy with  $^{90}\text{Y}$ -clivatuzumab tetraxetan and low-dose gemcitabine is active in advanced pancreatic cancer. *Cancer* 2012;118(22): 5497–506.
- [52] Parkkila S, Parkkila A-K, Saarnio J, Kivelä J, Karttunen TJ, Kaunisto K, et al. Expression of the membrane-associated carbonic anhydrase isozyme XII in the human kidney and renal tumors. *J Histochem Cytochem* 2000;48(12):1601–8.

# Fully Automated Production and Characterization of $^{64}\text{Cu}$ and Proof-of-Principle Small-Animal PET Imaging Using $^{64}\text{Cu}$ -Labelled CA XII Targeting 6A10 Fab

Luise Fiedler,<sup>\*[a]</sup> Markus Kellner,<sup>[b]</sup> Rosel Oos,<sup>[a]</sup> Guido Böning,<sup>[a]</sup> Sibylle Ziegler,<sup>[a]</sup> Peter Bartenstein,<sup>[a]</sup> Reinhard Zeidler,<sup>[b, c]</sup> Franz Josef Gildehaus,<sup>[a]</sup> and Simon Lindner<sup>\*[a]</sup>

$^{64}\text{Cu}$  is a cyclotron-produced radionuclide which offers, thanks to its characteristic decay scheme, the possibility of combining positron emission tomography (PET) investigations with radiotherapy. We evaluated the Alceo system from Comecor SpA to automatically produce  $^{64}\text{Cu}$  for radiolabelling purposes. We established a  $^{64}\text{Cu}$  production routine with high yields and radionuclide purity in combination with excellent operator radiation

protection. The carbonic anhydrase XII targeting 6A10 antibody Fab fragment was successfully radiolabelled with the produced  $^{64}\text{Cu}$ , and proof-of-principle small-animal PET experiments on mice bearing glioma xenografts were performed. We obtained a high tumor-to-contralateral muscle ratio, which encourages further in vivo investigations of the radioconjugate regarding a possible application in diagnostic tumor imaging.

## Introduction

As a powerful noninvasive imaging tool, positron emission tomography (PET) offers the possibility to visualize and monitor biochemical and physiological functions as well as pathophysiological processes in vivo. To investigate rapid molecular distribution and accumulation characteristics, short-lived PET radionuclides such as  $^{11}\text{C}$  ( $t_{1/2}=20.4$  min),  $^{68}\text{Ga}$  ( $t_{1/2}=67.7$  min) and  $^{18}\text{F}$  ( $t_{1/2}=109.8$  min) are commonly used.<sup>[1–6]</sup> For instance, [ $^{18}\text{F}$ ]FDG is a radiolabelled glucose molecule with rapid tumor uptake characteristics and is one of the most prominent tracers in the field of tumor imaging.<sup>[6,7]</sup> Radionuclides with longer half-lives such as  $^{89}\text{Zr}$  ( $t_{1/2}=3.27$  days) and  $^{124}\text{I}$  ( $t_{1/2}=4.18$  days), are needed to image molecules with slower biochemical processes and longer blood availability, such as antibodies.<sup>[8,9]</sup> Fragment antigen binding (Fab) fragments of antibodies, on the other hand, have shorter bioavailability than full-length antibodies, but much longer availability than small molecules, such as glucose.<sup>[10–12]</sup> Radiolabelling such molecules with an intermediate half-life PET nuclide such as  $^{64}\text{Cu}$  ( $t_{1/2}=12.7$  h) might therefore be promising. Furthermore, in addition to  $\beta^+$

and electron capture,  $^{64}\text{Cu}$  decay includes a significant  $\beta^-$  component (probability of  $39.0 \pm 3\%$ ).<sup>[13–15]</sup> Thus, the combination of PET imaging with radiotherapy may be feasible, which is not the case for  $^{124}\text{I}$  and  $^{89}\text{Zr}$ .<sup>[16–19]</sup>

Various kinds of molecules have been radiolabelled with  $^{64}\text{Cu}$  to investigate possible PET applications against a wide range of diseases. One of the most common  $^{64}\text{Cu}$ -radiolabelling methods is based on the use of a chelating agent to bind the radioactive metal to the carrier molecule. Copper offers well-established coordination chemistry which allows the use of various chelators, such as DiamSar, NOTA, NODA-GA, PCTA and their derivatives.<sup>[20,21]</sup> Using chelator-conjugated antibodies,  $^{64}\text{Cu}$  has been investigated in studies against pancreatic cancer,<sup>[22]</sup> malignant lymphoma,<sup>[23]</sup> breast cancer,<sup>[24]</sup> and carbonic anhydrase (CA) IX expressing malignant tissue.<sup>[25]</sup> Antibody fragments (Fab and F(ab)<sub>2</sub>), also radiolabelled with  $^{64}\text{Cu}$  via chelators, have been used in studies against ovarian cancer,<sup>[26]</sup> breast cancer,<sup>[26,27]</sup> and head and neck cancer.<sup>[28]</sup> Chelator molecules are further used to bind  $^{64}\text{Cu}$  to peptides, such as RGD<sub>2</sub>-BBN heterotrimers against prostate cancer,<sup>[29]</sup> and RGD peptides against gliomas.<sup>[30]</sup> Chelator conjugating is even used to radiolabel nanoparticles<sup>[31]</sup> and liposomes for breast cancer diagnosis.<sup>[32]</sup> Copper-labelled complexing agents such as ATSM or some bifunctional chelators have been further investigated for use as diagnostics against hypoxia<sup>[33,34]</sup> and Alzheimer's disease,<sup>[35,36]</sup> respectively.

Because chelators might change the pharmacokinetics and binding ability of the conjugated molecule, the development of chelator-free radiolabelling strategies is interesting. Using nanoparticles based on gallic acid is one way to ensure chelator-free radiolabelling, as the phenol groups interact strongly with  $^{64}\text{Cu}$ .<sup>[37–39]</sup> Promising preclinical results of such approaches have already been reported for studies against breast cancer.<sup>[37,38,40]</sup> A further method to generate  $^{64}\text{Cu}$ -labelled struc-

[a] L. Fiedler, R. Oos, PD Dr. G. Böning, Prof. S. Ziegler, Prof. P. Bartenstein, Dr. F. J. Gildehaus, Dr. S. Lindner  
Department of Nuclear Medicine, University Hospital, LMU Munich, Marchioninistrasse 15, 81377 Munich (Germany)  
E-mail: luise.fiedler@med.uni-muenchen.de  
simon.lindner@med.uni-muenchen.de

[b] Dr. M. Kellner, Prof. R. Zeidler  
Helmholtz-Zentrum München, German Research Center for Environmental Health, Research Group Gene Vectors, Marchioninistrasse 25, 81377 Munich (Germany)

[c] Prof. R. Zeidler  
Department of Otorhinolaryngology, University Hospital, LMU Munich, Marchioninistrasse 15, 81377 Munich (Germany)

 The ORCID identification number(s) for the author(s) of this article can be found under:  
<https://doi.org/10.1002/cmdc.201800130>.

tures is the use of radioactively doped starting material. As a result, the radionuclide is embedded in the structure's matrix, as is the case for  $^{64}\text{Cu}$ -containing quantum dots, which are under investigation for PET studies against gliomas.<sup>[41]</sup> Furthermore, structures like liposomes or micelles or even nanoparticles can be used to encapsulate  $^{64}\text{Cu}$ -linked molecules which might be useful to influence the molecule's properties, for instance, by increasing its hydrophilic properties.<sup>[39,42]</sup> Due to this wide range of promising applications for  $^{64}\text{Cu}$ , establishing a production routine was further investigated in this study.

The cyclotron production of  $^{64}\text{Cu}$  via the  $^{64}\text{Ni}(p,n)^{64}\text{Cu}$  reaction has already been extensively investigated.<sup>[18,19,43]</sup> Several research groups have established  $^{64}\text{Cu}$  production routines, but mostly with individual custom-made, semi-automated processes and equipment.<sup>[19,44–47]</sup> Comecer SpA (Castel Bolognese, Italy) developed an automatic setup, the so-called Alceo modules, to cover all processes regarding  $^{64}\text{Cu}$  production: electrochemical fabrication of the  $^{64}\text{Ni}$  target, cyclotron irradiation and subsequent dissolution of the target, purification and final preparation of the  $^{64}\text{Cu}$  product. All procedures can be performed automatically without manual intervention, which ensures a high level of radiation protection for the operator. Matarrese et al.<sup>[48]</sup> first introduced these modules, but used an individual modified electrochemical cell. Our study is focused on establishing a  $^{64}\text{Cu}$  routine production with the unmodified, commercially available first-generation Alceo modules (Figure 1) to perform preliminary PET imaging experiments.

The Alceo setup consists of the PRF (purification), the EDS (electrodeposition/dissolution/transfer/storage) and the PTS (ir-

radiation/cooling) unit. To prepare the irradiation target, a  $^{64}\text{Ni}$  solution circulates between the PRF and the electrochemical cell in the EDS module. A main part of the electrochemical cell is the so-called shuttle, which is a cylindrical hollow aluminum device (height 35 mm, diameter 28 mm) with an integrated platinum beaker. The ground area of this beaker is used as backing for  $^{64}\text{Ni}$  electrodeposition. The lid of the electrochemical cell equipped with a platinum rod anode is closed above the shuttle, which is placed on the gold-foiled brass cathode beneath (Figure 2). Through a tube system, the shuttle is automatically transferred to the PTS module, which is installed on the in-house biomedical cyclotron and positioned in the beam-line. Cooling of the shuttle backing and the nickel target during irradiation is maintained using water and helium, respectively.

The shuttle is delivered back to the EDS unit, and the irradiated target is dissolved using the circularly arranged capillaries between EDS and PRF. The target solution is purified by anion-exchange chromatography<sup>[49]</sup> in the PRF. Recovered nickel can be processed for repeated use as target material. The purified  $^{64}\text{CuCl}_2$  is sent to the TADDEO module (Comecer SpA) for volume reduction (Figure 1 D).

The produced  $^{64}\text{Cu}$  was further characterized, used for radiolabelling experiments, and the initial in vivo small-animal PET imaging experiments were performed. For this, the Fab fragment of the new 6A10 antibody (6A10 Fab) was used, which binds with high specificity to CA XII.<sup>[50,51]</sup> CA XII is a membrane enzyme that catalyzes the generation of bicarbonates for buffering purposes in cells that are covering their high energy de-

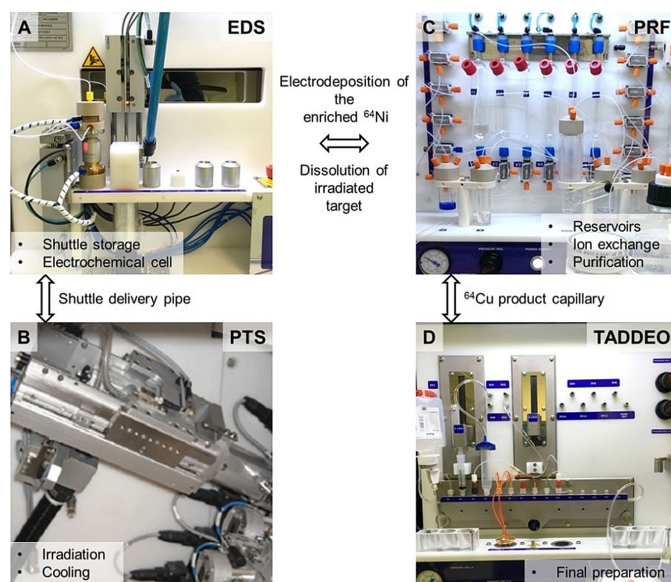


**Figure 1.** Modular setup of the Alceo system: The shuttle is transported between the EDS (A) and PTS (B) via a delivery pipe, EDS (A) and PRF (C) are connected by capillaries to enable the circulating fluid transport, and the final product is transferred from the PRF (C) through capillaries to the TADDEO module (D) for final processing.

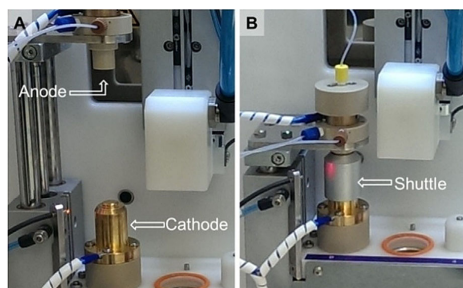


**Figure 2.** Electrochemical cell of the EDS module: A) open cell with marked positions of anode and cathode; B) shuttle in position for electrodeposition and dissolution with closed electrochemical cell.

mands by extensive anaerobic glycolysis.<sup>[50,51]</sup> This enzyme is expressed on various aggressively growing cancer cells,<sup>[52,53]</sup> such as renal carcinoma,<sup>[54–56]</sup> breast cancer,<sup>[57]</sup> ovarian tumors,<sup>[58]</sup> and gliomas.<sup>[59]</sup> The 6A10 Fab has already been radiolabelled with <sup>177</sup>Lu and investigated for potential use as a radiotherapy agent against glioma recurrence.<sup>[60]</sup> Further applications as a diagnostic tracer, radiolabelled with the PET nuclide <sup>64</sup>Cu, is now considered to extend the use of this biomolecule for tumor imaging.

Next to the establishment of an automated Cu production with the Alceo setup, the aim of our study was to evaluate the possibility of generating a <sup>64</sup>Cu-labelled 6A10 Fab for proof-of-principle PET experiments on mice bearing CA XII expressing tumor xenografts.

## Results and Discussion

### Target preparation and irradiation

Enriched <sup>64</sup>Ni was electrochemically deposited from an aqueous Ni(SO<sub>4</sub>)<sub>2</sub> solution in a dynamic cycle. In comparison with other research groups who used static electrochemical cells for nickel target deposition,<sup>[19,44,45,61,62]</sup> the Alceo setup uses the dynamic deposition method, in which the shuttle is part of the electrochemical cell, and the nickel is deposited directly on the shuttle's platinum beaker. This method prevents the accumulation of hydrogen at the cathode, which has been reported to disrupt the deposition process when using static setups.<sup>[46,63]</sup> To successfully produce a nickel target for irradiation, the flow of the electrolyte solution must be adjusted very accurately to 1.2–1.4 mL min<sup>-1</sup>. In this flow range, typical electrodeposition yields of up to 96% were reached. When using flows higher than 1.4 mL min<sup>-1</sup>, the yields radically decreased. Recovery and re-electrodeposition of already irradiated nickel material was accomplished with yields of up to 90%. The generated deposit (Figure 3B) was conically shaped, with a diameter of 7 mm, increasing thickness in the middle, and a rough, pitted surface. This appearance was most likely caused by the geometry of the electrochemical cell, as the anode is a platinum rod, and the cathode is a round-shaped platinum surface. The anode is

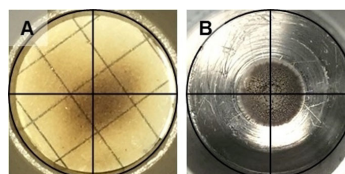


**Figure 3.** Result of the paper burn test shows the position of the beam on the shuttle (A), while B shows a <sup>64</sup>Ni-plating on the shuttle's platinum beaker.

positioned centrally above the cathode, which results in an increased deposition rate in the middle. Because the target gets very pointy and brittle at the tip if too much material is deposited, nickel amounts above 85 mg are not usable for further irradiation experiments.

A paper burn test was performed to determine the beam position on the shuttle required to effectively irradiate the nickel target. For that reason, a shuttle was equipped with a paper and irradiated for a short time. In Figure 3, panels A and B show the beam position on the burned paper and a representative nickel target. The cross in both figures indicates the center of the shuttle, where both <sup>64</sup>Ni and proton beam are located. This confirmed that the beam successfully hits the target during irradiation.

The beam energy was varied through the installation of aluminum foils of different thicknesses in the beam line. According to the <sup>64</sup>Ni(p,n)<sup>64</sup>Cu cross-section, the highest nuclear reaction yield can be expected at 11 MeV proton beam energy.<sup>[64,65]</sup> However, we observed an overall decreasing activity yield in correlation with the decreasing beam voltage. Proton energies of 11, 13.2 and 14.5 MeV resulted in average yields of 0.25 ± 0.15, 0.44 ± 0.14 and 0.72 ± 0.20 MBq/μA/h/mgNi, respectively. This can be explained by a decreased proton flux hitting the target with increasing degrader foil thickness. Table 1 contains a summary of 16 representative <sup>64</sup>Cu production runs with the corresponding amounts of used <sup>64</sup>Ni, irradiation parameter, and radioactive yields.

In comparing batches with similar amounts of nickel (B1 and B3, B5 and B7, B8 and B9), the yielded activity at the end of bombardment (EOB) was improved by elevating the beam current and duration. Increasing the amount of nickel target but using constant beam parameters (B12 and B13, B10 and B11, B16 and B15) also resulted in improved yields. Higher nickel amounts cannot be deposited, and longer irradiation times or higher currents are limited due to technical restrictions. Nevertheless, significant yield deviation was observed, even though similar nickel amounts and equal beam parameters were used (B13 and B15, B12 and B14). These variances are most likely due to an uneven quality of the nickel target caused by an unreliable electrodeposition process. The Alceo setup is characterized by a very long capillary circuit, which is used in different steps of the <sup>64</sup>Cu production. This can cause ionic cross-contaminations, which might disturb the electrochemistry process and can lead to irregular nickel deposition. Additionally, the pre-installed membrane pump is not able to establish a

**Table 1.** List of 16  $^{64}\text{Cu}$  production runs with the sample IDs, the corresponding amounts of  $^{64}\text{Ni}$ , beam parameters and resulting yields, decay corrected to the end of bombardment (EOB).

ID	$^{64}\text{Ni}$ [mg]	Beam parameters [MeV]	$[\mu\text{A}\cdot\text{h}]$	[MBq]	Yield EOB [MBq/ $\mu\text{A}\cdot\text{h}/\text{mgNi}$ ]
B1	46.9	14.5	18	660	
B2	58.0	14.5	60	2362	
B3	50.6	14.5	85	4443	
B4	41.0	14.5	100	3604	$0.72 \pm 0.20$
B5	84.5	14.5	57	3100	
B6	82.0	14.5	75	2509	
B7	83.5	14.5	100	5389	
B8	85.3	11.0	100	941	
B9	78.5	11.0	150	1702	
B10	24.0	11.0	150	1532	$0.25 \pm 0.15$
B11	39.7	11.0	150	2005	
B12	23.0	13.2	150	1826	
B13	42.0	13.2	150	2394	
B14	26.0	13.2	150	976	$0.44 \pm 0.14$
B15	42.6	13.2	150	3969	
B16	35.0	13.2	150	2118	

constant flow of the solution. Thus, to produce a reliable  $^{64}\text{Ni}$  target and consequently a predictable irradiation yield, modification of the pump and the electrochemical cycle is highly recommended to increase the irradiation output.

### Characterization

The irradiated target was dissolved in HCl, and the  $^{64}\text{Cu}$  was separated from nickel target material and irradiation by-products using anion-exchange chromatography. With a final volume of 9 mL, the  $^{64}\text{CuCl}_2$  was not suitable for radiolabelling purposes, so the product was evaporated to dryness and redissolved in HCl (400  $\mu\text{L}$ ; 0.1 M) using the TADDEO module. The final  $^{64}\text{CuCl}_2$  had an approximate pH 0.4 at the end of preparation (EOP). A half-life of  $12.7 \pm 0.5$  h was confirmed via dose calibrator measurement. The identity of the produced  $^{64}\text{Cu}$  was verified by gamma spectroscopy (Figure 4). Next to the 511 keV peak, the characteristic  $\gamma$ -peak of  $^{64}\text{Cu}$  at 1345 keV was identified. The radionuclide purity was calculated to be  $>99\%$  (EOP).

When irradiating enriched  $^{64}\text{Ni}$  with protons, the formation of radionuclide by-products has been reported.<sup>[19,45,46,66]</sup> Due to the limited purity of enriched  $^{64}\text{Ni}$  ( $<99.32\%$  purity), some impurities are expectable. To eliminate short-lived copper isotopes, anion-exchange purification of the product was performed after an overnight decay ( $\sim 12$  h), which resulted in excellent radionuclide purity at the end of preparation. All purification fractions were analyzed by gamma spectroscopy, and the overall contents of radionuclides were quantified. Table 2 lists the resulting contents of  $n=11$  separations in atomic percent (At%), decay corrected to EOB.

The cobalt isotopes  $^{55}\text{Co}$ ,  $^{57}\text{Co}$  and  $^{61}\text{Co}$  were identified with contents of  $0.03 \pm 0.10$ ,  $0.004 \pm 0.014$  and  $1.4 \pm 3.4$  At%, respectively. The amount of  $^{64}\text{Cu}$  was determined to be  $98.5 \pm$

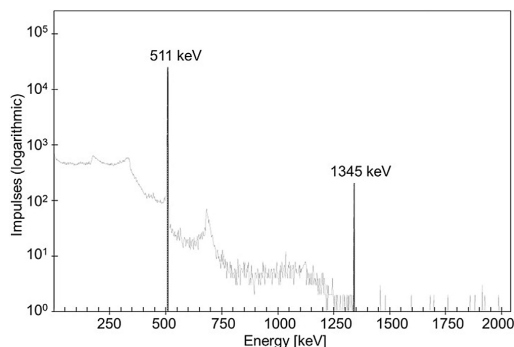


**Figure 4.** Exemplary gamma spectrum of the produced  $^{64}\text{Cu}$  with the annihilation peak (511 keV) and the copper-specific  $\gamma$ -peak at 1345 keV.

**Table 2.** Average amounts of irradiation products in atomic percent (At%) at EOB ( $n=11$ ). Nuclides that were not detected are declared as n.d. (not detectable). Gamma spectrometry measurements were performed 10–12 h post-EOB.

Element	Isotope	Half-life	At% @ EOB
Cobalt	55	17.5 h	$0.03 \pm 0.10$
	57	271.8 d	$0.004 \pm 0.014$
	61	1.7 h	$1.4 \pm 3.4$
Copper	60	23.7 min	n.d.
	61	3.4 h	n.d.
	62	9.7 min	n.d.
	64	12.7 h	$98.5 \pm 3.4$

$3.4$  At%. Radionuclides with short half-lives, such as  $^{60-62}\text{Cu}$ , were not detected in the examined sample. This supports the implementation of a 12 h time interval between EOB and EOP for elimination of any short-lived isotopes.

The molar activity ( $A_m$ ) of the produced  $^{64}\text{CuCl}_2$  was determined by titration with the chelator 1,4,8,11-tetraazacyclotetradecane-1,4,8,11-tetraacetic acid (TETA).<sup>[19]</sup> To do so, aliquots of TETA at different concentrations were radiolabelled with  $^{64}\text{Cu}$ , and the radioactive yield was determined with radio-TLC. Due to an equimolar reaction between metal and chelator, the molar activity ( $\text{Bq mol}^{-1}$ ) can be calculated. Non-radioactive metallic ion contaminations would compete with the  $^{64}\text{Cu}$  to complex with TETA, so this method determines the effective molar activity (eff.  $A_m$ ) of the entire  $^{64}\text{CuCl}_2$  product rather than the theoretical activity per mole  $^{64}\text{Cu}$ . To determine the theoretical  $A_m$ , a direct method such as mass spectrometry techniques is recommendable.<sup>[44,45]</sup> Because the eff.  $A_m$  is decisive for radiolabelling purposes, we focused on the TETA titration method in this study.

Improving the eff.  $A_m$  was accomplished by changing the solvent for cleaning of all the module reservoirs and capillaries prior to  $^{64}\text{Cu}$  production. We first used only Tracepur® water ( $\leq 1.0$  ppb Cu;  $\leq 1.0$  ppb Fe) and switched during development to a two-step method, which includes pre-cleaning with Trace-

pur® water and final rinsing with Ultrapur® water ( $\leq 0.1$  ppb Cu;  $\leq 0.3$  ppb Fe). To monitor the rinsing efficiency, diluted aliquots of decayed  $^{64}\text{CuCl}_2$  batches were analyzed with ICP-OES for metallic contaminations of Co, Cr, Mn, Ni, Zn, Cu and Fe. Metal contents of significance were found for Cu, Fe, Ni and Zn, and are plotted in Figure 5 in correlation with the determined effective molar activity.

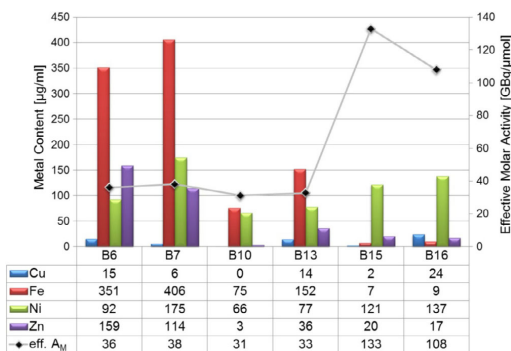


**Figure 5.** A representative comparison of the contents of non-radioactive metals ( $\mu\text{g mL}^{-1}$ ) and the corresponding molar activity ( $A_m$ ) [ $\text{GBq } \mu\text{mol}^{-1}$ ].

B6 and B7 show the results of a system that was rinsed with Tracepur® water using a small anion-exchange column (3 g resin) for separation. In both batches, remarkably high amounts of Fe and Zn were detected. The amount of resin was increased up to 9 g in B10 and B13, while rinsing was still carried out with Tracepur® water, resulting in decreased Fe and Zn contents.

Finally, cleaning of all production-relevant lines and cycles was performed with Ultrapur® water, leading to a decreased content of Fe in B15 and B16. Simultaneously, a significant improvement of the eff.  $A_m$  was reached using high-purity water for cleaning ( $120.5 \pm 17.7 \text{ GBq } \mu\text{mol}^{-1}$  in B15 and B16 versus  $34.5 \pm 3.1 \text{ GBq } \mu\text{mol}^{-1}$  in B6, B7, B10 and B13). Varying amounts of Cu and Ni were detected over all batches.

The amount of determined nickel in the product does not correlate with improvements made for purification and rinsing. We therefore assume that the majority of the nickel originates from the nickel target. Minor amounts of non-radioactive Ni and Zn can be attributed to  $^{64}\text{Cu}$  decay, as it is characterized by  $39.0 \pm 3\%$   $\beta^-$  decay to  $^{64}\text{Zn}$  ground state, and  $17.86 \pm 14\%$   $\beta^+$  and  $42.6 \pm 5\%$  electron capture decay to  $^{64}\text{Ni}$  ground state.<sup>[13–15]</sup> Co, Cr and Mn were not found in significant amounts.

An optimized molar activity of  $^{64}\text{Cu}$  is an important prerequisite for imaging purposes. Using different technical setups, processing methods and irradiation parameters, a wide range of possible molar activities has been published. Table 3 shows a comparison between the results presented in this study and previously published molar activities of other groups. With up to  $133 \text{ GBq } \mu\text{mol}^{-1}$ , our method generates moderate values,

**Table 3.** Comparison of the molar activities reported in previous studies and in this study, in correlation with the measurement methods used.

Authors	Molar activity [ $\text{GBq } \mu\text{mol}^{-1}$ ]	Measurement method
Ohya et al. <sup>[67]</sup>	$1170 \pm 1170$	ICP-MS
Avila-Rodriguez et al. <sup>[46]</sup>	$696 \pm 122$	Titration with TETA
Thieme et al. <sup>[44]</sup>	$1072 \pm 420$	ICP-MS
McCarthy et al. <sup>[19]</sup>	Up to 733	Titration with TETA
<b>Current study</b>	<b>Up to 133</b>	<b>Titration with TETA</b>
Obata et al. <sup>[62]</sup>	$118 \pm 67$	Titration & HPLC with ATSM
Jeffery et al. <sup>[45]</sup>	$89 \pm 37$	ICP-MS
Matarrese et al. <sup>[48]</sup>	$81 \pm 48$	HPLC

higher than those reported by Jeffery et al.,<sup>[45]</sup> Matarrese et al.<sup>[48]</sup> and Obata et al.,<sup>[62]</sup> but lower than those achieved by Avila-Rodriguez et al.,<sup>[46]</sup> McCarthy et al.,<sup>[19]</sup> Ohya et al.<sup>[67]</sup> and Thieme et al.<sup>[44]</sup> Our results can best be compared with those of Matarrese et al.,<sup>[48]</sup> who also worked with the Alceo modules. They reported an effective molar activity of  $81.4 \pm 48.1 \text{ GBq } \mu\text{mol}^{-1}$ , which was moderately improved to maximum  $133 \text{ GBq } \mu\text{mol}^{-1}$  in this study.

#### Limitations of the Alceo modules

By using the first-generation Alceo modules, an automatic production of  $^{64}\text{Cu}$  can be established. However, some improvements might be recommended to further optimize the process reproducibility and the molar activity of the  $^{64}\text{Cu}$  product. The modules are equipped with very long capillary circuits for all production steps, and the same lines are used for nickel electroplating and dissolving prior and post-irradiation. This might result in metal ion cross-contaminations, which must be removed by extensive rinsing procedures. A better way to diminish problems associated with those cross-contaminations would be to strictly separate the two cycles and to significantly shorten the fluid pathways. Furthermore, a setup based on disposable kits would even guarantee a production that is free of any contamination.

An improved reproducibility regarding the electroplating process can further be reached by installing a pump with a more stable performance, as the pre-installed device shows unequal pump velocity over a long operating time.

The initially produced  $^{64}\text{CuCl}_2$  is so far available in 9 mL, which results in a volume-concentration too low for radiolabelling purposes. In this study, the TADDEO module had to be used for volume reduction. With an integrated solution, for example, a pre-installed heating device for evaporation, the Alceo setup would enable a convenient production outcome of labelling-suitable  $^{64}\text{Cu}$ .

#### Radiolabelling and PET imaging

The 6A10 Fab, conjugated with *p*-NCS-benzyl-NODA-GA, was radiolabelled with  $^{64}\text{Cu}$  and purified with a nap-5 column (GE Healthcare, Munich, Germany). The radiochemical purity of the product was determined by radio-TLC to be  $> 93\%$ . In five syn-

thesis runs, we reached a final specific activity of the radiolabelled compound of  $208.6 \pm 49.7 \text{ MBq mg}^{-1}$ . A female SCID mouse, bearing a glioma xenograft on the right shoulder ( $\sim 370 \text{ mm}^2$ ) was injected with 14.7 MBq of the conjugate via a tail vein catheter and scanned by small-animal PET. The image is shown in Figure 6. The tumor-to-contralateral muscle ratio was calculated to be 12.

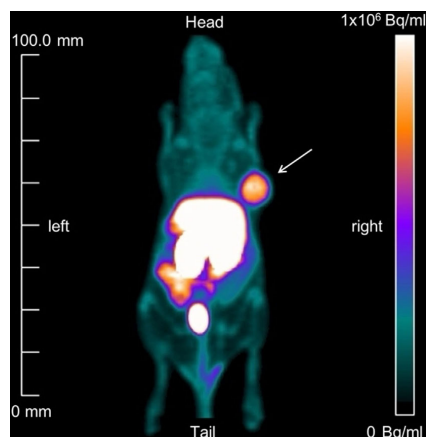


**Figure 6.** PET image of a mouse scanned 4 h after injection of 14.7 MBq of the radioconjugate. The tumor xenograft on the right shoulder is indicated with a white arrow.

The image also shows activity accumulation in organs such as kidney, liver, bladder, spleen and intestines. According to our previous work,<sup>[60]</sup> this accumulation pattern can be expected, as the metabolism of proteins with molecular weight similar to a Fab fragment ( $\sim 55 \text{ kDa}$ ) is dominated by kidney and liver. The calculated tumor-to-contralateral muscle ratio of 12 is notably high for a systemically applied Fab fragment, as Fabs undergo rapid degradation processes and are therefore much more short-lived in the blood than full-length antibodies.<sup>[10–12]</sup> This encourages further studies regarding the *in vivo* behavior of this  $^{64}\text{Cu}$ -labelled compound for diagnostic imaging of CA XII expressing tumors.

## Conclusions

The Comacer Alceo modules offer the possibility to produce  $^{64}\text{Cu}$  in good radioactive yields, high radiochemical purity, and good effective molar activity for radiolabelling of biomolecules. Due to the high grade of automatization an excellent radiation protection for the operator can be expected. Labelling of the 6A10 antibody Fab fragment and proof-of-principle small-animal PET experiments were accomplished and showed promising imaging results.

Further studies are considered to investigate the *in vitro* and *in vivo* characteristics of the  $^{64}\text{Cu}$ -labelled 6A10 Fab in regard

to a possible diagnostic application against CA XII expressing tumors.

## Experimental Section

Unless otherwise mentioned, all chemicals and expendable items were purchased from Sigma–Aldrich (Taufkirchen, Germany), Carl Roth (Karlsruhe, Germany), or Eppendorf (Hamburg, Germany). All glassware and capillaries were routinely cleaned prior to production with  $\text{HNO}_3$  (2 M), rinsed with water and dried with nitrogen. During the evaluation process in this work, the purity grade of the used water was continuously refined.

**Target preparation:** The electrolyte bath was prepared according to McCarthy et al.<sup>[19]</sup> The enriched  $^{64}\text{Ni}$  (20–90 mg, <99.32% purity, Chemotrade Chemiehandels-gesellschaft mbH, Düsseldorf, Germany) was dissolved in  $\text{HNO}_3$  (2 mL, 6 M), evaporated to dryness, re-dissolved in  $\text{H}_2\text{SO}_4$  (300  $\mu\text{L}$ , concentrated), diluted with  $\text{H}_2\text{O}$  (2 mL), evaporated to near dryness and diluted with  $\text{H}_2\text{O}$  (5 mL). The solution was adjusted to pH 9 with  $\text{NH}_3$ , and  $(\text{NH}_4)_2\text{SO}_4$  (0.3 mg) and  $\text{H}_2\text{O}$  (2 mL) were added to a final volume of 8–9 mL. Nickel deposition on the shuttle occurred under constant circulation of the solution with  $1.2\text{--}1.4 \text{ mL min}^{-1}$ , at 2.6 V and a current between 0–30  $\mu\text{A}$ , depending on the amount of nickel remaining in the solution. After 20–24 h, the solution turned colorless, which indicates the complete nickel deposition. By weighing the shuttle before and after electrodeposition, the amount of deposited nickel was determined. The circulation cycle and the plated nickel was rinsed with  $\text{H}_2\text{O}$  and dried with nitrogen.

**Irradiation:** For irradiation a PETtrace 800 series cyclotron from GE Healthcare (Uppsala, Sweden) was used. Confirmation of the correct shuttle position in the beam line was obtained by a paper burn test. For that purpose, a shuttle was equipped with a paper and irradiated for 16 s with 5  $\mu\text{A}$  at 13.2 MeV. Several irradiation conditions were tested. The initial 16 MeV beam was degraded by different aluminum foils. Using 320, 500 and 820  $\mu\text{m}$  foils resulted in beam voltages of 14.5, 13.2 and 11 MeV, respectively.<sup>[68]</sup> The irradiation took up to 5 h and current values between 20–30  $\mu\text{A}$  were tested. The temperature range of cooling water and helium was set to be at  $-20 \pm 5^\circ\text{C}$ .

**Purification and preparation of  $^{64}\text{Cu}$ :** After an overnight decay, the irradiated target was dissolved with HCl (5 mL, 6 M) at  $90^\circ\text{C}$  shuttle temperature over 1 h. A BioRad Econo-Column with AG1-X8 chloride form resin (200–400 mesh, BioRad, Hercules, CA, USA) was loaded with the solution. In three steps, unreacted nickel, co-produced cobalt and copper product were eluted with 6 M HCl (30 mL), 4 M HCl (15 mL) and 0.1 M HCl (9 mL), respectively. The  $^{64}\text{Cu}$  fraction was delivered to the TADDEO module and evaporated to dryness at  $160^\circ\text{C}$  in 1 h under a constant nitrogen flow, and finally re-dissolved in 400  $\mu\text{L}$ . To recover the decayed  $^{64}\text{Ni}$ , the first fraction was loaded on the AG1-X8 resin, eluted with 6 M HCl (30 mL), evaporated to dryness, re-dissolved in  $\text{H}_2\text{O}$  (20 mL), evaporated to dryness, re-dissolved in ethanol (15 mL) and evaporated to dryness. The residue was retreated with  $\text{HNO}_3$  (2 mL, 6 M) and further processed as previously explained, to prepare the electrochemical  $^{64}\text{Ni}$  solution.

**Characterization:** The pH of the copper fraction was determined with a pH meter by Mettler Toledo (Greifensee, Switzerland). All three purification fractions were analyzed by gamma spectroscopy (GC2020-CP5SL, Mirion Technologies (former Canberra) GmbH, Rüsselsheim, Germany) with the Gamma Analysis S501 software package), to calculate the overall radionuclide composition of the pro-

duction run and to determine the  $^{64}\text{Cu}$  purity. Using an ISOMED 2010 dose calibrator (MED Nuklear-Medizintechnik Dresden GmbH, Dresden, Germany), final product activity and half-life were verified. The specific activity of  $^{64}\text{Cu}$  was determined via titration with TETA (1,4,8,11-tetraazacyclotetradecane-1,4,8,11-tetraacetic acid, from Macrocylics, Dallas, TX, USA), as presented by McCarthy et al.<sup>[19]</sup> A copper stock solution in  $\text{NH}_4\text{OAc}$  (0.1 M, pH 5.5) with a concentration of 10 MBq per 30  $\mu\text{L}$  was prepared; 0.03–0.2  $\mu\text{g}$  of TETA and 10 MBq copper stock solution were diluted in  $\text{NH}_4\text{OAc}$  (300  $\mu\text{L}$ , 0.1 M, pH 5.5) and incubated for 30 min at 37 °C. Radio-TLC was performed on iTLC-SA strips (Agilent, Waldbronn, Germany) with NaCl (0.9%) as mobile phase ( $R_f(\text{TETA}) = 0.8\text{--}0.9$ ;  $R_f(^{64}\text{Cu}) = 0.0$ ). ICP-OES analysis was performed on decayed  $^{64}\text{Cu}$  aliquots at the analytical division of the Faculty for Chemistry and Pharmacy, LMU Munich, to determine non-radioactive metallic impurities (Co, Cr, Cu, Fe, Mn, Ni, Zn).

**Labelling:** The 6A10 Fab was conjugated with *p*-NCS-benzyl-NODA-GA (2,2'-(7-(1-carboxy-(4-(4-isothiocyanatobenzyl)amino)-4-oxobutyl)-1,4,7-triazacyclononane-1,4-diyl)diacetic acid from Chematech (Dijon, France) in phosphate buffer (400  $\mu\text{L}$  reaction volume, 0.1 M, pH 8.5) for 1 h at 37 °C. Not complexed chelator was removed using nap-5 columns (GE Healthcare, Munich, Germany). The conjugate was labelled with  $^{64}\text{CuCl}_2$  in  $\text{NH}_4\text{OAc}$  (500–600  $\mu\text{L}$  reaction volume, 0.1 M, pH 5.5) at 37 °C for 20 min followed by a nap-5 column purification. Radio-TLC on iTLC-SA strips (15–95 mm) in citric buffer (pH 4.5) was used for quality control ( $R_f(\text{Fab}) = 0.0\text{--}0.1$ ;  $R_f(\text{NODA-GA}) = 0.1\text{--}0.3$ ;  $R_f(\text{free } ^{64}\text{Cu}) = 0.1\text{--}1.0$ ).

**PET imaging:** The glioma cell line U87MG (American Type Culture Collection) was cultivated in Gibco MEM media by Thermo Fischer Scientific (Munich, Germany), supplemented with fetal bovine serum and L-glutamine (Biochrom Berlin, Germany) and kept at 5%  $\text{CO}_2$  and 37 °C in a CB150 incubator by Binder (Tuttlingen, Germany).  $5 \times 10^6$  U87MG cells were subcutaneously injected into the right shoulder of a female SCID mouse (6–8 weeks, 20–25 g). 14.7 MBq was injected through a tail vein catheter after a tumor growth time of 12 days. Under constant anesthesia (Isoflurane Vet. Med. Vapor, Drägerwerk, Lübeck) the mouse was scanned 4 h post-injection for 70 min (60 min emission and 10 min transmission) on an Inveon P120  $\mu\text{PET}$  scanner (Siemens, Munich, Germany; Inveon acquisition workplace, Siemens Medical Solutions, Knoxville, USA). PET images were analyzed with the Inveon Research Workplace software. Region-of-interest (ROI) analysis was performed using a tumor ROI based on 40% threshold (239  $\mu\text{L}$ ) and a background ROI (ellipsoid, 100 mL) in the contralateral thigh muscle. Average ROI counts were calculated. All animal experiments were performed in accordance to the current German animal protection laws and protocols of the local authorities.

## Conflict of interest

The authors declare no conflict of interest.

**Keywords:**  $^{64}\text{Cu}$  · 6A10 Fab · Comcer Alceo · positron emission tomography · solid targets

- [1] B. J. Hackel, R. H. Kimura, Z. Miao, H. Liu, A. Sathirachinda, Z. Cheng, F. Chin, S. S. Gambhir, *J. Nucl. Med.* **2013**, *54*, 1101–1105.
- [2] H. Chen, G. Niu, H. Wu, X. Chen, *Theranostics* **2016**, *6*, 78–92.
- [3] J. Oxboel, M. Brandt-Larsen, C. Schjoeth-Eskesen, R. Myschetzky, H. H. El-Ali, J. Madsen, A. Kjaer, *Nucl. Med. Biol.* **2014**, *41*, 259–267.

- [4] P. Bustany, M. Chatel, J. M. Delron, F. Darcel, P. Sgouropoulos, F. Soussaline, A. Syrota, *J. Neuro-Oncol.* **1986**, *3*, 397–404.
- [5] J. W. Hicks, H. F. Van Brocklin, A. A. Wilson, S. Houle, N. Vasdev, *Molecules* **2010**, *15*, 8260–8278.
- [6] I. Kayani, J. B. Bomanji, A. Groves, G. Conway, S. Gacinovic, T. Win, J. Dickson, M. Caplin, P. J. Ell, *Cancer* **2008**, *112*, 2447–2455.
- [7] H. Zhuang, M. Pourdehnad, E. S. Lambright, A. J. Yamamoto, M. Lanuti, P. Li, P. D. Mozley, M. D. Rossman, S. M. Albelda, A. Alavi, *J. Nucl. Med.* **2001**, *42*, 1412–1417.
- [8] G. W. Severin, J. W. Engle, R. J. Nickles, T. E. Barnhart, *J. Med. Chem.* **2011**, *7*, 389–394.
- [9] T. J. Wadas, E. H. Wong, G. R. Weisman, C. J. Anderson, *Chem. Rev.* **2010**, *110*, 2858–2902.
- [10] D. G. Covell, J. Barbet, O. D. Holton, C. D. V. Black, R. J. Parker, J. N. Weinstein, *Cancer Res.* **1986**, *46*, 3969–3978.
- [11] C. T. Mendl, L. Friedrich, I. Laitinen, M. Schlapschy, M. Schwaiger, H.-J. Wester, A. Skerra, *mAbs* **2015**, *7*, 96–109.
- [12] R. W. Kinne, K. Schemer, T. Behr, R. M. Sharkey, E. Palombo-Kinne, F. Emmrich, D. M. Goldenberg, F. Wolf, W. Becker, *Nucl. Med. Commun.* **1999**, *20*, 67–75.
- [13] C. Wanke, K. Kossert, O. J. Nähle, O. Ott, *Appl. Radiat. Isot.* **2010**, *68*, 1297–1302.
- [14] G. Wermann, D. Alber, W. Pritzkow, G. Riebe, J. Vogl, W. Görner, *Appl. Radiat. Isot.* **2002**, *56*, 145–151.
- [15] S. M. Qaim, T. Bisinger, K. Hilgers, D. Nayak, H. H. Coenen, *Radiochim. Acta* **2007**, *95*, 67–73.
- [16] A. H. Al Rayyes, Y. Ailouti, *World J. Nucl. Sci. Technol.* **2013**, *3*, 72–77.
- [17] M. Shokeen, C. J. Anderson, *Acc. Chem. Res.* **2009**, *42*, 832–841.
- [18] A. N. Asabella, G. L. Cascini, C. Altini, D. Paparella, A. Notaristefano, G. Rubini, *BioMed Res. Int.* **2014**, *2014*, 1–9.
- [19] D. W. McCarthy, R. E. Shefer, R. E. Klinkowstein, L. A. Bass, W. H. Margeneau, S. Cutler, C. J. Anderson, M. J. Welch, *Nucl. Med. Biol.* **1997**, *24*, 35–43.
- [20] M. S. Cooper, M. T. Ma, K. Sunassee, K. P. Shaw, J. D. Williams, R. L. Paul, P. S. Donnelly, P. J. Blower, *Bioconjugate Chem.* **2012**, *23*, 1029–1039.
- [21] C. J. Anderson, R. Ferdani, *Cancer Biother. Radiopharm.* **2009**, *24*, 379–393.
- [22] H. Wang, D. Li, S. Liu, R. Liu, H. Yuan, V. Krasnoperov, H. Shan, P. S. Conti, P. S. Gill, Z. Li, *J. Nucl. Med.* **2015**, *56*, 908–913.
- [23] Q. Xie, H. Zhu, F. Wang, X. Meng, Q. Ren, C. Xia, Z. Yang, *Molecules* **2017**, *22*, 641–650.
- [24] J. E. Mortimer, J. R. Bading, J. M. Park, P. H. Frankel, M. I. Carroll, T. T. Tran, E. K. Poku, R. C. Rockne, A. A. Raubitschek, J. E. Shively, D. M. Colcher, *J. Nucl. Med.* **2018**, *59*, 38–43.
- [25] A. Čepa, J. Ráliš, V. Král, M. Paurová, J. Kučka, J. Humajová, M. Lázníček, O. Lebeda, *Appl. Radiat. Isot.* **2018**, *133*, 9–13.
- [26] K. Lam, C. Chan, R. M. Reilly, *mAbs* **2017**, *9*, 154–164.
- [27] L. Y. Kwon, D. A. Scollard, R. M. Reilly, *Mol. Pharm.* **2017**, *14*, 492–501.
- [28] L. K. van Dijk, C. B. Yim, G. M. Franssen, J. H. Kaanders, J. Rajander, O. Solin, T. J. Gronroos, O. C. Boerman, J. Bussink, *Contrast Media Mol. Imaging* **2016**, *11*, 65–70.
- [29] E. Lucente, H. Liu, Y. Liu, X. Hu, E. Lacivita, M. Leopoldo, Z. Cheng, *Bioconjugate Chem.* **2018**, DOI: <http://doi.org/10.1021/acs.bioconjchem.8b00113>.
- [30] S. Sarkar, N. Bhatt, Y. S. Ha, P. T. Huynh, N. Soni, W. Lee, Y. J. Lee, J. Y. Kim, D. N. Pandya, G. I. An, K. C. Lee, Y. Chang, J. Yoo, *J. Med. Chem.* **2018**, *61*, 385–395.
- [31] D. Zeng, N. S. Lee, Y. Liu, D. Zhou, C. S. Dence, K. L. Wooley, J. A. Katzenellenbogen, M. J. Welch, *ACS Nano* **2012**, *6*, 5209–5219.
- [32] H. Lee, A. F. Shields, B. A. Siegel, K. D. Miller, I. Krop, C. X. Ma, P. M. LoRusso, P. N. Munster, K. Campbell, D. F. Gaddy, S. C. Leonard, E. Geretti, S. J. Blocker, D. B. Kirpotin, V. Moyo, T. J. Wickham, B. S. Hendriks, *Clin. Cancer Res.* **2017**, *23*, 4190–4202.
- [33] X. Nie, R. Laforest, A. Elvington, G. J. Randolph, J. Zheng, T. Voller, D. R. Abendschein, S. E. Lapi, P. K. Woodard, *J. Nucl. Med.* **2016**, *57*, 2006–2011.
- [34] S. E. Lapi, J. S. Lewis, F. Dehdashti, *Semin. Nucl. Med.* **2015**, *45*, 177–185.
- [35] N. Bandara, A. K. Sharma, S. Krieger, J. W. Schultz, B. H. Han, B. E. Rogers, L. M. Mirica, *J. Am. Chem. Soc.* **2017**, *139*, 12550–12558.
- [36] A. K. Sharma, J. W. Schultz, J. T. Prior, N. P. Rath, L. M. Mirica, *Inorg. Chem.* **2017**, *56*, 13801–13814.

- [37] Q. Jin, W. Zhu, D. Jiang, R. Zhang, C. J. Kutyreff, J. W. Engle, P. Huang, W. Cai, Z. Liu, L. Cheng, *Nanoscale* **2017**, *9*, 12609–12617.
- [38] S. Shen, D. Jiang, L. Cheng, Y. Chao, K. Nie, Z. Dong, C. J. Kutyreff, J. W. Engle, P. Huang, W. Cai, Z. Liu, *ACS Nano* **2017**, *11*, 9103–9111.
- [39] D. Psimadas, P. Bouziotis, P. Georgoulas, V. Valotassiou, T. Tsotakos, G. Loudos, *Contrast Media Mol. Imaging* **2013**, *8*, 333–339.
- [40] L. Cheng, S. Shen, S. Shi, Y. Yi, X. Wang, G. Song, K. Yang, G. Liu, T. E. Barnhart, W. Cai, Z. Liu, *Adv. Funct. Mater.* **2016**, *26*, 2185–2197.
- [41] W. Guo, X. Sun, O. Jacobson, X. Yan, K. Min, A. Srivatsan, G. Niu, D. O. Kiesewetter, J. Chang, X. Chen, *ACS Nano* **2015**, *9*, 488–495.
- [42] H. J. Seo, S. H. Nam, H.-J. Im, J.-Y. Park, J. Y. Lee, B. Yoo, Y.-S. Lee, J. M. Jeong, T. Hyeon, J. Who Kim, J. S. Lee, I.-J. Jang, J.-Y. Cho, D. W. Hwang, Y. D. Suh, D. S. Lee, *Sci. Rep.* **2015**, *5*, 15685.
- [43] C. Alliot, N. Michel, A.-C. Bonraisin, V. Bossé, J. Laizé, C. Bourdeau, B. M. Mokili, F. Haddad, *Radiochim. Acta* **2011**, *99*, 627–630.
- [44] S. Thieme, M. Walther, H.-J. Pietzsch, J. Henniger, S. Preusche, P. Mäding, J. Steinbach, *Appl. Radiat. Isot.* **2012**, *70*, 602–608.
- [45] C. M. Jeffery, S. V. Smith, A. H. Asad, S. Chan, R. I. Price, *AIP Conf.* **2012**, *1509*, 84–90.
- [46] M. A. Avila-Rodríguez, J. A. Nye, R. J. Nickles, *Appl. Radiat. Isot.* **2007**, *65*, 1115–1120.
- [47] J. Y. Kim, H. Park, J. C. Lee, K. M. Kim, K. C. Lee, H. J. Ha, T. H. Choi, G. I. An, G. J. Cheon, *Appl. Radiat. Isot.* **2009**, *67*, 1190–1194.
- [48] M. Matarrese, P. Bedeschi, R. Scardaoni, F. Sudati, A. Savi, A. Pepe, V. Masiello, S. Todde, L. Gianolli, C. Messa, F. Fazio, *Appl. Radiat. Isot.* **2010**, *68*, 5–13.
- [49] K. A. Kraus, F. Nelson, *Proc. Int. Conf. Peaceful Uses At. Energy* **1956**, *7*, 113–131.
- [50] C. Battke, E. Kremmer, J. Mysliwicz, G. Gondi, C. Dumitru, S. Brandau, S. Lang, D. Vullo, C. Supuran, R. Zeidler, *Cancer Immunol. Immunother.* **2011**, *60*, 649–658.
- [51] G. Gondi, J. Mysliwicz, A. Hulikova, J. P. Jen, P. Swietach, E. Kremmer, R. Zeidler, *Cancer Res.* **2013**, *73*, 6494–6503.
- [52] S. Ivanov, S.-Y. Liao, A. Ivanova, A. Daniilkovitch-Miagkova, N. Tarasova, G. Weirich, J. Maerill, M. A. Proescholdt, E. H. Oldfield, J. Lee, J. Zavada, A. Waheed, W. S. Sly, M. I. Lerman, E. J. Stanbridge, *Am. J. Pathol.* **2001**, *158*, 905–919.
- [53] R. M. Torczynski, A. P. Bollon (Cytoclonal Pharmaceuticals Inc.), US Pat. No. 5589579, **1996**.
- [54] A. J. Kivelä, S. Parkkila, J. Saarnio, T. J. Karttunen, J. Kivelä, A. K. Parkkila, S. Pastoreková, J. Pastorek, A. Waheed, W. S. Sly, H. Rajaniemi, *Histochem. Cell Biol.* **2000**, *114*, 197–204.
- [55] Ö. Türeci, U. Sahin, E. Vollmar, S. Siemer, E. Göttert, G. Seitz, A.-K. Parkkila, G. N. Shah, J. H. Grubb, M. Pfreundschuh, W. S. Sly, *Proc. Natl. Acad. Sci. USA* **1998**, *95*, 7608–7613.
- [56] S. Parkkila, A.-K. Parkkila, J. Saarnio, J. Kivelä, T. J. Karttunen, K. Kaunisto, A. Waheed, W. S. Sly, Ö. Türeci, I. Virtanen, H. Rajaniemi, *J. Histochem. Cytochem.* **2000**, *48*, 1601–1608.
- [57] C. C. Wykoff, N. Beasley, P. H. Watson, L. Campo, S. K. Chia, R. English, J. Pastorek, W. S. Sly, P. Patcliffe, A. L. Harris, *Am. J. Pathol.* **2001**, *158*, 1011–1019.
- [58] P. Hynninen, L. Vaskivuo, J. H. Saarnio, H. Haapasalo, J. Kivelä, S. Pastoreková, J. Pastorek, A. Waheed, W. S. Sly, U. Puistola, S. Parkkila, *Histopathology* **2006**, *49*, 594–602.
- [59] M. A. Proescholdt, C. Mayer, M. Kubitz, T. Schubert, S.-Y. Liao, E. J. Stanbridge, S. Ivanov, E. H. Oldfield, A. Brawanski, M. J. Merrill, *Neuro-Oncol.* **2005**, *7*, 465–475.
- [60] L. Fiedler, M. Kellner, A. Gosewisch, R. Oos, G. Böning, S. Lindner, N. Albert, P. Bartenstein, H.-J. Reulen, R. Zeidler, F. J. Gildehaus, *Nucl. Med. Biol.* **2018**, *60*, 55–62.
- [61] T. Toyota, T. Hanafusa, T. Oda, I. Koumura, T. Sasaki, E. Matsuura, H. Kumon, T. Yano, T. Ono, *J. Radioanal. Nucl. Chem.* **2013**, *298*, 295–300.
- [62] A. Obata, S. Kasamatsu, D. W. McCarthy, M. J. Welch, H. Saji, Y. Yonekura, Y. Fujibayashi, *Nucl. Med. Biol.* **2003**, *30*, 535–539.
- [63] I. Rose, C. Whittington, *Nickel Plating Handbook*, 2014, Nickel Institute, Brussels (Belgium): <https://nickelinstitute.org/>.
- [64] F. Szelecsényi, G. Blessing, S. M. Qaim, *Appl. Radiat. Isot.* **1993**, *44*, 575–580.
- [65] R. Adam Rebeles, P. Van den Winkel, A. Hermanne, F. Tárkányi, *Nucl. Instrum. Methods Phys. Res. Sect. B* **2009**, *267*, 457–461.
- [66] J. C. Manrique-Arias, M. A. Avila-Rodríguez, *Appl. Radiat. Isot.* **2014**, *89*, 37–41.
- [67] T. Ohya, K. Nagatsu, H. Suzuki, M. Fukada, K. Minegishi, M. Hanyu, T. Fukumura, M.-R. Zhang, *Nucl. Med. Biol.* **2016**, *43*, 685–691.
- [68] Data received from Comecer SpA, <https://www.comecer.com/>.

Manuscript received: February 26, 2018

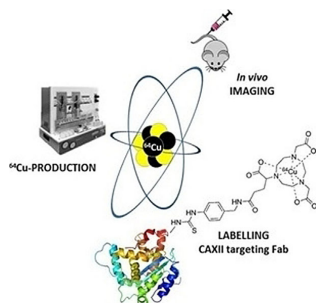
Revised manuscript received: April 9, 2018

Accepted manuscript online: April 18, 2018

Version of record online: ■■■ 0000

## FULL PAPERS

**Ideal decay:** An automated  $^{64}\text{Cu}$  production system using the first-generation Alceo setup was established and evaluated. Volume, pH, radionuclide purity, non-radioactive metal impurities, and molar activity of the product were determined. The carbonic anhydrase XII targeting 6A10 Fab fragment was radio-labelled with the produced  $^{64}\text{Cu}$ , and proof-of-principle small-animal PET imaging was performed.



L. Fiedler,\* M. Kellner, R. Oos, G. Böning,  
S. Ziegler, P. Bartenstein, R. Zeidler,  
F. J. Gildehaus, S. Lindner\*

■ ■ - ■ ■

**Fully Automated Production and  
Characterization of  $^{64}\text{Cu}$  and Proof-of-  
Principle Small-Animal PET Imaging  
Using  $^{64}\text{Cu}$ -Labelled CA XII Targeting  
6A10 Fab**

## List of Figures

---

Figure 2-1: Schematic drawing of the pH regulation in a tumor cell. Next to extruding H <sup>+</sup> with exchange or transport mechanisms, bicarbonate is used as a buffer system. The escaped CO <sub>2</sub> is extracellularly converted into bicarbonate by carbonic anhydrases and transported back into the cell.....	5
Figure 2-2: Reaction mechanism of the formation of bicarbonate catalyzed by carbonic anhydrases.....	5
Figure 2-3: Schematic illustration of an antibody structure containing the N-terminated binding sites on the Fab-domains, the C-terminated Fc-domain and the allocation in heavy and light chains.....	6
Figure 3-1: Structural drawing of the [ <sup>177</sup> Lu]LuDTPA-Fab.....	11
Figure 3-2: Coronal (A) and transversal (B) SPECT/CT image of a mouse 5 h after the injection of 16.1 MBq <sup>177</sup> Lu-6A10 Fab. The tumor on the right shoulder is indicated by white arrows.....	13
Figure 3-3: Structural drawing of the [ <sup>64</sup> Cu]CuNODA-GA-Fab.....	14
Figure 3-4: PET images of M1 and M2 4 h after the injection of 14.7 MBq and 13.9 MBq of the <sup>64</sup> Cu-6A10 Fab, respectively. Tumors on the right shoulder are indicated with white arrows.....	16
Figure 3-5: PET images of M4 and M5 23 h after the injection of 9.6 MBq and 14.2 MBq of the <sup>64</sup> Cu-6A10 Fab, respectively. Tumors on the right shoulder are indicated with white arrows.....	16
Figure 3-6: Biodistribution results 6 h and 5 h after injecting tumor xenograft bearing mice with 4.3 ± 0.4 MBq <sup>177</sup> Lu-6A10 Fab (n = 4) [107] and 13.1 ± 2.4 MBq <sup>64</sup> Cu-6A10 Fab (n = 2).....	17
Figure 3-7: Biodistribution results 24 h after injecting tumor xenograft bearing mice with 4.3 ± 0.4 MBq <sup>177</sup> Lu-6A10 Fab (n = 4) [107] and 13.1 ± 2.4 MBq <sup>64</sup> Cu-6A10 Fab (n = 2).....	18



## List of Tables

---

Table 3-1: Comparison of the biodistribution results (in %ID/g) gained using n = 2 and n = 4 mice injected with <sup>64</sup> Cu- and <sup>177</sup> Lu-labelled 6A10 Fab, respectively. ....	17
Table 3-2: Tumor volume, applied activity and the correlating Tu/Cl values generated from biodistribution and PET data of each mouse investigated with the <sup>64</sup> Cu-compound.....	19



## Danksagung

---

Herzlichen Dank möchte ich an dieser Stelle an **Dr. Simon Lindner** und **Dr. Franz Josef Gildehaus** richten, für die Möglichkeit zur Bearbeitung eines abwechslungsreichen Themas, für ihre fachliche Unterstützung und die vielen konstruktiven Diskussionen und Anregungen. Des Weiteren danke ich **Priv. Doz. Dr. Guido Böning** für die Betreuung und, ebenso wie **Prof. Dr. Peter Bartenstein**, für die Möglichkeit zur Promotion an der Klinik und Poliklinik für Nuklearmedizin.

Während dieser Arbeit durfte ich sehr große Hilfsbereitschaft von vielen Kollegen erfahren, wofür ich mich an dieser Stelle von ganzem Herzen bedanken möchte. **Prof. Dr. Reinhard Zeidler** und **Dr. Markus Kellner**, für die schier unerschöpfliche Bereitstellung an Wissen und forschungsrelevanten Grundmaterial. **Dr. Andreas Hergesell**, für seinen beherzten Einsatz während der Inbetriebnahme des Feststofftargets. **Rosel Oos**, für die Unterstützung bei sämtlichen tierexperimentellen Arbeiten und für die Pflege der Versuchstiere. **Prof. Dr. Sibylle Ziegler**, für ihr stets rekordverdächtig schnelles Korrekturlesen meiner Arbeit. **Dr. Sarah Pfeiffer**, für ihre Hilfe während meiner Einarbeitungszeit im Labor und, gemeinsam mit **Sandra Haller**, für die kameradschaftliche und leider viel zu kurze Bürogemeinschaft. **Dr. Christian Zach**, **Dr. Andreas Delker**, **Karin Bormann-Giglmaier**, **Dr. Barbara Ungern-Sternberg** und **allen weiteren Nuk-Kollegen**, für die freundliche Arbeitsatmosphäre und für das stets hilfreiche Teilen von interdisziplinärem Fachwissen. **Marcel Simmet**, **Jens Wiemer**, **Astrid Gosewisch**, **Magdalena Lindner**, **Julia Brosch** und **Larissa Ermoschkin**, für die vielfältige Unterstützung, völlig unabhängig ob nun Experimente geplant und durchgeführt wurden, Ort und Zeit der nächsten Nahrungsaufnahme diskutiert wurde, oder es einfach mal wieder Zeit für eine Pause war.

**Meine Eltern** haben mir stets ihren unerschütterlichen Glauben an mich spüren lassen, wofür ich mich an dieser Stelle von ganzen Herzen bedanken möchte. Außerdem danke ich meinen Freunden **Andi**, **Chrissi**, **Unger** und **Timo** für ihre moralische Unterstützung während der letzten Jahre.

Mein größter Dank gilt meiner besseren Hälfte **Flo**, der durch seine grenzenlose Geduld, seinen aufbauenden Optimismus und seine bedingungslose Unterstützung während meiner Promotion sicherlich selbst einen Dokortitel verdient hätte.